The Dissertation Committee for Naeem Akl
certifies that this is the approved version of the following dissertation:

Root-MUSIC-Based Methods for Blind Network-Assisted Diversity Multiple Access

Committee:

Ahmed Tewfik, Supervisor

Gustavo de Veciana

Haris Vikalo

John Gilbert

Sanjay Shakkottai

Root-MUSIC-Based Methods for Blind Network-Assisted Diversity Multiple Access

by

Naeem Akl

DISSERTATION

Presented to the Faculty of the Graduate School of

The University of Texas at Austin

in Partial Fulfillment

of the Requirements

for the Degree of

DOCTOR OF PHILOSOPHY

THE UNIVERSITY OF TEXAS AT AUSTIN

December 2018

Dedicated to whom I love.

Acknowledgments

First and foremost, I thank Allah, the almighty for everything.

I am very grateful to Prof. Ahmed Tewfik for all his guidance and support throughout my years at UT. I find myself privileged to work with a very sharp researcher and an extremely humble person. I am sure he knows how much I owe him respect, and I have told him several times how proud I am to be one of his students.

I would also like to thank my committee members professors Gustavo de Veciana, Haris Vikalo, Sanjay Shakkottai and John Gilbert for their guidance and useful feedback.

Special thanks to Prof. Zaher Dawy who encouraged me to complete graduate studies and has always been a great advisor and friend.

I thank Sara and Zeina with whom I have been friends for nine years and I wish them the best in their careers.

I cannot find words to express my gratitude to my roommates Mohamad and

Hamza. I felt I was rather living with my family. I am also very grateful to our close friend Baker who gave me great tips during my preparation for the technical interviews. I am so lucky to have awesome friends like Hassan, Mahdi and Saadallah. Along with Mohamad, Hamza and Baker, we had fun outdoor activities and enjoyed having dinner together. I loved giving the team hard time over board games.

I sincerely thank my parents Khozaey and Souad for their love and endless sacrifices. I thank my sisters Lara and Bahaa, my brothers Bilal, Ali and Waseem, Lara's daughters Lamya and Lina, and Bahaa's sons Ali and Bilal for being there for me every time I needed them.

Last but not least, special thanks to Amena, who I plan to spend my life with, for all her support.

Root-MUSIC-Based Methods for Blind Network-Assisted Diversity Multiple Access

Publication No. _____

Naeem Akl, Ph.D.
The University of Texas at Austin, 2018

Supervisor: Ahmed Tewfik

Packet collisions in wireless networks degrade the throughput and impede the system performance. The collided packets are typically corrupted and get discarded. Channelization methods avoid collisions through fixed assignment of communication resources to the system users, but they do not take into account the randomness of packet arrivals. Statistical multiplexing optimally adapts the allocation of resources to the instantaneous traffic demands of the users. However, it is only possible in the downlink wherein the data streams are managed by one station. Random-access methods mimic statistical multiplexing by dynamically assigning resources to users. A slot is wasted if the channel incurs a collision, and the collided packets have to be retransmitted.

First, we present a cross-layer design for providing multiple access to a shared wireless link. While retransmissions are controlled by the medium access con-

trol (MAC) layer, this creates sufficient diversity to recover the collided packets in the physical (PHY) layer. Both the number and identities of the involved transmitters in a collision are unknown to the receiver. The signal separation is done blindly using root-MUSIC-like algorithms. We solve the collision resolution problem in four network-operation modes: synchronous blocking mode, synchronous non-blocking mode, asynchronous blocking mode and asynchronous non-blocking mode.

Second, we evaluate the decoding performance of the algorithms in block-fading channels with additive white Gaussian noise. We analytically demonstrate the effect of signal-to-noise ratio and the number of retransmissions on the signal separation capability of the proposed methods for a given number of collided packets.

Third, we evaluate the network throughput and mean packet queueing delay for the proposed collision resolution algorithms analytically and numerically. We derive conditions for stability of the queueing network as function of the mean packet arrival rates.

Table of Contents

Acknowledgments **v**

Abstract **vii**

List of Tables **xiii**

List of Figures **xiv**

Chapter 1. Introduction **1**

1.1 Network-Assisted Diversity Multiple Access (NDMA) 2

1.2 Overview of Related Work 4

1.2.1 Network Coding 6

1.2.2 Zigzag Decoding 8

1.2.3 Blind Signal Separation 10

1.2.4 Modulation-Induced Cyclostationarity Approaches . . . 12

1.3 Network Protocol 14

1.4 Contributions 21

1.5 Notation and Abbreviations 22

1.6 Organization 24

Chapter 2. A Root-MUSIC Method for Resolving Synchronous Collisions Using Retransmission Diversity **25**

2.1 Vandermonde Matrix 26

2.2 Root-MUSIC BNDMA 27

2.2.1 Transmission Scheme 28

2.2.2 Detection of K 30

2.2.3 Identification of the K Transmitters 31

2.2.4 Decoding of the K Packets 32

2.2.5 Asymptotic Throughput 33

2.3 Perturbation Analysis 33
2.3.1 Perturbation of the Noise Projection Matrix P_{U_n} 35
2.3.2 Angular Displacements of the Characteristic Complex Exponentials $\{r_k\}_k$ 37
2.3.3 Individual Distributions of Angular Shifts $\{\Delta\omega_k\}_k$ . . . 38
2.3.4 Joint Distribution of Angular Shifts $\{\Delta\omega_k\}_k$ 41
2.4 Noise Averaging 43
2.5 Numerical Experiments 45
2.6 Conclusion 50

Chapter 3. Non-Blocking Scheme for Blind Network-Assisted Diversity Multiple Access in Synchronous Channels 51
3.1 Root-MUSIC-Like Collision Resolution Algorithm 52
3.1.1 Transmission Scheme 53
3.1.2 Detection of K 55
3.1.3 Identification of the K Transmitters 57
3.1.4 Decoding of the K Packets 58
3.2 Probability Distribution of the Collision Resolution Interval Length 58
3.2.1 Brute-force Approach to Compute $P(m)$ in Exponential Time 60
3.2.2 Recursive Approach to Compute $P(m)$ in Polynomial Time 66
3.3 Queueing Analysis 70
3.3.1 Notation 71
3.3.2 Number of Buffered Packets at a Transmitter 72
3.3.3 Characterization of the New Packet Arrivals Per Slot . . 73
3.3.4 Probability Generating Function of the Number of Buffered Packets 74
3.3.5 Steady-State Probability p_e of an Empty Buffer 76
3.3.6 Interpretation of the Network Convergence Condition . 77
3.3.7 Throughput Analysis 79
3.3.8 Delay Analysis 80
3.4 Results 81
3.5 Conclusion 86

Chapter 4. Asynchronous Blind Network-Assisted Diversity Multiple Access **88**
4.1 System Model 89
4.2 Asynchronous Non-Blocking Mode 91
4.2.1 Transmission Scheme 92
4.2.2 Expressions of Collected Packets 94
4.2.3 General Expression of Received Matrix of Packets Y_n . . 95
4.2.4 Decoding of S 97
4.2.5 Pitfalls of Decoding Algorithm 98
4.2.5.1 Pitfall Scenario I 98
4.2.5.2 Pitfall Scenario II 100
4.3 Modified Transmission-Reception Algorithm 102
4.3.1 Transmission Scheme 103
4.3.2 Expression of Y_n 103
4.3.3 Detection of Pitfall Scenario II 105
4.3.4 Identifiability of the K Active Transmitters 106
4.3.5 Decoding of S 108
4.3.6 Symbol Asynchronization 112
4.4 Asynchronous Blocking Mode 113
4.5 Results 114
4.6 Conclusion 119

Chapter 5. Conclusion **120**
5.1 Summary 120
5.2 Future Research Directions 120

Appendices **122**

Appendix A. Appendix to Chapter 3 **123**
A.1 Rank(W_n) 123
A.2 Computation of $P(m, i)$ 126

Appendix B. Appendix to Chapter 4 **131**
B.1 Rank(W_n) 131

Bibliography **137**

List of Tables

1.1 List of Abbreviations 23

List of Figures

1.1 Last two collided mixtures collected by the access point. Involved transmitters TX A and TX B are within the range of each other. 17

1.2 Last two collided mixtures collected by the access point. Involved transmitters TX A and TX B are within the range of each other. Involved transmitter TX C is a hidden node with respect to TX A and TX B. 19

2.1 Transmission scheme of K packets that collide synchronously at the receiver at $t = 0$. 29

2.2 Variation of the number of correctly detected transmitters out of $K = 5$ versus $SNR = 10\log_{10}(1/\sigma^2)$ for $N - K = 1, 2, 3$ and 5. 46

2.3 Variation of symbol error rate (SER) versus $SNR = 10\log_{10}(1/\sigma^2)$ for $N - K = 1, 2, 3$ and 5. 47

2.4 Theoretical and numerical results of the mean squared error $E[\Delta\omega_1^2]$ versus the number of received packets N for two SNR conditions: SNR = 0dB and SNR = 30dB. $K = 2$, $\omega_1 = \pi/4$, $\omega_2 = 3\pi/4$. 48

2.5 Distribution of $(\Delta\omega_1 + \Delta\omega_2)/2$ for $K = 2$, $N = 7$, SNR = 0dB, $\omega_1 = \pi/4$, $\omega_2 = 3\pi/4$. 49

3.1 Transmission scheme of $K = 4$ transmitters. 54

3.2 All collision scenarios in a network of $\tilde{K} = 4$ transmitters. Collision resolution interval (CRI) length m is measured in slots. . 62

3.3 Subgrouping of collision patterns corresponding to a collision resolution interval (CRI) of length $m = 5$. 68

3.4 Variation of symbol error rate (SER) versus $\text{SNR} = 10\log_{10}(1/\sigma^2)$ for two transmission schemes and different number of stacked packets m. $\tilde{K} = 8$. 82

3.5 Probability mass function of the collision resolution length m for two data arrival rates λ. $\tilde{K} = 16$. 83

3.6 Network throughput versus data arrival rate λ for different network sizes $\tilde{K}$. 84

3.7 Maximum network throughput versus network size $\tilde{K}$ for the original scheme [1] and the proposed scheme. 85
3.8 Packet queueing delay versus data arrival rate λ for the original scheme [1] and the proposed scheme. $\tilde{K} = 16$. 86

4.1 Transmission scheme of $K = 3$ packets aligned with the start of a symbol duration 93
4.2 Modified transmission scheme of $K = 3$ packets aligned with the start of a symbol duration 104
4.3 Network throughput versus mean data arrival rate λ for three network operation modes, $\tilde{K} = 20$. 114
4.4 Packet queueing delay versus data arrival rate λ for three network operation modes, $\tilde{K} = 20$. 115
4.5 Maximum network throughput $\eta_{\max}$ versus network size $\tilde{K}$ for the asynchronous blocking mode: $\eta_{\max} = \tilde{K}/(\tilde{K}+2)$. 117
4.6 Absolute difference between rank of packets S and that of a full rank matrix of same dimensions as S versus the number of collided packets K. 118
4.7 Symbol error rate versus $SNR = 10\log_{10}(1/\sigma^2)$ for $K = 3$ collided packets and N collected mixtures of packets in fully synchronous and fully asynchronous network operation modes, $\tilde{K} = 8$. 119

Chapter 1

Introduction

The maximum achievable throughput in wireless networks is reduced by interference. Since the wireless medium is shared, concurrent utilization of the same network resources leads to packet collisions. The collided mixture is corrupted and thus typically discarded. This results in wasting the communication resources and degrading the network throughput. In addition, the discarded packets have to be retransmitted. This incurs additional delay for the successful communication of both the collided packets and the newly arrived packets queued at the transmitters. Therefore, multiaccess schemes are required to manage the channel access, boost the network throughput and cut down the end-to-end delay.

Modular designs in the medium access control (MAC) and physical (PHY) layers approach the collision problem from different perspectives. For example, transmissions could be based on fixed allocation of communication resources in order to avoid collisions as in time-division multiple access (TDMA), and they could be contention-based as in ALOHA and rely on the MAC layer functionality to retransmit the collided packets [2]. The former schemes are poor in

bursty data networks while the latter schemes suffer under heavy network load. PHY approaches like code-division multiple access (CDMA) spreading [3] and interference alignment [4] [5] rely on signal processing to separate collided signals but do not exploit the MAC capabilities.

Cross-layer designs for collision resolution consider both the randomness of data arrival at the transmitters and the multi-reception capability enabled by signal processing as an attempt to improve the system performance [6]. For example, [7] jointly optimizes the MAC and PHY layer by combining interference alignment for transmit beamforming with opportunistic packet transmission for interference management but assumes all nodes have multiple antennas. Two MAC protocols are advised in [8] and [9] for successive interference cancellation (SIC). The random access protocol in [8] is only applied to establish a connection between the nodes and the base station using power domain multiplexing of preamble transmissions. In [9] messages are exchanged before data transmission in order to determine if the receiver can support additional interference from currently inactive nodes and still decode the desired signal using SIC.

1.1 Network-Assisted Diversity Multiple Access (NDMA)

Network-assisted diversity multiple access (NDMA), first introduced in [10], is a cross-layer communication protocol that enables shared access to a communication channel and provides a solution for resolving packet colli-

sions. In the case of simultaneous transmissions on the same frequency band, collided data is not discarded but rather stored by the receiver. The receiver relies on MAC layer functionality and requests packet retransmissions from the involved transmitters. This creates the necessary diversity to separate the collided packets using advanced signal processing in the PHY layer. Orthogonal training sequences are appended to the transmitted packets to enable the identification of the active transmitters. The channel between each transmitter and the receiver is assumed to vary independently over the time slots. The scheme is extended in [11] to dispersive channels.

The use of orthogonal codes to detect the active transmitters renders the collision resolution algorithm highly sensitive to any lack of synchronization. Moreover, the orthogonal sequences scale with the size of the network which wastes the communication resources. A blind version of NDMA (BNDMA) is presented in [1]. The number and identity of the involved transmitters in a collision is unknown beforehand to the receiver. Each transmitter issues weighted replicas of its packet until the packet is acknowledged by the receiver. The weights encode the signatures of the transmitters, which helps the receiver identify the set of involved transmitters in a collision. Inspecting the structure of the collected mixtures of collided packets at the receiver, an analogy is made in [1] between the problem of active user identification in collision resolution and the problem of direction of arrival (DoA) estimation in multiple-antenna communication systems. An Estimation of Signal Parameters via Rotational

Invariance Technique (ESPRIT)-like method is then suggested for active user identification and collision resolution.

In this work we present a set of BNDMA schemes for resolving packet collisions. We distinguish our work from [1] in two respects. First, maintaining the analogy with the DoA estimation problem, we suggest a root-MUltiple SIgnal Classification (MUSIC)-like method for resolving collisions. Second, [1] considers the collision resolution problem in the synchronous blocking mode, whereas we also support three other network-operation modes: synchronous non-blocking mode, asynchronous blocking mode and asynchronous non-blocking mode.

1.2 Overview of Related Work

While in NDMA only the nodes involved in a collision have to retransmit, in [12] a randomly selected set of network nodes join the collision resolution interval (CRI). If the packet of a node collides, the node retransmits that packet. Else, it sends what it overhears. Retransmissions occur in a TDMA fashion. At the end of the CRI the receiver tries to separate the collided packets based on maximum likelihood. A limitation is that orthogonal sequences are required to detect the collision multiplicity. The cooperative random scheme is improved in [13] such that nodes have location information of the other nodes. The scheme is extended in [14] for the multichannel case.

Network-assisted diversity can be combined with spatial diversity as in [15].

Moreover, it can be combined with other multiple access schemes. For example, [16] presents a successive interference cancellation tree-splitting algorithm for medium access. The tree algorithm is combined with an NDMA source-separation scheme in [17–19] provided that sufficient retransmissions have been received at a tree branch. The main limitation of [17–19] is that orthogonal sequences need to be used in order to identify the active user set in each round of the tree-splitting algorithm.

In [20], NDMA is viewed as repetition Automatic Repeat reQuest (ARQ) because of the retransmissions, i.e. the time diversity is provided by repetition coding. [20] suggests to use incremental redundancy ARQ so that K collided packets are decoded in less than K slots whenever feasible. However, [20] requires extra control channels for active user identification. No extra channels are required for our scheme.

In [21], a frequency-domain multipacket receiver that uses single-carrier frequency-domain equalization (SC-FDE) is proposed for collision resolution. The technique uses NDMA as the MAC protocol. The performance depends on the level of correlation of the channel coefficients, and thus it requires uncorrelated channels for the different retransmissions or a frequency domain form of interleaving. Moreover, the channel coefficients need to be estimated in order to perform the equalization. This is challenging to do in the uplink direction in presence of collisions.

In the blind version of NDMA it is required to estimate the number of collided signals K. We detect K using a rank test. Due to noise, this number might be under-estimated or over-estimated. Different methods to identify the order of the mixture of information sources can be found in [22–26].

Below we summarize related work beyond NDMA.

1.2.1 Network Coding

Network coding refers to intelligently mixing signals at network nodes as opposed to simple forwarding [27]. The types of codes to apply (linear, random,...) and polynomial-time algorithms for encoding and decoding are discussed for instance in [28–30]. Network coding could be intra-session or inter-session [31]. The former mixes packets of same sessions (sources) mostly for reliability, while the latter mixes packets of different sessions as an approach to increase the network throughput. Network coding could be done in the analog (physical) domain as in [32] or the digital domain as in [33].

We distinguish our work from network coding approaches that aim at creating opportunities to reduce the number of data transmissions and increase the throughput. Examples of such approaches are [32–37]. The main difference is that they assume the receiver at the time of decoding has knowledge of a subset of the collided signals, or it knows how the collided mixture is

composed of its individual components. We do not assume the receiver has such network layer information. The mentioned network coding approaches describe different methods to acquire such knowledge. For instance, in [32] traffic flow information is provided via control packets. In [33] a node overhears and stores the transmissions of its neighbors. It also relies on exchange of reception reports and educated guessing (as in routing computations) to learn the neighbor state. The format of a coded packet is modified to include identifying information of the individual mixed packets and their next hops. In [34] and [36] an encoding vector is stored in the packet header to help later in decoding. In [37] transmitters are simply assumed to know when their packets are overheard by other nodes in the network. It should be noted that these network coding approaches still require a medium access scheme that could be TDMA [33], ALOHA [38] [39] or simply our scheme.

On the other hand, network coding could also be used to provide a medium access and collision resolution scheme as in [38–40]. We again distinguish our work from theirs. In [38] and [39], a collision represents a linear combination of packets. The receiver should collect enough combinations to separate the packets. [38] employs coding over blocks of symbols, while [39] tries to estimate the number of transmissions that optimizes the network throughput before quitting a collision resolution interval. In both works it is assumed that the receiver knows the set of active transmitters in each slot, for instance via appending a CDMA-encoded preamble to each transmitted packet [39]. In our

case the receiver identifies the active transmitters blindly. It should be noted that the idea of acquiring enough combinations of packets to enable decoding is also found in [41] although [41] does not coin the term *physical network coding*. Extensions of [41] are presented in [40, 42, 43]. A limitation of such schemes is that they rely on receiving one or more collision-free packets and thus cannot resolve every collision pattern even at infinite signal-to-noise ratio (SNR).

The various network coding approaches listed above rely on SIC to subtract a detected or known signal from a mixture of collided signals before trying to decode the other signals. It should be noted that SIC is not specific to network coding [8,9,16,44,45]. However, its main limitation is that it relies on *capture effect*, where one collided signal should have significantly higher power compared to others for successful decoding. Thus, capture effect is random and cannot always be relied upon [6]. For recovery of collided packets based on capture effect refer to [46–49].

1.2.2 Zigzag Decoding

Transmitters in 802.11 networks resend their packets when the packets collide. They do so after waiting for random times. Thus the same collided packets probably collide again at different offsets. Zigzag decoding introduced in [50] exploits this misalignment and searches for chunks that are interference-free in one collided mixture but experience interference in others. The receiver

subtracts these chunks from the mixtures where they experience interference. This way it is likely that the receiver obtains new interference-free chunks which the receiver uses to fully decode the collided packets. Therefore zigzag decoding depends on the asynchrony of the collisions and combines joint decoding and interference cancellation to resolve collisions.

Zigzag decoding requires that the offsets of K packets within K collided mixtures are all different. Compared to zigzag decoding, our work does not depend on the collision pattern but rather applies in both synchronous and asynchronous modes. Moreover, in zigzag decoding an interference-free chunk is decoded and then processed before it is deducted from other collided mixtures. In the case the receiver incorrectly decodes a symbol, the error propagates to the subsequent iterations of the decoding procedure [51]. The decoding errors also limit the maximum number of collided packets that can be separated [50].

[52] and [53] present two variants of zigzag decoding in satellite or underwater acoustic sensor networks and in wireless sensor networks respectively. Both schemes suggest that each packet is augmented with its flipped replica so that a replica of the same packet is easily identified. Moreover, the channel over the two replicas is expected to be correlated. Zigzag decoding is then employed to resolve the collisions. A major drawback of the two schemes is that they only apply in wireless networks that can afford to augment each transmitted packet with its replica. Ideally, full throughput should be achieved in absence

of collisions.

[54] uses zigzag decoding to separate two collided packets from a single transmission. However, it applies zigzag decoding in a cooperative setting in the sense that the two packets are identical and simply transmitted by two nodes in the network (for instance a source and a relay).

While zigzag decoding resolves a collision of K packets by K retransmissions, [55] suggests to separate packets in ZigBee [56] using a single transmission. However, the method should be able to discern a number of amplitude levels that grows exponentially with K. Thus the authors in [55] claim it applies to a maximum of four collided packets. A similar limitation holds for [57]. The proposed method in [57] falls under asynchronous multiuser detection [58] except that all users have the same signature waveform. It relies on the symbol misalignment of the collided signals which are extracted via oversampling and a Viterbi-like algorithm. Channel coding is integrated with the method in [57] to reduce the bit-error rate [59]. We make no assumptions about symbol alignment.

1.2.3 Blind Signal Separation

In our work the receiver blindly identifies the set of active transmitters. We therefore look at blind signal separation schemes used for collision resolution. We do not consider blind multiuser detection based on known signature wave-

forms as in [60–63] due to bandwidth expansion caused by spreading.

Collisions are resolved using independent component analysis in [64] in the synchronous blocking mode. The collision multiplicity K is detected using the minimum description length (MDL) criterion. The receiver thus requires at least $K + 2$ slots to resolve the collision, which is a larger packet delay compared to ours. For signal separation, independent component analysis (ICA) assumes independence and non-Gaussianity of the mixture components. Moreover, over consecutive time slots the channel tends to be correlated. Thus the performance of the scheme in [64] drops for slow fading channels [65]. The channel in [64] is assumed quasi-static, i.e. it is constant during a slot but varies independently between two slots. This is avoided in our case and in [1] by controlling the phase of the transmitted signals. A cooperative version of [64] is presented in [66] and assumes a fully-connected network. Techniques like the iterative least-squares with projections (ILSP) [67] and iterative least-squares with SIC [68] could be used instead of ICA and exhibit similar performance. ICA is integrated with ALOHA in [69] for tag collision resolution in multi-antenna radio frequency identification.

In [70–73], users are blindly separated in the sense that no pilot signals are needed to estimate the mixing matrix and recover the collided signals. Instead, the methods separate the users based on the different user delays, carrier frequency offsets, pulse shapes and oversampling. The different polyphase

components are viewed as independent mixtures of the user signals. However, these methods best apply for two-user separation. Improved error performance is obtained at the cost of bandwidth expansion.

Sparse signal separation techniques may also apply for collision resolution whenever the source signals are sparse in a transformed domain like time-frequency [74]. These techniques are only applicable under the sparsity assumption. This is typical only for particular modulation schemes like frequency hopping.

A semi-blind collision resolution scheme is described in [75]. It is based on embedding known symbols in the packets. The approach is semi-blind because the number of embedded symbols is less than training-based approaches. The receiver is assumed to be equipped with an antenna array and spreading is employed. We assume single-antenna nodes and no spreading.

1.2.4 Modulation-Induced Cyclostationarity Approaches

The above collision-resolution algorithms either require synchronous transmissions as in [1] or depend on the asynchrony of the received signals for successful decoding as in [50]. We highlight two approaches in [76] and [77] that resolve collisions independent of the alignment of the received packets. In both methods the receiver exploits the cyclostationarity properites exhibited by the baseband signals at the transmitters. The cyclostationarity is modulation-induced.

In [76] the transmitted signals are modulated by known amplitude variations at the symbol rate. In [77] the symbols are modulated by polynomial phase sequences. Since the modulation is done at the symbol rate there is no bandwidth expansion. However, it is a form of color code that the receiver uses to distinguish among the transmitters.

Both [76] and [77] assume the receiver has an antenna array, while in our case all nodes have single antennas. In [76] it is assumed that only one signal in the mixture of collided signals is of interest to the receiver. It is also required that the receiver either knows or estimates the arrival time of the desired signal. We do not require knowledge of the arrival times of the desired signals for collision resolution. On the other hand, in [77] the receiver separates the packets by solving a number of eigenvalue problems that is the size of the codebook from which the color codes are selected. It is recommended that this number should be eight times the size of the network population in order to increase the chance that the collisions may be resolved. Compared to ours, this is prohibitive complexity since it depends on the network size as opposed to the multiplicity of the collision. In addition, [77] applies only to binary phase shift keying (BPSK) modulation, whereas we support higher-order modulation schemes.

1.3 Network Protocol

In the following chapters we show how collided packets are extracted from a collected mixture. We only provide a high-level description of the channel access protocol followed by the network nodes. A detailed design of the network protocol is beyond the scope of this work. In this section we show how our collision resolution methods may be potentially incorporated into a real network protocol. For this purpose, we suggest a modification to the infrastructure-based IEEE 802.11 MAC protocol.

The basic version of the protocol is based on carrier sense multiple access with collision avoidance (CSMA/CA). There is an optional mode to avoid hidden terminals. These two mechanisms are referred to as distributed coordination function (DCF). We refer to [78] for a summary of the IEEE 802.11 MAC protocol.

In the basic mode, a node that has a packet to send waits until the channel is idle for a duration of DCF inter-frame spacing (DIFS). If the channel was previously busy, the node waits for an additional random time within the range of a contention window. If more than one node wants to access the channel, the one whose waiting time ends first gains access while the others wait again for an idle channel state. Those delayed to the next cycle stop their timers, wait for an idle state of duration DIFS and then start their counters again as opposed to selecting a new random waiting time. On the other hand, if the

timers of more than one node expire simultaneously, a collision occurs. The contention window doubles (up to a maximum), which is known as exponential backoff. Then the nodes have to contend again for channel access. Whenever a node successfully sends a packet to the access point (AP), the AP sends an acknowledgement (ACK) back. It does so after waiting for an idle channel state for a duration of short inter-frame spacing (SIFS). SIFS is shorter than DIFS so that an ACK always has higher priority over data packets.

The hidden terminal problem [79] refers to the situation in which two nodes are within the range of the AP but not visible to each other. While one node is active, the other node senses an idle channel state and issues a transmission. This leads to a collision at the AP, and the collided packets are discarded. The request-to-send (RTS)/ clear-to-send (CTS) extension of the 802.11 protocol partially solves the hidden terminal problem. Whenever a node has data to send, it contends for channel access according to the basic protocol described above. Upon accessing the channel, the node sends an RTS to the AP. All nodes that hear the RTS set their net allocation vector (NAV) as specified in the duration field of the RTS packet. If the AP successfully receives the RTS, it sends a CTS after SIFS and the recipients adjust their NAVs again. This way a hidden terminal is notified that the channel is reserved for the duration in its NAV. The node that gains channel access and the AP exchange data packets and ACKs. They only have to sense an idle channel state for SIFS. The exchanged packets carry information that helps to update the NAVs of

the other nodes. In this mode of the protocol collisions are only possible when sending RTS packets. This mode results in non-negligible overhead but is useful for delay-sensitive applications.

[80] defines an enhancement of the IEEE 802.11 MAC protocol to include the collision recovery mechanism described in [1]. [80] assumes the infrastructure basic service set (BSS) is compact, collisions are synchronous and there are no hidden terminals. When a collision occurs, each involved node retransmits its packet after a recovery inter-frame space (RIFS). RIFS is chosen to be longer than SIFS but shorter than DIFS so that the CRI is not interrupted. The process repeats until the maximum number of retransmissions is reached or the AP acknowledges the collided packets.

We modify the IEEE 802.11 MAC protocol to handle collisions. In a BSS, we assume all nodes are within the range of the AP but might be out of range of each other. Denote by a round-trip time (RTT) double the maximum propagation delay between two nodes that are visible to each other. Moreover, collisions at the AP are not necessarily synchronous. In this section we assume the network operates in blocking mode, so a node refrains from sending a packet to the AP if it detects a busy channel state. All packets have the same length. Similarly to [80], we define a recovery inter-frame space (RIFS). We choose RIFS such that SIFS + RTT $<$ RIFS $<$ DIFS. This sets an upper limit on RTT or equivalently the basic service area (BSA). In the discussion below

we also assume RTT is less than double the contention window slot time but this could be easily removed. We present two example scenarios that illustrate the enhanced MAC protocol. We also highlight the nonidealities due to the different propagation delays among the network nodes.

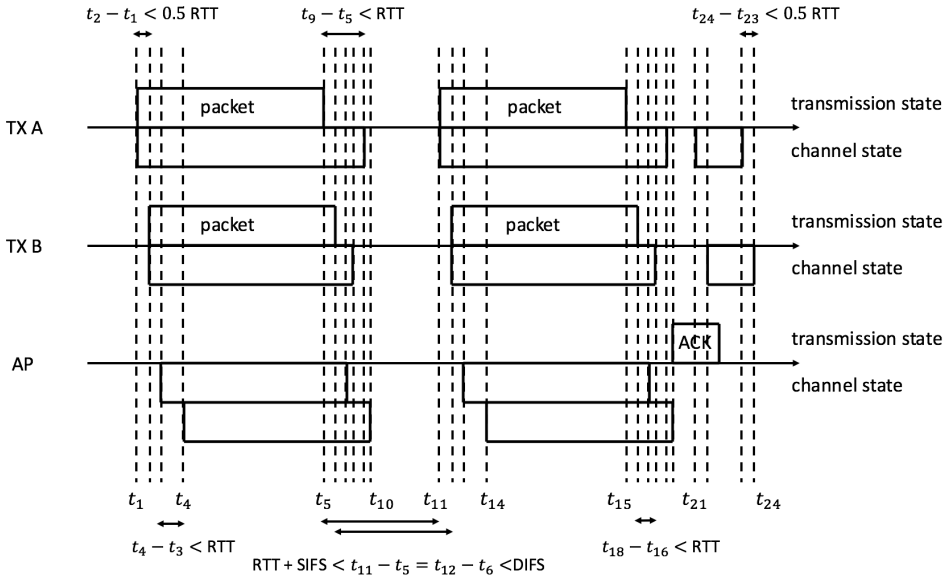

Figure 1.1: Last two collided mixtures collected by the access point. Involved transmitters TX A and TX B are within the range of each other.

Consider the collision scenario in figure 1.1. Two transmitters TX A and TX B are visible to the AP and to each other. We show when each node is actively sending a packet. We also show the channel state as detected by each node. The channel state is marked as busy whenever a node issues a transmission or detects the transmissions of other nodes. Suppose the AP sends an ACK at the end of preceding activity (not shown in the figure). Due to different prop-

agation delays from the AP to TX A and TX B, the two transmitters receive the ACK at different times, and the time gap is at most half an RTT. TX A and TX B seek channel access, so they wait for an idle channel state of DIFS plus the timeout of their backoff counters. The backoff time in the modified protocol is optional. In the example of figure 1.1, TX A is closer than TX B to the AP. Since the contention window slot time is greater than half the RTT, a collision is possible (though might not be necessary) only if the two counters are equal, or counter A is greater than counter B by one. In both cases, the difference between the instants when TX A and TX B issue their packets is less than half an RTT, and the difference between the instants of arrival of the packets at the AP is less than one RTT. In figure 1.1, $t_2 - t_1 < 0.5$ RTT and $t_4 - t_3 <$ RTT. In addition, since the collision involves no hidden terminals, TX A and TX B detect a busy channel state for at most one RTT after they stop transmission: $t_9 - t_5 <$ RTT and $t_8 - t_6 <$ RTT. TX A and TX B wait for RIFS $= t_{11} - t_5 = t_{12} - t_6$. Since RIFS $>$ SIFS + RTT, the channel is clear for at least SIFS. If no ACK is received, TX A and TX B retransmit their packets according to a transmission scheme that is defined later. The process repeats until the AP acknowledges the collided packets or requests to terminate the current collision resolution interval. Assuming the AP sends an ACK, the propagation delays to TX A and TX B are different. Thus, TX A and TX B detect an idle channel state at different instants, and the time gap is again at most half an RTT: $t_{24} - t_{23} < 0.5$ RTT. In figure 1.1 we only show the last two packets sent by each active transmitter before the collision is resolved.

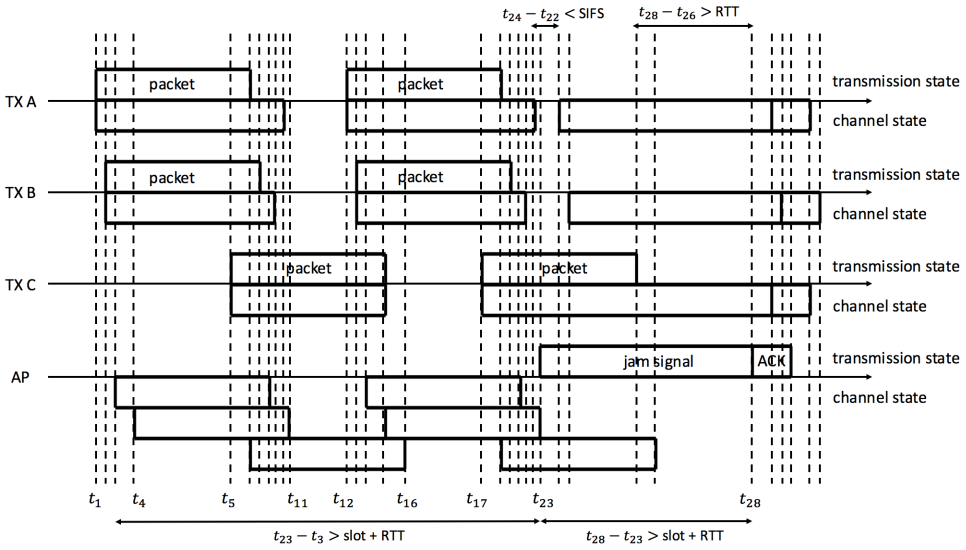

Figure 1.2: Last two collided mixtures collected by the access point. Involved transmitters TX A and TX B are within the range of each other. Involved transmitter TX C is a hidden node with respect to TX A and TX B.

Figure 1.2 illustrates the same collision scenario as figure 1.1 except for an additional involved transmitter TX C. TX C is visible to the AP but hidden from TX A and TX B. It detects an idle channel state and issues a packet while TX A and TX B are active. The packets collide at the AP, and each involved transmitter waits for RIFS between two consecutive transmissions. In the design example of figure 1.2, we select the initial transmission time of TX C so that TX A and TX B are active when TX C is idle and vice versa. In this scenario, the two collided mixtures at the AP overlap in time, so the AP cannot detect the start and end of each mixture: $t_{23} - t_3 >$ slot + RTT. (In this context a slot refers to the duration of a packet and should not be confused

with a contention window slot time.) In addition, suppose the AP manages to decode the collided packets and sends an ACK. In this case, the ACK collects interference from the receive circuitry, and only the currently inactive subset of TX A, TX B and TX C detects the ACK. Instead, the AP sends a jam signal once it decodes the packets. From the example of figure 1.1, a group of visible nodes detect a busy channel state for at most one time slot plus an RTT. Therefore, the duration of the jam signal should be greater than one slot plus an RTT so that it is detected by all involved transmitters: $t_{28} - t_{23} >$ slot + RTT. TX A, TX B and TX C no longer retransmit their packets once the jam signal is detected, and an ACK is issued by the AP. The interference collected by the jam signal from the receive circuity is irrelevant since the jam signal carries no useful information. In figure 1.2 we only show the last two packets sent by each active transmitter before the collision is resolved.

We use random backoff to limit the collision multiplicity K. As pointed out in [80], the value of K impacts both the complexity of signal processing at the AP and the achieved throughput. In the extreme case, no backoff timers are used, which increases the decoding complexity and maximizes the throughput. The protocol should be further modified to handle channel estimation for collision resolution under various channel conditions.

1.4 Contributions

We design a set of methods for resolving packets collisions in multiaccess communication networks. We focus on the signal processing that enables the extraction of packets from a collided mixture. The primary contributions of this work can be summarized as follows:

- We design a set of blind network-assisted diversity multiple access (BNDMA) schemes for the collision resolution problem. The solutions build on the root-MUSIC algorithm [81] for direction of arrival estimation using antenna arrays. We consider the collision resolution problem in four network-operation modes: synchronous blocking (SB) mode in Chapter 2, synchronous non-blocking (SN) mode in Chapter 3, asynchronous blocking (AB) mode in Chapter 4 and asynchronous non-blocking (AN) mode also in Chapter 4. In the asynchronous modes we neither assume slot nor symbol synchronization.

- We evaluate the noise performance of the decoding scheme under additive white Gaussian noise in Chapter 2. We carry out a first-order perturbation analysis and derive closed-form expressions for the individual and joint distributions of the angular perturbations of the roots computed by root-MUSIC. We consider the SB mode for the analysis but the results hold true for the other modes. We illustrate the noise-averaging effect as function of the number of retransmissions N within a collision resolution

interval and derive the rate of convergence over N of the computed roots towards their true values.

- We carry out throughput and delay analysis of the collision resolution algorithm in the SN mode in Chapter 3. [1] presents a queueing analysis for BNDMA schemes in the SB mode. On contrary to the SB mode, a naive approach to do the throughput and delay analysis for the SN mode is exponentially complex in the size of the network. We perform the analysis recursively in polynomial-order complexity. The analyses for the AN and the AB modes are similar to the SN and SB modes respectively.

1.5 Notation and Abbreviations

All vectors $\overrightarrow{v}$ are column vectors and have arrow symbols on top. The transpose of $\overrightarrow{v}$ is $\overrightarrow{v}^T$ and the conjugate transpose of $\overrightarrow{v}$ is $\overrightarrow{v}^H$. Similar transpose notation is used for matrices. For an L-element vector $\overrightarrow{v}$, $\overrightarrow{v}[l]$ is its l^{th} element, $1 \leq l \leq L$. The vector holding elements l through h of $\overrightarrow{v}$ is denoted as $\overrightarrow{v}[l:h]$, $1 \leq l \leq h \leq L$. For a general matrix M of dimensions $R \times C$, $M[r,c]$ is the element of M at the r^{th} row and c^{th} column, $1 \leq r \leq R$, $1 \leq c \leq C$. Moreover, $M[r_l : r_h, c_l : c_h]$ is the submatrix of M holding the elements between rows r_1 and r_h inclusive and columns c_l and c_h inclusive, $1 \leq r_l \leq r_h \leq R$, $1 \leq c_l \leq c_h \leq C$. For indexing in matrices, r is a short-hand notation for $r : r$, and a single : is used to select all rows or columns. For instance, $M[r,:]$ is the r^{th} row of M, $M[:,c]$ is the c^{th} column of M, and $M[:,:]$

is the entire matrix M. The conjugate of complex value z is z^*.

The table below summarizes the acronyms used in this work.

Table 1.1: List of Abbreviations

ACK	ACKnowledgement
ALOHA	Additive Links On-line Hawaii Area
AP	Access Point
ARQ	Automatic Repeat reQuest
AB	Asynchronous Blocking
AN	Asynchronous Non-blocking
BNDMA	Blind Network-assisted Diversity Multiple Access
BPSK	Binary Phase Shift Keying
BSA	Basic Service Area
BSS	Basic Service Set
CDMA	Code-Division Multiple Access
CRC	Cyclic Redundancy Check
CRI	Collision Resolution Interval
CSMA/CA	Carrier Sense Multiple Access with Collision Avoidance
CTS	Clear-To-Send
DCF	Distributed Coordination Function
DIFS	DCF Inter-Frame Spacing
DoA	Direction of Arrival
ESPRIT	Estimation of Signal Parameters via Rotational Invariance Technique
ICA	Independent Component Analysis
ILSP	Iterative Least-Squares with Projections
LHS	Left-Hand Side
MAC	Medium Access Control
MDL	Minimum Description Length
M/G/1	Markov arrival process, IID service times with a General CDF, one server
MSE	Mean-Squared Error
MUSIC	MUltiple SIgnal Classification
NAV	Net Allocation Vector
NDMA	Network-assisted Diversity Multiple Access

Table 1.1 (continued)

PGF	Probability Generating Function
PHY	Physical
RHS	Reft-Hand Side
RIFS	Recovery Inter-Frame Space
RTS	Request-To-Send
RTT	Round-Trip Time
SB	Synchronous Blocking
SC-FDE	Single-Carrier Frequency Domain Equalization
SER	Symbol Error Rate
SIC	Successive Interference Cancellation
SIFS	Short Inter-Frame Spacing
SN	Synchronous Non-blocking
SNR	Signal-to-Noise Ratio
SVD	Singular Value Decomposition
TDMA	Time-Division Multiple Access
TX	Transmitter

1.6 Organization

We present an algorithm to resolve synchronous packet collisions in Chapter 2 and analyze its noise performance. The method is extended in Chapter 3 to the non-blocking mode in which an idle transmitter may join the set of active transmitters and contact the receiver before the current collision is resolved. A throughput and delay analysis of the non-blocking mode is carried out. In Chapter 4 we forgo synchronization and support immediate transmissions. Concluding remarks and future research directions are presented in Chapter 5.

Chapter 2

A Root-MUSIC Method for Resolving Synchronous Collisions Using Retransmission Diversity

We present a root-MUSIC type blind network-assisted diversity multiple access (BNDMA) scheme for collision resolution in block-fading synchronous channels. The scheme relies on weighted retransmissions of the collided packets, and the active set of transmitters is identified using root-MUSIC by computing characteristic roots of the transmitters as analogous to direction-of-arrival (DoA) estimation problems. We also perform a first-order perturbation analysis of the algorithm. Expressions of the individual and joint distributions of the noise-induced angular shifts of the computed roots are derived. These expressions are analyzed in relation to the signal-to-noise ratio and the number of retransmissions made within the collision-resolution interval. Results are verified in simulation.

Perturbation analysis for subspace decomposition in general is examined for instance in [82–85]. Results on perturbation analysis for MUSIC-type sub-

space methods do exist in the literature in the context of DoA estimation. The dependence of performance on the signal-to-noise ratio (SNR), array size N, number of snapshots P, angular separation of the signals, etc. is studied numerically in [86–88]. Analytical results for the mean-squared errors (MSEs) of the DoA estimates are derived in [85], [89–91]. These results give insight on the effect of the array geometry, model error parameters, array size N, and the number of snapshots P on the performance of DoA estimation.

In the next section we summarize important properties of the Vandermonde matrix needed for our solution. Our root-MUSIC BNDMA scheme is incrementally defined in Section 2.2. The set of active transmitters is detected blindly by solving for the characteristic complex exponentials $\{r_k\}_k$. In Section 2.3 we derive first-order approximations of both the individual and the joint distributions of the angular displacements $\{\Delta\omega_k\}_k$ of $\{r_k\}_k$ in the complex plane. We prove these shifts are jointly Gaussian and fully characterize the means and covariances. While in [85] it is shown that the MSE of a DoA estimate monotonically decreases with the number of sensors N, in Section 2.4 we argue that the MSE decays quadratically in the number of stacked packets N. Section 2.5 presents numerical results and Section 2.6 concludes the chapter.

2.1 Vandermonde Matrix

This section summarizes important properties of the Vandermonde matrix that will be used in the design of the transmission and decoding schemes. Consider matrix A

$$A = \begin{pmatrix} 1 & 1 & 1 & \dots & 1 \\ \alpha_1 & \alpha_2 & \alpha_3 & \dots & \alpha_K \\ \alpha_1^2 & \alpha_2^2 & \alpha_3^2 & \dots & \alpha_K^2 \\ \vdots & \vdots & \vdots & \dots & \vdots \\ \alpha_1^{N-1} & \alpha_2^{N-1} & \alpha_3^{N-1} & \dots & \alpha_K^{N-1} \end{pmatrix} \tag{2.1}$$

A is an $N \times K$ Vandermonde matrix where $N > K$. Each column of A is a geometric progression. Assuming all $\{\alpha_k\}_{k=1}^K$ are distinct complex numbers, any subset of the columns of A is full rank. In addition, since $N > K$, A has a non-trivial left null space $A_\perp$. For a Vandermonde matrix A, $A_\perp$ fully identifies the elements $\{\alpha_k\}_{k=1}^K$. This is because $A_\perp^H A = 0$, so equation

$$\overrightarrow{Z}^H A_\perp A_\perp^H \overrightarrow{Z} = 0 \tag{2.2}$$

admits roots $\{\alpha_k\}_{k=1}^K$, where $\overrightarrow{Z} = [1, z, z^2, \dots, z^{N-1}]^T$.

2.2 Root-MUSIC BNDMA

Consider a network of $\tilde{K}$ transmitters and one receiver. All nodes have single antennas, and all transmissions occur on the same frequency band. The minimum transmission unit is a packet of P symbols, where $P > \tilde{K}$. A packet duration is 1 slot $= P \times \tau$, where τ is the symbol duration. Each transmitter $\tilde{k}$

is characterized by a complex exponential $r_{\tilde{k}}$, and the receiver is aware of this assignment. Only K transmitters, $1 \leq K \leq \tilde{K}$, have data to send and thus access the channel. The number and identities of the active transmitters are unknown to the receiver. Transmissions are synchronized, so all the packets from the K active transmitters arrive at the receiver at the same instant. Until the K packets get decoded, all inactive transmitters stay inactive. During this collision resolution interval (CRI), we assume fading is constant. For ease of notation, we denote by $\overrightarrow{s}_k$ the original packet issued by transmitter k scaled by fading. Once packets $\{\overrightarrow{s}_k\}_{k=1}^{K}$ are decoded, fading is removed by single-channel (collision-free) methods. We first describe the transmission scheme. Then we show how the receiver detects K, identifies the K transmitters and decodes the received packets.

2.2.1 Transmission Scheme

We follow the transmission scheme of [1]. For the case $K = 1$ both the transmitter and the receiver detect a contention-free channel (error-detecting code checking, carrier sensing, etc.). No collision occurs and the packet is decoded correctly at high SNR. The transmitter does not have to do any retransmissions of the same packet.

On the other hand, figure 2.1 shows the transmission scheme adopted by each transmitter if $K > 1$. Each transmitter k sends its packet $\overrightarrow{s}_k$. The K packets arrive at the receiver at time $t = 0$, i.e. the start of slot $n = 1$. During

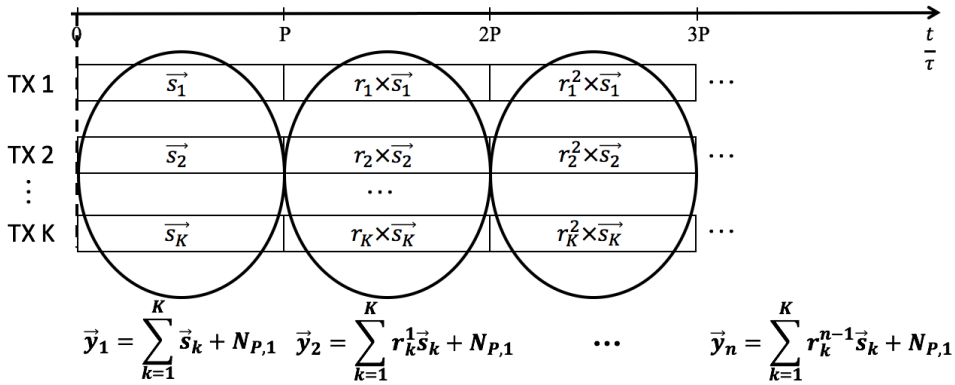

Figure 2.1: Transmission scheme of K packets that collide synchronously at the receiver at $t = 0$.

this slot, the receiver collects packet $\overrightarrow{y}_1 = \sum_{k=1}^{K} \overrightarrow{s}_k + \mathcal{N}_{P,1}$ that is corrupted due to collision, even at high SNR. $\mathcal{N}_{a,b}$ is a noise matrix of dimension $a \times b$. Collision is detected by the receiver and the transmitters.

The receiver will not be able to decode the K packets within a single slot since $K > 1$ and all the packets occupy the same frequency band. In this case, each transmitter k sends a contiguous packet $r_k \times \overrightarrow{s}_k$ that will exactly fit within slot $n = 2$. During slot $n = 2$, the receiver collects $\overrightarrow{y}_2 = \sum_{k=1}^{K} r_k \overrightarrow{s}_k + \mathcal{N}_{P,1}$. Suppose the receiver fails again in decoding the original K packets $\{\overrightarrow{s}_k\}_{k=1}^{K}$. The transmitters continue to send their contiguous transmissions of the weighted packets. In its n^{th} transmission, transmitter k sends packet $r_k^{n-1} \overrightarrow{s}_k$ and the receiver collects during slot n packet $\overrightarrow{y}_n = \sum_{k=1}^{K} r_k^{n-1} \overrightarrow{s}_k + \mathcal{N}_{P,1}$.

2.2.2 Detection of K

At the end of each time slot n, the receiver stacks the n already collected vectors $\{\overrightarrow{y}_1^T, \overrightarrow{y}_2^T, \ldots, \overrightarrow{y}_n^T\}$ vertically into matrix Y_n. Note that matrix Y_n can be expressed as

$$Y_n = \begin{pmatrix} \overrightarrow{y}_1^T \\ \overrightarrow{y}_2^T \\ \vdots \\ \overrightarrow{y}_n^T \end{pmatrix} = \begin{pmatrix} 1 & 1 & \ldots & 1 \\ r_1 & r_2 & \ldots & r_K \\ \vdots & \vdots & \ldots & \vdots \\ r_1^{n-1} & r_2^{n-1} & \ldots & r_K^{n-1} \end{pmatrix} \times \begin{pmatrix} \overrightarrow{s}_1^T \\ \vdots \\ \overrightarrow{s}_K^T \end{pmatrix} + \mathcal{N}_{n,P} \tag{2.3}$$

or shortly

$$Y_n = W_n \times S + \mathcal{N}_{n,P} \tag{2.4}$$

We have $P > \tilde{K} \geq K$ and the packets $\{\overrightarrow{s}_k\}_{k=1}^K$ of the K transmitters are independent, so rank$(S) = K$. But S is a $K \times P$-matrix, so rank$(W_n \times S) =$ rank(W_n). However, W_n holds the coding vectors $\{\overrightarrow{w}_{k,n}\}_{k=1}^K$ of the K transmitters as its columns. Since each transmitter k is assigned a different complex number r_k, W_n is a Vandermonde matrix whose rank is K whenever $n > K$. From (2.4), if $n > K$ then K is also the rank of Y_n in the noiseless case. In presence of noise, the receiver is still able to detect the actual rank of Y_n at high SNR as that of the noiseless case by thresholding the small singular values of Y_n. Therefore, the receiver builds matrix Y_n and checks its true

(noiseless) rank at the end of every slot n. Once $\text{rank}(Y_n)$ stops growing with n, the receiver detects K as

$$K = \text{rank}(Y_n) \tag{2.5}$$

The receiver stops expanding Y_n at $n = N > K$:

$$Y_N = W_N \times S + \mathcal{N}_{N,P} \tag{2.6}$$

2.2.3 Identification of the K Transmitters

At high SNR, Y_N in (2.6) has a non-trivial left null space of dimension $N - K$. Let $\hat{U}_\perp$ hold as columns the basis vectors of the left null space of Y_N. The receiver computes $\hat{U}_\perp$ by performing the singular value decomposition (SVD) of Y_N:

$$Y_N = \left([\hat{U}_\parallel \quad \hat{U}_\perp]\right) \hat{\Sigma} \hat{V}^H \tag{2.7}$$

From (2.6), Y_N and W_N have the same left null space in the noiseless case:

$$\hat{U}_\perp^H W_N \underset{\text{SNR}\to\infty}{\longrightarrow} 0 \tag{2.8}$$

However, W_N is a Vandermonde matrix. As discussed in Section 2.1, $\hat{U}_\perp$ thus fully identifies the elements $\{r_k\}_{k=1}^K$. Therefore, after computing $\hat{U}_\perp$ from the SVD of Y_N, the receiver solves equation

$$J(z) = \overrightarrow{w'}_N^H \times \hat{U}_\perp \hat{U}_\perp^H \times \overrightarrow{w'}_N = 0 \tag{2.9}$$

for z, where coding vector $\overrightarrow{w'}_N$ is given by

$$\overrightarrow{w'}_N = \left[1, z^1, \ldots, z^{N-1}\right]^T \tag{2.10}$$

Equation (2.9) yields K unit complex exponentials $\{r_k\}_{k=1}^K$ that indicate to the receiver the identity of the K transmitters. On the other hand, in presence of noise, $\hat{U}_\perp$ will not exactly describe the left null space of W_N. In this case, the receiver still computes $\hat{U}_\perp$ from Y_N and solves (2.9). Then the receiver chooses the K solutions closest to the unit circle and the individual elements of set $\{r_{\tilde{k}}\}_{\tilde{k}=1}^{\tilde{K}}$ to identify the K active transmitters. Optimal methods that account for the distributions of angular displacements $\{\Delta\omega_k\}_k$ of $\{r_k\}_k$ derived in Section 2.3 may also be utilized.

2.2.4 Decoding of the K Packets

Having identified the K complex exponentials $\{r_k\}_{k=1}^K$, the receiver constructs the Vandermonde matrix W_N as in (2.3). The order of the columns of W_N is unimportant. From (2.6), the matrix of decoded packets is obtained as

$$\hat{S} = (W_N^H W_N)^{-1} W_N^H Y_N \tag{2.11}$$

Matrix $W_N^H W_N$ is full rank and thus admits an inverse. In the noiseless case $\hat{S}$ is exactly S. The k^{th} row of $\hat{S}$ is the decoded packet of the transmitter whose coding vector is the k^{th} column in constructed matrix W_N.

2.2.5 Asymptotic Throughput

As mentioned previously, $N-K$ is the number of columns of $\hat{U}_\perp$ which defines the left null space of Y_N. Referring to the SVD of Y_n in (2.7), these columns correspond to the $N-K$ singular values of the noise-only subspace. Since K is fixed in a given communication scenario, the receiver gains better approximation of the noise-only subspace by stacking more packets $\overrightarrow{y}_n$ to matrix Y_n in order to increase N and consequently $\text{rank}(\hat{U}_\perp) = N-K$. Lower SNR requires extra packets $\overrightarrow{y}_n$ to be collected for the same performance. At high SNR, $N-K \sim \mathcal{O}(1)$. This implies that the decoding delay N (measured in slots) is of the order of the number of active transmitters K. During this time, K distinct packets are correctly decoded. The asymptotic throughput becomes

$$\lim_{K\to\infty} \frac{K}{N} = 100\% \tag{2.12}$$

2.3 Perturbation Analysis

Perturbation analysis refers to the effect of observation noise $\mathcal{N}_{N,P}$ in (2.6) on the accuracy of detecting characteristic roots $\{r_k\}_k$ or equivalently

$\{\omega_k\}_k$ from Y_N ($\omega_k = \angle r_k$), which in turn affects the reconstruction of coefficient matrix W_N and the decoding of packets S. We do perturbation analysis for root-MUSIC in the context of collision resolution, which differs from DoA estimation in several respects. First, we focus on the noise averaging effect that is achieved by stacking a large number of packets N in Y_N, whereas in DoA estimation the number of sensors N cannot be flexibly varied. Second, we only consider packet transmissions of fixed symbol size P. In DoA estimation it is crucial to increase the time-averaging factor P to get better estimates of the spatial covariance matrix of the antenna array. Third, in (2.7) we decompose the measurement matrix Y_N itself. The observation error $\mathcal{N}_{N,P}$ is assumed to follow a complex Gaussian distribution. In DoA estimation it is typical to do subspace decomposition of the sample covariance matrix computed from Y_N, in which case the approximation error of the covariance matrix is modeled by a complex Wishart distribution [92], [93].

The signal component of Y_N in (2.6) can be expressed by SVD as

$$X = W_N \times S = U_{\parallel}\Sigma_s V_s^H + U_{\perp}\Sigma_n V_n^H \tag{2.13}$$

where $U_{\parallel}$ and $U_{\perp}$ constitute an orthonormal basis for the left singular vectors of X, V_s and V_n form an orthonormal basis for the right singular vectors, Σ_s is a diagonal matrix holding the K non-zero singular values of X, and Σ_n is a matrix of $(N-K)\times(N-K)$ zeros.

The SVD of the noisy signal Y_N in (2.6) can be re-expressed as

$$Y_N = X + \Delta X = \hat{U}_{\|}\hat{\Sigma}_s\hat{V}_s^H + \hat{U}_{\perp}\hat{\Sigma}_n\hat{V}_n^H \tag{2.14}$$

where the perturbation $\Delta X = \mathcal{N}_{N,P}$ in (2.6) leads to a perturbation of the singular vectors $U_{\|}$, $U_{\perp}$, V_s and V_n and the singular values $\mathrm{diag}(\Sigma_s)$ and $\mathrm{diag}(\Sigma_n)$. In particular, a perturbation of $U_{\perp}$ leads to a perturbation of the noise subspace projection matrix:

$$\hat{P}_{U_n} = \hat{U}_{\perp}\hat{U}_{\perp}^H = P_{U_n} + \Delta P_{U_n} = U_{\perp}U_{\perp}^H + \Delta P_{U_n} \tag{2.15}$$

This leads to a displacement of the roots $\{r_k\}_k$ generated by

$$\overrightarrow{w'}_N(z)^H \times P_{U_n} \times \overrightarrow{w'}_N(z) = 0 \tag{2.16}$$

for an arbitrary coding vector $\overrightarrow{w'}_N(z) = \left[1, z^1, \ldots, z^{N-1}\right]^T$, which impacts the identification of the set of active transmitters.

2.3.1 Perturbation of the Noise Projection Matrix P_{U_n}

Referring to [82], for an arbitrary matrix X of SVD as in (2.13), a perturbation ΔX leads to a first-order perturbation $\Delta U_{\|}$ of the form

$$\Delta U_{\|} = U_{\|}R + U_{\perp}U_{\perp}^H\Delta X V_s\Sigma_s^{-1} \tag{2.17}$$

where $R = D \odot (U_{\|}^H \Delta X V_s \Sigma_s + \Sigma_s V_s^H \Delta X^H U_{\|})$ and $\odot$ is the Hadamard product. D is a $K \times K$ matrix whose first diagonal elements are zero while the off-diagonal elements have the form $D[k_1, k_2] = 1/(\sigma_{k_2}^2 - \sigma_{k_1}^2), 1 \leq k_1 \neq k_2 \leq K$. Values $\{\sigma_k\}_k$ correspond to the K non-zero singular values of X whose rank is K.

Define the signal subspace projection matrix as $P_{U_s} = U_{\|} U_{\|}^H$. By the orthonormality of the left singular vectors of X we have

$$P_{U_s} + P_{U_n} = I \tag{2.18}$$

Therefore,

$$\Delta P_{U_n} = -\Delta P_{U_s} = -\Delta U_{\|} U_{\|}^H - U_{\|} \Delta U_{\|}^H \tag{2.19}$$

Substituting (2.17) in (2.19) and noting that $R^H = -R$ we have

$$\Delta P_{U_n} = -P_{U_n} \Delta X X^+ - X^{+H} \Delta X^H P_{U_n} \tag{2.20}$$

where

$$X^+ = V_s \Sigma_s^{-1} U_{\|}^H \tag{2.21}$$

2.3.2 Angular Displacements of the Characteristic Complex Exponentials $\{r_k\}_k$

Denote by $d_k = 1$ and ω_k the respective magnitude and angle of characteristic complex exponential r_k of transmitter k, i.e. $r_k = d_k \exp(j\omega_k)$. A coding vector $\overrightarrow{w}_k$ of transmitter k is defined as

$$\overrightarrow{w}_k = \overrightarrow{w'}_N(r_k) = [1, \exp(j\omega_k), \ldots, \exp\left(j(N-1)w_k\right)]^T \tag{2.22}$$

where $\overrightarrow{w'}_N(z)$ is an arbitrary coding vector as in (2.16). By definition of $U_\perp$ in (2.13) we have

$$\overrightarrow{w}_k^H P_{U_n} \overrightarrow{w}_k = 0, \quad 1 \le k \le K \tag{2.23}$$

Because of ΔX, perturbed roots $\{\hat{r}_k\}_k$ are generated by (2.16) as approximations for $\{r_k\}_k$. Define

$$\overrightarrow{w}_k^{(1)} = \frac{d\overrightarrow{w'}}{dz}(r_k) = [0, \exp(j\omega_k), \ldots, (N-1)\cdot\exp\left(j(N-1)\omega_k\right)]^T \tag{2.24}$$

Referring to [89], (2.16) can be approximated as a first-order perturbed version of (2.23) as follows:

$$\begin{aligned}(\overrightarrow{w}_k^H - j\overrightarrow{w}_k^{(1)^H}\Delta\omega_k - \overrightarrow{w}_k^{(1)^H}\Delta r_k + \text{h.o.t}) \times (P_{U_n} + \Delta P_{U_n}) \\ \times (\overrightarrow{w}_k + j\overrightarrow{w}_k^{(1)}\Delta\omega_k + \overrightarrow{w}_k^{(1)}\Delta r_k + \text{h.o.t}) = 0\end{aligned} \tag{2.25}$$

where h.o.t refers to higher order terms to be neglected in a first-order analysis. (2.25) implies perturbation ΔP_{U_n} of noise projection matrix U_n expectedly shifts root r_k to new position $(1+\Delta r_k)\exp(j(\omega_k+\Delta\omega_k))$ in the complex plane. The real and imaginary parts in the left-hand side of (2.25) should be equated to zero. Unless higher-order terms are considered, $\Delta r_k = 0$. Moreover, the identification of the active set of users depends on the angles of the detected roots. A first-order approximation of the angular shift $\Delta\omega_k$ is given by

$$\Delta\omega_k = \frac{\overrightarrow{w}_k^{(1)^H} P_{U_n} \Delta X X^+ \overrightarrow{w}_k - \overrightarrow{w}_k^H X^{+^H} \Delta X^H P_{U_n} \overrightarrow{w}_k^{(1)}}{2j \overrightarrow{w}_k^{(1)^H} P_{U_n} \overrightarrow{w}_k^{(1)}} \tag{2.26}$$

Note that $\Delta\omega_k$ in (2.26) is real-valued.

2.3.3 Individual Distributions of Angular Shifts $\{\Delta\omega_k\}_k$

Recall that $\Delta X = \mathcal{N}_{N,P}$ has dimensions $N \times P$. We assume noise is independent for the different packet symbols, so the columns of ΔX are independent. We assume noise is also independent over the different slot durations, so the entries of each column of ΔX are independent. We finally assume each entry $\Delta X_{n,p}$ of ΔX is circularly symmetric complex normal of mean zero $E[\Delta X_{n,p}] = 0$, variance $E[\Delta X_{n,p}^* \Delta X_{n,p}] = \sigma^2$ and relation $E[\Delta X_{n,p} \Delta X_{n,p}] = 0$. Therefore, we may associate a complex matrix normal distribution to ΔX:

$$\Delta X \sim \mathcal{CN}(0_{N\times P}, \sigma^2 I_{N\times N}, I_{P\times P}) \tag{2.27}$$

The first argument in $\mathcal{CN}(\cdot,\cdot,\cdot)$ is the mean, the second argument describes the dependencies among the entries of a single column (covariance matrix), and the third argument describes dependencies among the different columns. This is equivalent to

$$\mathrm{vec}(\Delta X) \sim \mathcal{CN}(0_{NP}, \sigma^2 I_{P\times P} \otimes I_{N\times N}) \tag{2.28}$$

where $\mathcal{CN}(\mu,\Gamma)$ is the complex multivariate normal distribution of mean μ and covariance matrix Γ,

$$\mathrm{vec}(\Delta X) = [\Delta X_{1,1},\ldots,\Delta X_{N,1},\Delta X_{1,2},\ldots,\Delta X_{N,2},\ldots,\Delta X_{1,P},\ldots,\Delta X_{N,P}]^T \tag{2.29}$$

and $A \otimes B$ is the Kronecker product of two arbitrary matrices $A \in \mathcal{C}^{m\times n}$ and $B \in \mathcal{C}^{p\times q}$. Define

$$\overrightarrow{C}_k^H = \frac{\overrightarrow{w}_k^{(1)^H} P_{U_n}}{\overrightarrow{w}_k^{(1)^H} P_{U_n} \overrightarrow{w}_k^{(1)}} \tag{2.30}$$

$$\overrightarrow{D}_k = X^+ \overrightarrow{w}_k \tag{2.31}$$

Using (2.27), $\overrightarrow{C}_k^H \Delta X \overrightarrow{D}_k$ is distributed as

$$\overrightarrow{C}_k^H \Delta X \overrightarrow{D}_k \sim \mathcal{CN}(0, \sigma^2 \overrightarrow{C}_k^H I_{N\times N} \overrightarrow{C}_k, \overrightarrow{D}_k^H I_{P\times P} \overrightarrow{D}_k) \tag{2.32}$$

By a transformation as in (2.28), $\overrightarrow{C}_k^H \Delta X \overrightarrow{D}_k$ is a simple complex random variable of distribution

$$\overrightarrow{C}_k^H \Delta X \overrightarrow{D}_k \sim \mathcal{CN}(0, \sigma^2 \overrightarrow{D}_k^H \overrightarrow{D}_k \overrightarrow{C}_k^H \overrightarrow{C}_k) \tag{2.33}$$

Using the fact that $P_{U_n} P_{U_n}^H = P_{U_n}$, we have

$$\overrightarrow{C}_k^H \overrightarrow{C}_k = 1/\left(\overrightarrow{w}_k^{(1)^H} P_{U_n} \overrightarrow{w}_k^{(1)} \right) \tag{2.34}$$

Moreover, using (2.21) and $V_s^H V_S = I$ we have

$$\overrightarrow{D}_k^H \overrightarrow{D}_k = \overrightarrow{w}_k^H U_\parallel \Sigma_s^{-1} \Sigma_s^{-1} U_\parallel^H \overrightarrow{w}_k \tag{2.35}$$

Both $\overrightarrow{C}_k^H \overrightarrow{C}_k$ and $\overrightarrow{D}_k^H \overrightarrow{D}_k$ are real numbers. $\Delta\omega_k$ in (2.26) can be expressed as

$$\Delta\omega_k = \frac{\left(\overrightarrow{C}_k^H \Delta X \overrightarrow{D}_k \right) - \left(\overrightarrow{C}_k^H \Delta X \overrightarrow{D}_k \right)^H}{2j} = \mathrm{Im}\left(\overrightarrow{C}_k^H \Delta X \overrightarrow{D}_k \right) \tag{2.36}$$

where $\mathrm{Im}(z)$ is the imaginary part of complex variable z. As a first-order approximation, (2.33) and (2.36) imply that $\Delta\omega_k$ is a real Gaussian scalar distributed as

$$\Delta\omega_k \sim \mathcal{N}\left(0, \frac{\sigma^2}{2} (\overrightarrow{D}_k^H \overrightarrow{D}_k)(\overrightarrow{C}_k^H \overrightarrow{C}_k) \right) \tag{2.37}$$

2.3.4 Joint Distribution of Angular Shifts $\{\Delta\omega_k\}_k$

We now prove that angular shifts $\{\Delta\omega_k\}_k$ are jointly Gaussian for a first-order analysis. Denote by $D_{k,p}$ the p^{th} element of vector $\overrightarrow{D}_k$ and by $\overrightarrow{\Delta X}_p$ the p^{th} column of matrix ΔX, $1 \leq p \leq P$. Define K arbitrary real coefficients $\{\alpha_k\}_{k=1}^K$. Using (2.36), the weighted sum $\sum_k \alpha_k \Delta\omega_k$ can be expressed as

$$\begin{aligned}\sum_k \alpha_k \Delta\omega_k &= \sum_k \alpha_k \operatorname{Im}\left(\sum_p D_{k,p} \overrightarrow{C}_k^H \overrightarrow{\Delta X}_p\right) \\ &= \sum_p \operatorname{Im}\left(\left(\sum_k \alpha_k D_{k,p} \overrightarrow{C}_k^H\right) \overrightarrow{\Delta X}_p\right) \\ &= \sum_p \operatorname{Im}\left(\overrightarrow{\beta}_p^H \overrightarrow{\Delta X}_p\right)\end{aligned} \tag{2.38}$$

The second equality in (2.38) follows from the linearity of the imaginary operator. While row vector $\overrightarrow{\beta}_p^H$ is N-dimensional, it is a weighted sum of only K vectors $D_{k,p}\overrightarrow{C}_k^H$. Moreover, there are P such vectors $\{\overrightarrow{\beta}_p^H\}_p$. Therefore, the problem of selecting K coefficients $\{\alpha_k\}_k$ so that all vectors $\{\overrightarrow{\beta}_p^H\}_p$ are zero vectors admits NP equations. It is thus overdetermined and admits no non-trivial solutions for $\{\alpha_k\}_k$ almost surely. Since the entries of vectors $\{\overrightarrow{\Delta X}_p\}_p$ are complex Gaussian, and assuming set $\{\alpha_k\}_k$ is non-trivial, $\sum_k \alpha_k \Delta\omega_k$ in (2.38) is a weighted sum of real Gaussians and is thus Gaussian-distributed. Therefore, angular shifts $\{\Delta\omega_k\}_k$ in (2.37) are jointly Gaussian.

Given that variables $\{\Delta\omega_k\}_k$ are jointly Gaussian, the joint distribution is fully characterized by the mean vector and covariance matrix. All angular shifts $\{\Delta\omega_k\}_k$ have zero mean as in (2.37). For the covariance matrix, we evaluate $E[\Delta\omega_k\Delta\omega_l]$ using (2.36):

$$\begin{aligned} 4E[\Delta\omega_k\Delta\omega_l] &= E[(\overrightarrow{C}_k^H\Delta X\overrightarrow{D}_k)(\overrightarrow{C}_l^H\Delta X\overrightarrow{D}_l)^H] \\ &+ E[(\overrightarrow{C}_k^H\Delta X\overrightarrow{D}_k)^H(\overrightarrow{C}_l^H\Delta X\overrightarrow{D}_l)] \\ &- E[(\overrightarrow{C}_k^H\Delta X\overrightarrow{D}_k)^H(\overrightarrow{C}_l^H\Delta X\overrightarrow{D}_l)^H] \\ &- E[(\overrightarrow{C}_k^H\Delta X\overrightarrow{D}_k)(\overrightarrow{C}_l^H\Delta X\overrightarrow{D}_l)] \end{aligned} \tag{2.39}$$

$\overrightarrow{C}_k^H\Delta X\overrightarrow{D}_k$ is a weighted sum of the entries of ΔX. These entries are independent, have zero mean and are circularly symmetric. Thus, the last two expectations in (2.39) are zero. By linearity of the expectation we have

$$4E[\Delta\omega_k\Delta\omega_l] = \overrightarrow{C}_k^H E[\Delta X\overrightarrow{D}_k\overrightarrow{D}_l^H\Delta X^H]\overrightarrow{C}_l + \overrightarrow{D}_k^H E[\Delta X^H\overrightarrow{C}_k\overrightarrow{C}_l^H\Delta X]\overrightarrow{D}_l \tag{2.40}$$

Note the following:

$$\begin{aligned} E[\Delta X\overrightarrow{D}_k\overrightarrow{D}_l^H\Delta X^H] &= E[(\sum_p D_{k,p}\overrightarrow{\Delta X}_p)(\sum_p D_{l,p}^*\overrightarrow{\Delta X}_p^H)] \\ &= \sum_p\sum_{p'} D_{k,p}D_{l,p'}^* E\left[\overrightarrow{\Delta X}_p\overrightarrow{\Delta X}_{p'}^H\right] \\ &= \sum_p D_{k,p}D_{l,p}^*\sigma^2 I_{N\times N} \\ &= \sigma^2\left(\overrightarrow{D}_l^H\overrightarrow{D}_k\right) I_{N\times N} \end{aligned} \tag{2.41}$$

where the second equality in (2.41) is implied by the linearity of expectation, while the third equality is obtained by utilizing the distribution of ΔX in (2.27). Similarly,

$$E[\Delta X^H \overrightarrow{C}_k \overrightarrow{C}_l^H \Delta X] = \sigma^2 \left(\overrightarrow{C}_l^H \overrightarrow{C}_k \right) I_{P\times P} \tag{2.42}$$

Plugging (2.41) and (2.42) in (2.40) we have

$$\begin{aligned} E[\Delta\omega_k \Delta\omega_l] &= \frac{\sigma^2}{4} \left[\left(\overrightarrow{D}_l^H \overrightarrow{D}_k \right) \left(\overrightarrow{C}_k^H \overrightarrow{C}_l \right) + \left(\overrightarrow{D}_k^H \overrightarrow{D}_l \right) \left(\overrightarrow{C}_l^H \overrightarrow{C}_k \right) \right] \\ &= \frac{\sigma^2}{2} \operatorname{Re} \left(\left(\overrightarrow{D}_l^H \overrightarrow{D}_k \right) \left(\overrightarrow{C}_k^H \overrightarrow{C}_l \right) \right) \end{aligned} \tag{2.43}$$

where $\operatorname{Re}(z)$ is the real part of complex variable z. For the case $k = l$, note that (2.43) becomes the variance of $\Delta\omega_k$ as in (2.37). The matrix holding $E[\Delta\omega_k \Delta\omega_l], 1 \leq k, l \leq K$ in (2.43) defines the first-order approximation of the covariance matrix of the joint distribution of $\{\Delta\omega_k\}_k$.

2.4 Noise Averaging

We derive an upper bound on the variance of $\Delta\omega_k$ in (2.37). Using (2.35),

$$\overrightarrow{D}_k^H \overrightarrow{D}_k = \left| \Sigma_s^{-1} U_\parallel^H \overrightarrow{w}_k \right|_2^2 = \sum_{k'=1}^{K} \frac{1}{\sigma_{k'}^2} \left| \overrightarrow{U}_{\parallel k'}^H \overrightarrow{w}_k \right|_2^2 \tag{2.44}$$

where $|v|_2$ is the $\mathcal{L}_2$ norm of vector (or scalar) v, set $\{\sigma_k\}_k$ is the set of K non-zero singular values of X along the diagonals of Σ_s, and $\overrightarrow{U_{\|}}_k$ is the k^{th} column of $U_{\|}$. By Cauchy-Schwarz inequality, we obtain

$$\overrightarrow{D}_k^H \overrightarrow{D}_k \leq \sum_{k'=1}^{K} \frac{1}{\sigma_{k'}^2} \left| \overrightarrow{U_{\|}}_{k'} \right|_2^2 |\overrightarrow{w}_k|_2^2 = N \left(\sum_{k'=1}^{K} \frac{1}{\sigma_{k'}^2} \right) \tag{2.45}$$

where the columns of $U_{\|}$ have unit norm, and $|\overrightarrow{w}_k|_2^2 = N$ using (2.22).

Moreover, (2.34) implies

$$(\overrightarrow{C}_k^H \overrightarrow{C}_k)^{-1} = \left| U_{\perp}^H \overrightarrow{w}_k^{(1)} \right|_2^2 = \left| U_{\perp}^H \overrightarrow{u}_{\overrightarrow{w}_k^{(1)}} \right|_2^2 \left| \overrightarrow{w}_k^{(1)} \right|_2^2 \tag{2.46}$$

where $\overrightarrow{u}_{\overrightarrow{w}_k^{(1)}}$ is a unit vector in the direction of $\overrightarrow{w}_k^{(1)}$. Using (2.24),

$$\left| \overrightarrow{w}_k^{(1)} \right|_2^2 = 1 + 2^2 + \cdots + (N-1)^2 = \frac{(N-1)^3}{3} + \frac{(N-1)^2}{2} + \frac{(N-1)}{6} \tag{2.47}$$

(2.46) becomes

$$(\overrightarrow{C}_k^H \overrightarrow{C}_k)^{-1} \geq \left| U_{\perp}^H \overrightarrow{u}_{\overrightarrow{w}_k^{(1)}} \right|_2^2 \frac{(N-1)^3}{3} = p_{N,k} \frac{(N-1)^3}{3} \tag{2.48}$$

We now prove by contradiction that $p_{N,k}$ is strictly positive. Assume $p_{N,k} = 0$. By definition of $p_{N,k}$ and since spaces $U_{\perp}$ and $U_{\|}$ are orthogonal, $\overrightarrow{w}_k^{(1)}$ has to be spanned by the columns of $U_{\|}$. Let vector $\overrightarrow{v}$ hold the first K entries of

$\overrightarrow{w}_k^{(1)}$ and matrix M hold the first K rows of $U_{\|}$. M is a $K \times K$ Vandermonde matrix and is full rank. We therefore have

$$U_{\|} \times \left(M^{-1}\overrightarrow{v}\right) = \overrightarrow{w}_k^{(1)} \tag{2.49}$$

Denote by $\overrightarrow{u}_{\|,n}^H$ the n^{th} row of $U_{\|}$ and $\overrightarrow{w}_k^{(1)}[N]$ the N^{th} entry of $\overrightarrow{w}_k^{(1)}$. From (2.49),

$$\left|\overrightarrow{w}_k^{(1)}[N]\right|_2 = \left|\overrightarrow{u}_{\|,N}^H \times \left(M^{-1}\overrightarrow{v}\right)\right|_2 \leq K \times \left|M^{-1}\overrightarrow{v}\right|_2 \tag{2.50}$$

The inequality in (2.50) follows from Cauchy-Schwarz relation and the fact that all entries of $U_{\|}$ have norm less than unity since the columns of $U_{\|}$ are orthonormal. From (2.24), the left hand side of (2.50) is unbounded as N grows, while the right hand side of (2.50) is independent of N. This is a contradiction. Therefore, $p_{N,k}$ in (2.48) is strictly positive. For a fixed number of transmitters K we lower-bound $p_{N,k}$ by a positive constant. Combining (2.37), (2.45) and (2.48), we obtain an upper limit on the variance of angular shift $\Delta\omega_k$ that drops for higher signal powers $\{\sigma_{k'}\}_{k'}$ relative to the noise power σ^2. It also decays quadratically in the number of observed packets N.

2.5 Numerical Experiments

Consider a network of $\tilde{K} = 32$ transmitters and one receiver. Consider a CRI in which only $K = 5$ transmitters are active. The $\tilde{K}$ transmitters are

assigned equally-spaced complex exponentials $\{r_{\tilde{k}}\}_{\tilde{k}=1}^{\tilde{K}}$ between 0 and π, and the K transmitters are randomly selected. Each packet is of length $P = 1000$ symbols, and each symbol is -1 or 1 (no fading). S is thus 5×1000. We vary σ^2 in (2.27) on a log-scale for an SNR range between -20 dB and 20 dB, where the SNR is defined as $\text{SNR} = 10\log_{10}(1/\sigma^2)$. The simulation is run 500 times and we compute mean statistics.

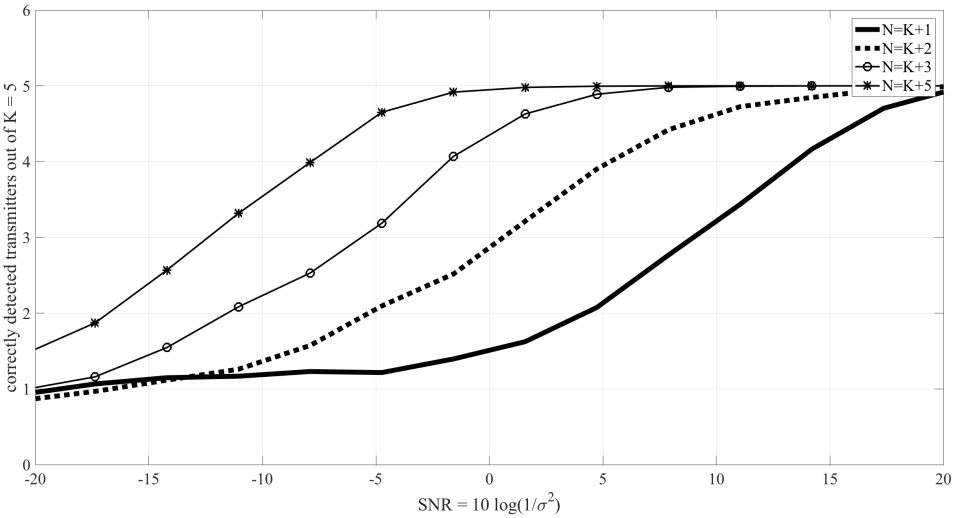

Figure 2.2: Variation of the number of correctly detected transmitters out of $K = 5$ versus $SNR = 10\log_{10}(1/\sigma^2)$ for $N - K = 1, 2, 3$ and 5.

In figure 2.2 we check the number of correctly detected transmitters out of K within the superset of $\tilde{K}$ transmitters. Here we assume that the receiver correctly detects K using the rank test in Section 2.2.2. The number of correctly identified active transmitters is checked versus the SNR and the number of stacked packets N in Y_N, where $N - K \in \{1, 2, 3, \text{ and } 5\}$. As expected,

the number of correctly identified transmitters increases with the SNR. It also increases with N as the receiver acquires a more accurate representation of the noise subspace $U_\perp$. It should be noted that minimum SNR and N values for correct identification of all active transmitters depend on the collision multiplicity K.

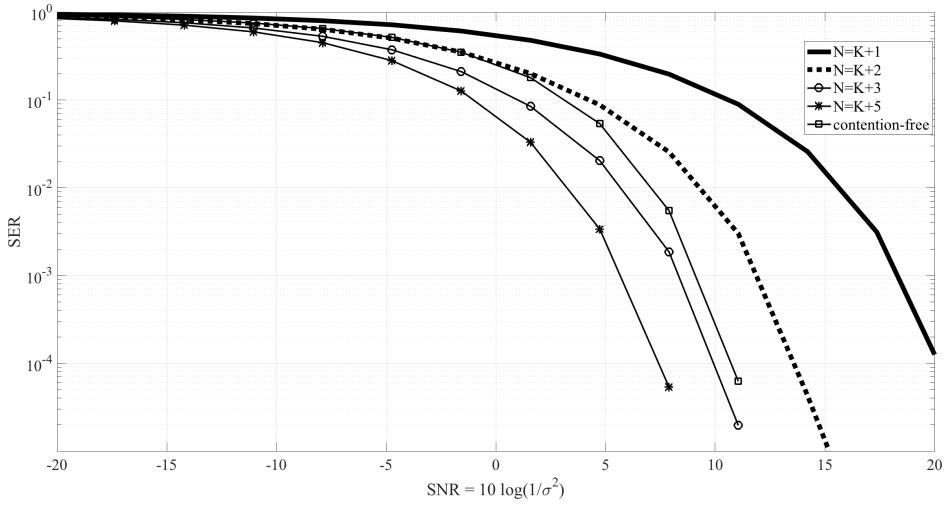

Figure 2.3: Variation of symbol error rate (SER) versus $SNR = 10\log_{10}(1/\sigma^2)$ for $N - K = 1, 2, 3$ and 5.

We also check the symbol error rate (SER) of the decoded packets assuming all K active transmitters are correctly identified by the receiver. Figure 2.3 shows that the SER drops for larger SNR and N values. For the sake of reference, we also plot the SER-versus-SNR curve for a contention-free channel (as in TDMA). In the latter case, $K = 5$ packets are sent to the receiver in 5 consecutive time slots. Better performance is obtained with root-MUSIC and

sufficient noise-averaging (large N) in the case of a collision at the cost of a longer CRI.

We now verify the theoretical results of Section 2.3 for the individual and joint distributions of the angular perturbations $\{\Delta\omega_k\}_k$. We also verify the noise-averaging effect of Section 2.4. Consider two simultaneously active transmitters 1 and 2 of respective characteristic complex exponentials r_1 and r_2 where $\omega_1 = \angle r_1 = \pi/4$ and $\omega_2 = \angle r_2 = 3\pi/4$. Packets $\overrightarrow{s}_1$ and $\overrightarrow{s}_2$ consist of a real random sequence of ± 1s and of length $P = 1000$. The experiment is repeated 1000 times and mean-statistics are computed.

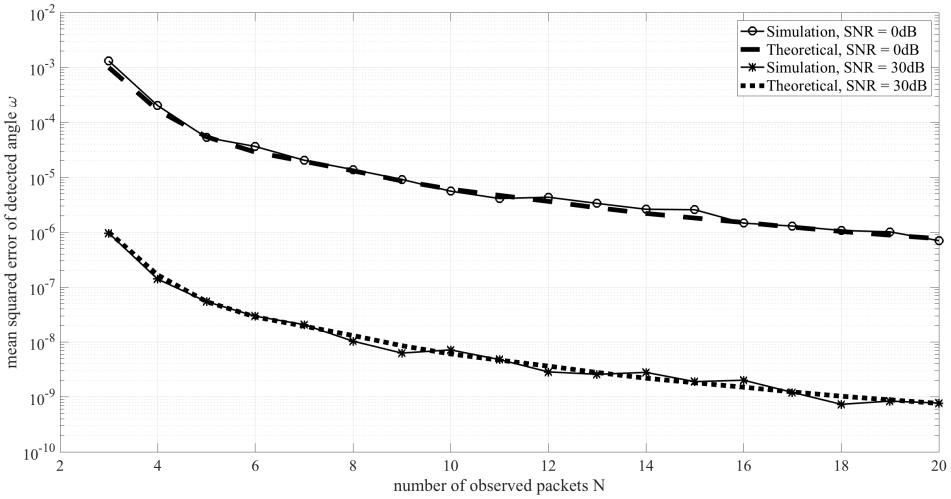

Figure 2.4: Theoretical and numerical results of the mean squared error $E[\Delta\omega_1^2]$ versus the number of received packets N for two SNR conditions: SNR = 0dB and SNR = 30dB. $K = 2$, $\omega_1 = \pi/4$, $\omega_2 = 3\pi/4$.

In figure 2.4 we plot the MSE for estimating ω_1 versus N for two SNR conditions. As expected, the MSE decays for larger values of N (noise-averaging effect) and higher SNR. Moreover, we compute the theoretical curves using (2.37). The matching between the theoretical and simulation curves indicates that the first-order perturbation analysis is accurate for predicting the statistics of $\Delta\omega_k$.

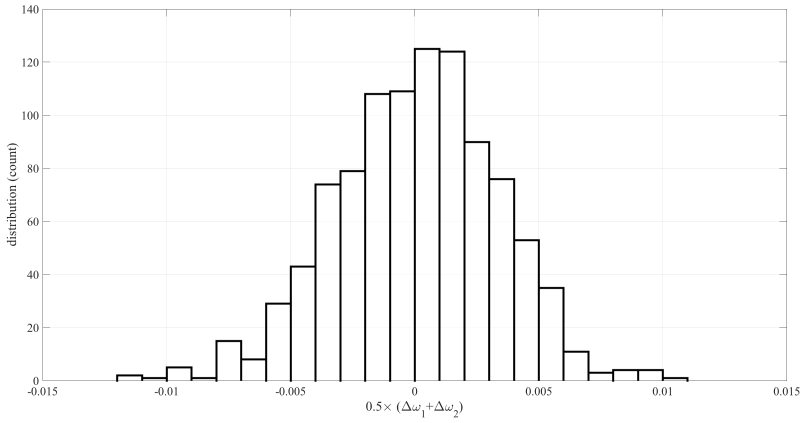

Figure 2.5: Distribution of $(\Delta\omega_1 + \Delta\omega_2)/2$ for $K = 2$, $N = 7$, SNR = 0dB, $\omega_1 = \pi/4$, $\omega_2 = 3\pi/4$.

Moreover, figure 2.5 shows a histogram of the average of the two angular shifts $\Delta\omega_1$ and $\Delta\omega_2$. The plot fairly has a Gaussian bell shape. This is expected for a weighted sum of jointly Gaussian random variables as we derived in Section 2.3.4. In addition, for the plot in figure 2.5, the simulated MSE is 1.0679e-05. By computing the covariance matrix of $\Delta\omega_1$ and $\Delta\omega_2$ using (2.43), the theoretical MSE is given by

$$E\left[\left(\frac{\Delta\omega_1+\Delta\omega_2}{2}\right)^2\right] = \begin{pmatrix}0.5 & 0.5\end{pmatrix} \times \mathrm{Cov}\begin{pmatrix}\Delta\omega_1\\ \Delta\omega_2\end{pmatrix} \times \begin{pmatrix}0.5\\ 0.5\end{pmatrix} = 1.1871\text{e-}05 \tag{2.51}$$

which is of the same order as the simulated MSE.

2.6 Conclusion

A root-MUSIC-like BNDMA scheme for collision resolution is presented for synchronized transmissions and a block-fading channel. The algorithm achieves high asymptotic throughput, and its decoding complexity depends on the number of collided packets. Analytical results on the performance of the algorithm under various SNR conditions and noise-averaging are derived and verified in simulations.

Chapter 3

Non-Blocking Scheme for Blind Network-Assisted Diversity Multiple Access in Synchronous Channels

We design a root-MUSIC method for resolving packet collisions in synchronous packet-switched networks using Blind Network-Assisted Diversity Multiple Access (BNDMA). As opposed to typical BNDMA schemes, the method operates in non-blocking mode. Idle transmitters at the start of a collision resolution interval may join the set of active transmitters and contact the receiver before the end of the interval. A naive queueing analysis of the proposed scheme is exponentially complex in the size of the network. We carry out a computationally efficient analysis of the network throughput and queueing delay. We show that the suggested scheme reduces the queueing delay of the buffered packets at the transmitters without sacrificing the maximum throughput achieved by standard BNDMA. Further insights are derived from the numerical experiments.

Throughput analysis of (B)NDMA in the synchronous blocking mode can be

found in [1, 94–96]. In [94] the BNDMA scheme is also generalized to allow transmitters with higher data rates to send more than one packet within a single collision resolution interval (CRI). Analysis for an adaptive version of NDMA is presented in [97]. The receiver updates its statistics (false alarm and detection probabilities) based on previously resolved collisions and embedded queueing state information in order to improve the detection of the active transmitters and prioritize the channel access of heavily loaded users.

This chapter is organized as follows. In the next section we present our root-MUSIC BNDMA scheme for resolving collisions. In Section 3.2 we derive the probability distribution of the CRI length which depends on the number of involved transmitters within a collision and consequently the data arrival rate at each transmitter. While a naive computation of the probability distribution is exponentially complex in the network size, we carry out the derivation in polynomial-order complexity. The derived probability distribution is then used in Section 3.3 for the queueing analysis. We characterize both the network throughput and the queueing delay under the proposed scheme. Section 3.4 holds numerical results, and Section 3.5 concludes the chapter.

3.1 Root-MUSIC-Like Collision Resolution Algorithm

A network comprises $\tilde{K}$ transmitters and one receiver, all with single antennas. The network is packet-switched, and a packet has P symbols ($P >$

$\tilde{K}$) and extends over one time slot. Thus, 1 slot = $P \times \tau$, where τ is one symbol duration. Each transmitter k is assigned a unique complex exponential r_k that is known to the receiver. Without loss of generality, transmitter k sends at most one (raw) packet $\overrightarrow{s}_k$ within a CRI. Upon collision, retransmissions are necessary. In its n^{th} transmission of packet $\overrightarrow{s}_k$, transmitter k issues packet $r_k^{(n-1)}\overrightarrow{s}_k$. A transmitter that is idle upon the start of a CRI may still join the set of active transmitters during the CRI. At the end of the CRI, K packets corresponding to K active transmitters are decoded by the receiver, where $1 \leq K \leq \tilde{K}$. The count and identities of the active transmitters during a CRI are unknown to the receiver beforehand. We assume the transmissions are synchronized, so a packet fits within the slot boundaries. Moreover, we assume fading along each channel between a transmitter and the receiver is constant over a CRI. For ease of notation, we subsume the fading into packets $\{\overrightarrow{s}_k\}_{k=1}^{K}$. Once these packets are decoded, fading is removed using single channel (collision-free) methods. We first illustrate the transmission scheme. Then we describe how the receiver detects the number and identities of the active transmitters and decodes the collided packets.

3.1.1 Transmission Scheme

As in [1], transmitter k scales its n^{th} transmission of packet $\overrightarrow{s}_k$ by $r_k^{(n-1)}$. The main difference is that transmitter k that is idle at the start of a CRI ($t = 0$) might still issue its first packet $\overrightarrow{s}_k$ during slot n_k of the CRI (assum-

ing the latter has not ended yet) and thus $\overrightarrow{s}_k$ is received at $t = (n_k - 1)P\tau$, $n_k \in \mathcal{Z}^+$. For the purpose of clarity, we illustrate the transmission scheme for a specific communication scenario in figure 3.1. However, the expression of the collected mixture(s) of packets is presented afterwards for the general case.

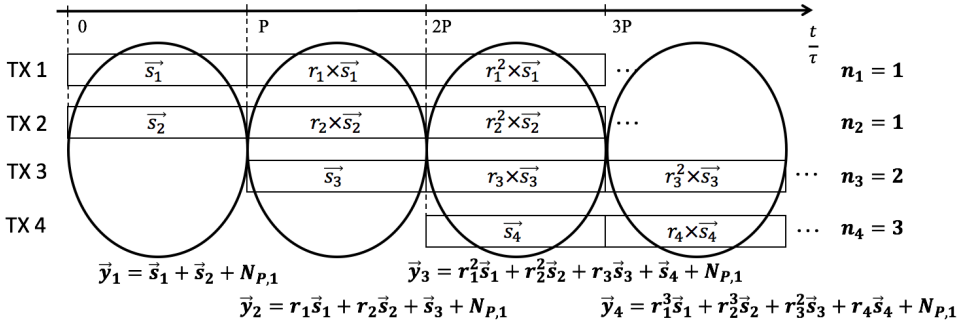

Figure 3.1: Transmission scheme of $K = 4$ transmitters.

Transmitters 1 and 2 initially send their unweighted packets. At $t = 0$, the receiver collects $\overrightarrow{y}_1 = \overrightarrow{s}_1 + \overrightarrow{s}_2 + \mathcal{N}_{P,1}$. Due to collision, the receiver is unable to decode packets $\overrightarrow{s}_1$ and $\overrightarrow{s}_2$. Transmitters 1 and 2 then send packets $r_1\overrightarrow{s}_1$ and $r_2\overrightarrow{s}_2$ respectively. In addition, transmitter 3 joins the set of active transmitters. Since this is the first time transmitter 3 sends its packet, transmitter 3 sends $\overrightarrow{s}_3$. The receiver collects at $t = P\tau$ packet $\overrightarrow{y}_2 = r_1\overrightarrow{s}_1 + r_2\overrightarrow{s}_2 + \overrightarrow{s}_3 + \mathcal{N}_{P,1}$. In the next time slot, transmitter 4 joins the active set. At $t = 2P\tau$ the receiver collects $\overrightarrow{y}_3 = r_1^2\overrightarrow{s}_1 + r_2^2\overrightarrow{s}_2 + r_3\overrightarrow{s}_3 + \overrightarrow{s}_4$. Notice that all transmitters follow the same transmission algorithm independent of the time they join the active set. No more transmitters get involved

in the scenario of figure 3.1. By the time the receiver manages to decode the packets, only 4 transmitters are active, i.e. $K = 4$.

3.1.2 Detection of K

At the end of each time slot n, the receiver stacks the n already collected vectors $\{\overrightarrow{y}_1, \overrightarrow{y}_2, \ldots, \overrightarrow{y}_n\}$ horizontally into matrix Y_n. A general expression for Y_n is given by

$$\begin{aligned} Y_n &= \begin{pmatrix} \overrightarrow{y}_1 & \overrightarrow{y}_2 & \ldots & \overrightarrow{y}_n \end{pmatrix}^T \\ &= \begin{pmatrix} \overrightarrow{w}_{1,n}^{(n_1-1)} & \overrightarrow{w}_{2,n}^{(n_2-1)} & \ldots & \overrightarrow{w}_{K,n}^{(n_K-1)} \end{pmatrix} \times \begin{pmatrix} \overrightarrow{s}_1^T \\ \overrightarrow{s}_2^T \\ \vdots \\ \overrightarrow{s}_K^T \end{pmatrix} + \mathcal{N}_{n,P} \\ &= W_n \times S + \mathcal{N}_{n,P} \end{aligned} \tag{3.1}$$

In (3.1), n_k refers to the slot index in which transmitter k joins the set of active transmitters in a given communication scenario, i.e. packet of transmitter k is received for the first time at $t = (n_k - 1)P\tau$. In the example of figure 3.1, $n_1 = n_2 = 1$, $n_3 = 2$ and $n_4 = 3$. Moreover, $\overrightarrow{w}_{k,n}^{(n_k-1)}$ is a shifted version of the coding vector $\overrightarrow{w}_{k,n}$ of transmitter k defined as follows

$$\overrightarrow{w}_{k,n}^{(n_k-1)} = \Big[\underbrace{0, \ldots, 0}_{(n_k-1) \text{ zeros}}, r_k^0, r_k^1, \ldots, r_k^{n-n_k} \Big]^T \tag{3.2}$$

Notice that (3.1) is a general expression for Y_n that applies to all values of n

even if not all K transmitters have yet joined the active set. It also applies to an arbitrary value of K. The matrix of shifted coding vectors in (3.1) is denoted as W_n. In the special case where $n_k = 1$ for $1 \leq k \leq K$, W_n becomes a Vandermonde matrix and Y_n in (3.1) admits the same structure as [1]. In the latter case, (3.1) resembles the response of a linear antenna array of N sensors on which a mixture of K signals impinge at angles of arrival equal to the arguments of the complex exponentials $\{r_k\}_{k=1}^{K}$.

The receiver builds matrix Y_n and checks its true (noiseless) rank at the end of every slot n assuming high SNR. Since matrix S in (3.1) holds random packets as its rows, it is full rank. Thus, the rank of Y_n is the same as that of W_n. Referring to Appendix A.1, rank(W_n) grows to K and saturates at K for $n \geq \max(K, n_1, \ldots, n_K)$. Therefore, the receiver detects K by iteratively collecting packets $\{\overrightarrow{y}_n\}_n$ and checking the rank of constructed matrix Y_n over index n. K is then the saturating value of rank(Y_n) for n large enough. Note that saturation is only detected when at least $n = K+1$ packets are collected. Thus, K packets are decoded by the proposed algorithm within at least $K+1$ slots whenever K is unknown beforehand. At stopping time $n = m > K$, the received matrix is

$$Y_m = W_m \times S + \mathcal{N}_{m,P} \tag{3.3}$$

3.1.3 Identification of the K Transmitters

Since $m > K$ and W_m is full rank, W_m admits a non-trivial left null space of dimension $m - K$. Moreover, from (3.3), Y_m and W_m have the same left null space at high SNR. Therefore, the receiver computes the left null space of W_m by computing that of Y_m. Let $U_\perp$ be the matrix whose columns define the basis of the left null space of Y_m. $U_\perp$ may be easily computed from the singular value decomposition (SVD) of Y_m as the $m - K$ left singular vectors corresponding to the noise-only singular values of Y_m. Consider the system of $m - 1$ equations

$$\overrightarrow{w'}_m^{(n-1)^H} \times U_\perp U_\perp^H \times \overrightarrow{w'}_m^{(n-1)} = 0, \quad 1 \leq n \leq m-1 \tag{3.4}$$

where $\overrightarrow{w'}_m^{(n-1)} = \big[\underbrace{0, \ldots, 0}_{(n-1) \text{ zeros}}, 1, z^1, \ldots, z^{m-n}\big]^T$. Since $U_\perp$ defines the left null space of W_m, and by inspecting the columns of W_m in (3.1), note that characteristic complex exponential r_k of transmitter k is a solution of equation $n = n_k$ of set (3.4). Therefore, the receiver identifies the K active transmitters by solving the set of equations (3.4) and selecting the K complex solutions that are closest to the unit circle and the individual elements of set $\{r_{\tilde{k}}\}_{\tilde{k}=1}^{\tilde{K}}$. In addition to obtaining the k^{th} solution r_k, the receiver also recovers shift $n_k - 1$ based on the index of the corresponding generating equation in set (3.4). In the special case where $n_k = 1$ for $1 \leq k \leq K$ (this in enforced in the transmission scheme of [1]), the receiver needs to solve only the first equation of (3.4).

This is similar to the root-MUSIC method for DoA estimation.

3.1.4 Decoding of the K Packets

Having obtained $\{r_k\}_{k=1}^{K}$ and $\{(n_k-1)\}_{k=1}^{K}$, the receiver constructs matrix W_m according to (3.1). From (3.3), the receiver decodes the matrix of raw packets S as

$$\hat{S} = ((W_m)^H W_m)^{-1} (W_m)^H Y_m \tag{3.5}$$

Referring to Appendix A.1, $((W_m)^H W_m)^{-1}$ exists almost surely. Note that the ordering of the columns of W_m is unimportant, since a shuffling of the columns of W_m simply yields an analogous shuffling of the rows of S.

3.2 Probability Distribution of the Collision Resolution Interval Length

We do throughput and delay analysis for the collision resolution algorithm of Section 3.1. Consider a network of $\tilde{K}$ transmitters. Each transmitter may send only one packet per CRI according to the transmission scheme of Section 3.1.1. New packets that become available within a CRI at an already involved transmitter are buffered in an infinitely long queue at the transmitter, so no packets are dropped. We examine the network in the steady state.

We do not consider the transient state during the network startup phase, but we show when the network converges to the steady state. Packets of data are assumed to arrive at each transmitter according to a Poisson distribution of mean λ packets/slot. By definition, once the network reaches steady state, the number of queued packets at a transmitter admits a steady state distribution. Moreover, there exists a unique probability p_e that a transmitter queue is empty at the start of each CRI in the steady state. This probability is traffic-dependent, and is common to all transmitters in the symmetric case (same λ).

We carry out the throughput and delay analysis at two levels. In this section we take a network-level perspective. We assume there exists a unique stationary probability p_e, and we derive the probability distribution of the CRI length m for an arbitrary network size $\tilde{K}$ and rate λ. This distribution will be function of unknown parameter p_e. In the next section, we take a single-node perspective and examine the probability generating function (PGF) of the number of queued packets at a transmitter given the derived distribution of the CRI length m within the network. We combine the two perspectives and show when the queues of the network transmitters converge to steady state, as well as how to compute p_e in the latter case. This completes the description of the distribution of the CRI length m and the PGF of the number of buffered packets at a transmitter. We then evaluate the throughput and delay of the network under the proposed collision resolution scheme.

For the purpose of computing the distribution of the CRI length in this section, we follow the following outline. In Section 3.2.1, we introduce the notion of collision trees. A collision tree $\mathcal{T}_K$ shows all possible collision patterns that yield the same CRI length $m = K + 1$. We compute the probability of such a CRI length by summing the probabilities of all collision patterns within the tree. Unfortunately, we show that the number of collision patterns in a collision tree $\mathcal{T}_K$ grows exponentially with the number of active transmitters K. Thus, a brute-force approach to compute the distribution of the CRI length becomes infeasible for large networks. This motivates Section 3.2.2 in which we present a polynomial-time recursive solution to compute the distribution of the CRI length. We again use the notion of collision trees $\mathcal{T}_K$, but this time we introduce the concept of first-level and second-level partitions of $\mathcal{T}_K$. We show that the probabilities associated to a second level partition of a collision tree $\mathcal{T}_K$ may be expressed as function of the probabilities associated to the first-level partitions of collision tree $\mathcal{T}_{K-1}$. This establishes the recursion over the number of active transmitters K and allows us to compute the probability of a particular CRI length m in polynomial time.

3.2.1 Brute-force Approach to Compute $P(m)$ in Exponential Time

For a network size $\tilde{K}$, the number of active transmitters within a CRI is $0 \leq K \leq \tilde{K}$. Assume the SNR is high enough so that K packets may be

decoded within $K+1$ slots. The extension of the throughput analysis to the general case $K+w, w \geq 1$ is straightforward. Therefore, given $\tilde{K}$, the CRI length m is bounded as $1 \leq m \leq \tilde{K}+1$. The lower equality corresponds to the case when the buffers of all the $\tilde{K}$ transmitters are empty at the start of a CRI. The higher equality corresponds to the case when all $\tilde{K}$ transmitters are involved in the CRI. As opposed to [1], the probability mass function $P(m)$ admits no closed form. This is because an inactive transmitter may join a CRI upon a new packet arrival without waiting for the current CRI termination, so two CRIs of the same length m may occur for different collision patterns.

Suppose at time instant t_0 a CRI has just ended and consider an arbitrary transmitter TX. The probability that TX has an empty buffer at t_0 is p_e, and new packets arrive at TX according to a Poisson distribution of rate λ. Therefore, the probability that TX is inactive for the next $(i-1)$ slots relative to instant t and then issues a packet at the i^{th} time slot is given by

$$p_i = \begin{cases} 1-p_e, & i=1 \\ p_e e^{-(i-2)\lambda}(1-e^{-\lambda}), & i \geq 2 \end{cases} \tag{3.6}$$

Consider a selection of $\tilde{K}-K$ transmitters. Define q_K as the probability that this particular selection is inactive at least for the next $K+1$ time slots relative to t_0. Then,

$$q_K = [p_e e^{-K\lambda}]^{(\tilde{K}-K)}, 0 \leq K \leq \tilde{K} \tag{3.7}$$

Define

$$\binom{a}{a_1, a_2, \ldots, a_j} = \frac{a!}{a_1! a_2! \ldots a_j!} \tag{3.8}$$

for natural numbers a, $a_1, a_2, \ldots, a_j$, $j \geq 1$ such that $a_1 + a_2 + \ldots a_j = a$ and $a!$ denotes the factorial of a.

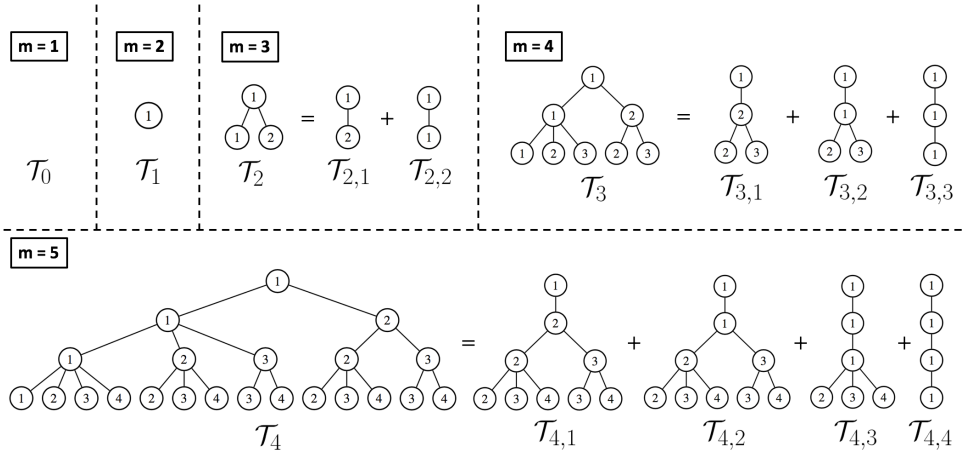

Figure 3.2: All collision scenarios in a network of $\tilde{K} = 4$ transmitters. Collision resolution interval (CRI) length m is measured in slots.

In a network of $\tilde{K}$ transmitters, a CRI of length $m = 1$ starts at instant t_0 if all $\tilde{K}$ transmitters have empty buffers. The collision pattern for $m = 1$ may be represented by an empty collision tree $\mathcal{T}_0$ as shown in figure 3.2. This happens with probability

$$P(\mathcal{T}_0) = \binom{\tilde{K}}{0, \tilde{K} - 0} q_0 \tag{3.9}$$

A CRI of length $m = 2$ starts at t_0 if only one of the $\tilde{K}$ transmitters has a non-empty buffer at $t = 0$, and no packets arrive at any of the other transmitters for the next $m-1 = 1$ slot. The collision pattern for $m = 2$ may be represented by a single-node collision tree $\mathcal{T}_1$ in figure 3.2 of height unity corresponding to a single active transmitter. The value in the node is the index of the slot relative to t_0 during which the active transmitter issues its first packet. A CRI of $m = 2$ occurs with probability

$$P(\mathcal{T}_1) = \binom{\tilde{K}}{1, \tilde{K}-1} q_1 \left[\binom{1}{1} p_1 \right] \tag{3.10}$$

A CRI of length $m = 3$ starts at t_0 in two scenarios: two transmitters have non-empty buffers at t_0, or one transmitter has a non-empty buffer at t_0 and one or more packets arrive at another transmitter during the time slot that starts at t_0. In both scenarios all other transmitters have empty buffers up to at least $m-1 = 2$ slots following t_0. The two collision patterns for $m = 3$ may be represented by collision tree $\mathcal{T}_2$ in figure 3.2 of height two (corresponding to two active transmitters) and two paths from the root to the leaves. The left path describes the first scenario. The right path describes the second scenario. The values inside the nodes indicate the relative slot indices during which the active transmitters issue their first packet transmissions. A CRI of $m = 3$ occurs with probability

$$P(\mathcal{T}_2) = \binom{\tilde{K}}{2, \tilde{K}-2} q_2 \left[\binom{2}{2, 0} p_1^2 + \binom{2}{1, 1} p_1 p_2 \right] \tag{3.11}$$

Collision tree $\mathcal{T}_3$ in figure 3.2 illustrates the five possible scenarios so that a CRI of length $m = 4$ starts at t_0. These scenarios are represented by the five distinct paths from the root of $\mathcal{T}_3$ to its leaves. An easy way to generate $\mathcal{T}_3$ is to consider an ordered set of three active transmitters $\{\mathrm{TX}_\alpha, \mathrm{TX}_\beta, \mathrm{TX}_\gamma\}$ and assume all other transmitters are inactive. The ordering of the active set is based on the transmission time of the first packet of each transmitter. TX_α should be active in the first time slot after t_0 or otherwise a CRI of $m = 1$ will occur. This generates the topmost level of $\mathcal{T}_3$. Given TX_α is active in slot $i_1 = 1$, TX_β should become active in either slots 1 or 2 following t_0 or otherwise a CRI of $m = 2$ will occur. This generates the second level of $\mathcal{T}_3$. Given that TX_α and TX_β are active in the respective slots $i_1 = 1$ and $i_2, i_1 \leq i_2 \leq 2$, TX_γ should become active in slot $i_3, i_2 \leq i_3 \leq 3$ or otherwise a CRI of $m = 3$ will occur. This generates the third level of $\mathcal{T}_3$. A CRI of $m = 4$ then occurs with probability

$$\begin{aligned} P(\mathcal{T}_3) = \binom{\tilde{K}}{3, \tilde{K}-3} q_3 \Bigg[\binom{3}{3,0,0} p_1^3 + \binom{3}{2,1,0} p_1^2 p_2 \\ + \binom{3}{2,0,1} p_1^2 p_3 + \binom{3}{1,2,0} p_1 p_2^2 + \binom{3}{1,1,1} p_1 p_2 p_3 \Bigg] \end{aligned} \tag{3.12}$$

It is now straightforward to give a general expression for the probability of a CRI of arbitrary length m. Inspecting equations (3.9), (3.10), (3.11) and (3.12), note the following:

- The binomial term outside the brackets counts the possible splits of the $\tilde{K}$ transmitters given that K transmitters are active.

- The q_K term ensures that the $\tilde{K} - K$ transmitters are actually inactive.
- Each term inside the brackets corresponds to a collision pattern or equivalently a path from the root to a leaf of collision tree $\mathcal{T}_K$.
- Each product of p_k's inside the brackets computes the probability of one collision pattern given an ordered selection of K active transmitters.
- The multinomial terms inside the brackets count the number of such orderings while splitting the set of K transmitters over the CRI slots.

The probability that a CRI of length $m = K+1$ slots starts at t_0 is then given by

$$\begin{aligned} p(\mathcal{T}_K) &= \binom{\tilde{K}}{K, \tilde{K}-K} q_K \times \left[\sum_{\pi_K \in \mathcal{T}_K} \binom{K}{c_1, c_2, \ldots, c_K} p_1^{c_1} p_2^{c_2} \ldots p_K^{c_K} \right] \\ &= \binom{\tilde{K}}{K, \tilde{K}-K} q_K \left[\sum_{\pi_K \in \mathcal{T}_K} p(\pi_K) \right] \end{aligned} \tag{3.13}$$

where

$$\pi_K = (i_1, i_2, \ldots, i_K) \in \mathcal{T}_K \quad \text{iff} \quad \begin{cases} i_1 = 1 \\ i_1 \leq i_2 \leq 2 \\ \vdots \\ i_{K-1} \leq i_K \leq K \end{cases} \tag{3.14}$$

$$c_l = \sum_{k=1}^{K} \mathbf{1}\{i_k == l\}, \quad 1 \leq l \leq K \tag{3.15}$$

and p_k, q_K and the multinomial terms in (3.13) are defined in (3.6), (3.7) and (3.8) respectively. $\mathbf{1}\{\cdot\}$ in (3.15) is the indicator function.

(3.13) admits no closed form. Figure 3.2 shows all possible collision trees $\mathcal{T}_K$ for a network of size $\tilde{K} = 4$. The number of paths in (3.14) is equal to the number of leaves of $\mathcal{T}_K$. The latter is lower-bounded by the number of leaves of a full binary tree of height K. Therefore, the number of collision patterns considered when computing $P(m = K + 1)$ in (3.13) grows exponentially in K.

3.2.2 Recursive Approach to Compute $P(m)$ in Polynomial Time

We now derive a recursive solution to compute $P(m)$ in (3.13). It is useful to define the following normalization

$$\tilde{p}(\mathcal{T}_K) = \frac{p(\mathcal{T}_K)}{\binom{\tilde{K}}{K,\tilde{K}-K} q_K} \tag{3.16}$$

We first compute $\tilde{p}(\mathcal{T}_K)$ recursively and then use (3.16) to recover $p(\mathcal{T}_K)$. $\mathcal{T}_K$ represents the set of all paths as defined in (3.14). We introduce the following partition of $\mathcal{T}_K$:

$$\mathcal{T}_{K,k} = \begin{cases} \{\pi_K | \pi_K \in \mathcal{T}_K, i_k = 1, i_{k+1} > 1\}, & 1 \leq k < K \\ \{(i_1 = 1, i_2 = 1, \ldots, i_K = 1)\}, & k = K \end{cases} \tag{3.17}$$

This is easily interpreted as splitting collision tree $\mathcal{T}_K$ at the nodes along its leftmost path. The partitions of trees $\mathcal{T}_2$, $\mathcal{T}_3$ and $\mathcal{T}_4$ are shown in figure 3.2. Notice that

$$\begin{cases} \mathcal{T}_{K,k} \cap \mathcal{T}_{K,k'} = \emptyset, 1 \leq k \neq k' \leq K \\ \bigcup_{k=1}^{K} \mathcal{T}_{K,k} = \mathcal{T}_K \end{cases} \tag{3.18}$$

so

$$\tilde{p}(\mathcal{T}_K) = \sum_{k=1}^{K} \tilde{p}(\mathcal{T}_{K,k}) = \sum_{k=1}^{K} \sum_{\pi_K \in \mathcal{T}_{K,k}} \tilde{p}(\pi_K) \tag{3.19}$$

where $\tilde{p}(\pi_K)$ follows from (3.13) and (3.16). By (3.19), $\tilde{p}(\mathcal{T}_K)$ may be computed from set $\{\tilde{p}(\mathcal{T}_{K,k})\}_k$. We now define a second-level partition of collision subtree $\mathcal{T}_{K,k}$:

$$\mathcal{T}_{K,k,l} = \begin{cases} \{\pi_K | \pi_K \in \mathcal{T}_{K,1}, i_{l+1} = 2, i_{l+2} > 2\}, & k = 1, 1 \leq l \leq K-2 \\ \{\pi_K | (i_1 = 1, i_2 = 2, \ldots, i_K = 2)\}, & k = 1, l = K-1 \\ \{\pi_K | \pi_K \in \mathcal{T}_{K,k}, i_{k+l-1} \leq 2, i_{k+l} > 2\}, & 1 < k \leq K-1, 1 \leq l \leq K-k \\ \{\pi_K | \pi_K \in \mathcal{T}_{K,k}, i_K = 2\}, & 1 < k \leq K-1, l = K-k+1 \\ \{\pi_K | (i_1 = 1, i_2 = 1, \ldots, i_K = 1)\}, & k = K, l = 1 \end{cases} \tag{3.20}$$

The partitions of $\mathcal{T}_{K,k}$ for $K = 4$ and $1 \leq k \leq K$ are shown in figure 3.3. Again

$$\tilde{p}(\mathcal{T}_{K,k}) = \sum_{l=1}^{\min(K-1,K-k+1)} \tilde{p}(\mathcal{T}_{K,k,l}) = \sum_{l=1}^{\min(K-1,K-k+1)} \sum_{\pi_K \in \mathcal{T}_{K,k,l}} \tilde{p}(\pi_K) \tag{3.21}$$

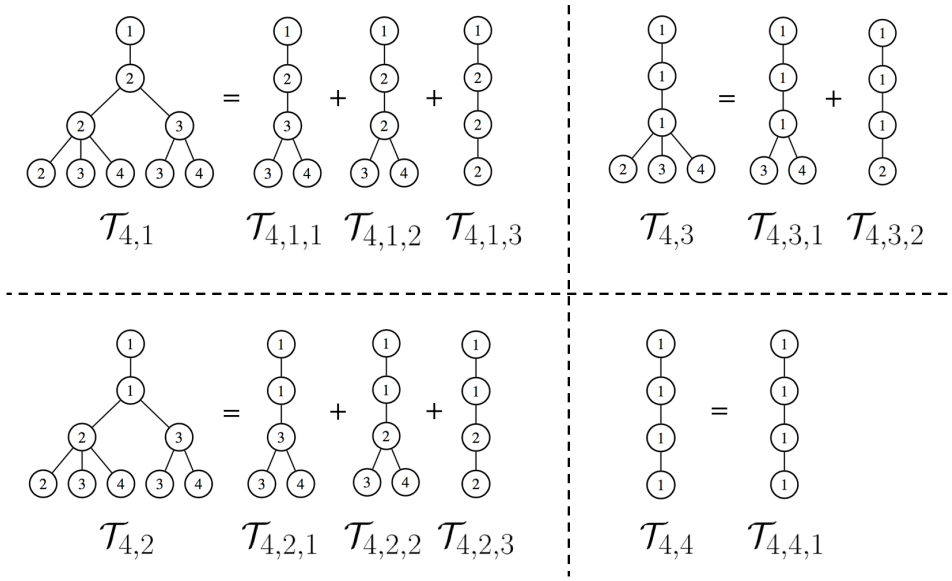

Figure 3.3: Subgrouping of collision patterns corresponding to a collision resolution interval (CRI) of length $m = 5$.

The significance of the partition in (3.20) follows from the theorem below:

Theorem: the number of paths from the root to a leaf in subtrees $\mathcal{T}_{K,k,l}$ and $\mathcal{T}_{K-1,l}$ is the same. Select the j^{th} path $\pi_K^{(j)}$ from $\mathcal{T}_{K,k,l}$ and its counterpart $\pi_{K-1}^{(j)}$ from $\mathcal{T}_{K-1,l}$, then the ratio of $\tilde{p}(\pi_K^{(j)})$ to $\tilde{p}(\pi_{K-1}^{(j)})$ is independent of j.

Corollary: $\tilde{p}(\mathcal{T}_{K,k}) = \sum_l \tilde{p}(\mathcal{T}_{K,k,l}) = \sum_l \sum_{\pi_K \in \mathcal{T}_{K,k,l}} \tilde{p}(\pi_K) = \sum_l \nu_l \sum_{\pi_{K-1} \in \mathcal{T}_{K-1,l}} \tilde{p}(\pi_{K-1}) = \sum_l \nu_l \tilde{p}(\mathcal{T}_{K-1,l})$. Thus, $\tilde{p}(\mathcal{T}_{K,k})$ may be computed recursively from $\{\tilde{p}(\mathcal{T}_{K-1,l})\}_l$.

In particular:

$$\tilde{p}(\mathcal{T}_{K,k}) = \begin{cases} Kp_1 \sum_{l=1}^{K-1} \binom{l}{0,l} \alpha^l \beta^{K-l-1} \tilde{p}(\mathcal{T}_{K-1,l}), & k = 1 \\ \frac{K}{k} p_1 \sum_{l=k-1}^{K-1} \binom{l}{k-1,l-k+1} \alpha^{l-k+1} \beta^{K-l-1} \tilde{p}(\mathcal{T}_{K-1,l}), & 1 < k \leq K \end{cases} \tag{3.22}$$

where

$$\begin{cases} \alpha = \frac{p_2}{p_1} \\ \beta = \frac{p_{i+1}}{p_i}, \quad i > 1 \end{cases} \tag{3.23}$$

and probabilities $\{p_i\}, i \geq 1$ are defined in (3.6).

The proofs of the theorem and the corollary follow from examining the structures of $\mathcal{T}_{K,k}$ and $\mathcal{T}_{K,k,l}$ defined in (3.14), (3.17) and (3.20). Then we directly substitute the expressions of $\{\tilde{p}(\pi_K)\}$ in (3.13) into those of $\tilde{p}(\mathcal{T}_{K,k})$ and $\tilde{p}(\mathcal{T}_{K,k,l})$ stated in (3.19) and (3.21) respectively. As an illustration, note that

$$\frac{\tilde{p}((1,2,3,4) \in \mathcal{T}_{4,1,1})}{\tilde{p}((1,2,3) \in \mathcal{T}_{3,1})} = \frac{\binom{4}{1,1,1,1} p_1 p_2 p_3 p_4}{\binom{3}{1,1,1} p_1 p_2 p_3} = 4p_4 = 4p_1 \alpha \beta^2 \tag{3.24}$$

$$\frac{\tilde{p}((1,2,3,3) \in \mathcal{T}_{4,1,1})}{\tilde{p}((1,2,2) \in \mathcal{T}_{3,1})} = \frac{\binom{4}{1,1,2,0} p_1 p_2 p_3^2}{\binom{3}{1,2,0} p_1 p_2^2} = 4p_3 \beta = 4p_1 \alpha \beta^2 \tag{3.25}$$

(3.24) and (3.25) imply

$$\tilde{p}(\mathcal{T}_{4,1,1}) = 4p_1 \alpha \beta^2 \tilde{p}(\mathcal{T}_{3,1}) \tag{3.26}$$

Similarly,

$$\tilde{p}(\mathcal{T}_{4,1,2}) = 4p_1\alpha^2\beta\tilde{p}(\mathcal{T}_{3,2}) \tag{3.27}$$

$$\tilde{p}(\mathcal{T}_{4,1,3}) = 4p_1\alpha^3\tilde{p}(\mathcal{T}_{3,3}) \tag{3.28}$$

so

$$\tilde{p}(\mathcal{T}_{4,1}) = 4p_1(\alpha\beta^2\tilde{p}(\mathcal{T}_{3,1}) + \alpha^2\beta\tilde{p}(\mathcal{T}_{3,2}) + \alpha^3\tilde{p}(\mathcal{T}_{3,3})) \tag{3.29}$$

which follows (3.22). The recursive solution to compute $P(m = K + 1) = P(\mathcal{T}_K)$ is summarized in Algorithm 1.

Algorithm 1

Input: $\{\tilde{p}(\mathcal{T}_{K-1,k})\}_{k=1}^{K-1}$
Output: $p(\mathcal{T}_K)$, $\{\tilde{p}(\mathcal{T}_{K,k})\}_{k=1}^{K-1}$
1: Compute $\{\tilde{p}(\mathcal{T}_{K,k})\}_{k=1}^{K-1}$ using (3.22)
2: Compute $\tilde{p}(\mathcal{T}_K)$ using (3.19)
3: Compute $p(\mathcal{T}_K)$ using (3.16)
Base case: (3.9), (3.10) and (3.11)

3.3 Queueing Analysis

Recall that t_0 denotes a time instant at which a CRI has just ended and a new CRI started. Let t_1 be the instant at which the new CRI ends. Denote

by B_0 and B_1 the number of packets buffered at a particular transmitter k^* at respective instants t_0 and t_1. Define the probability generating function (PGF) of a discrete non-negative random variable X as

$$G_X(z) = E[z^X] = \sum_{x=0}^{\infty} p_X(x) z^x, z \in \mathcal{C}, |z| \leq 1 \tag{3.30}$$

where $\mathcal{C}$ is the set of complex numbers and $p_X(x) = P(X = x)$. In this section, we evaluate $G_1(z)$, the PGF of B_1, as function of $G_0(z)$, the PGF of B_0. We then equate $G_1(z)$ and $G_0(z)$ in order to obtain a general PGF of the number of buffered packets just before the start of a CRI in the network steady state. This is then used to derive the probability of an empty buffer p_e at a transmitter in the steady state and the network convergence condition. Having obtained p_e, we evaluate the throughput and delay of the network under the proposed collision resolution scheme.

3.3.1 Notation

Let $P(m, i)$ be the probability of occurrence of two simultaneous events: a CRI of length m starts at instant t_0, and transmitter k^* gets involved in that CRI in the i^{th} slot, where $1 \leq i < m$. The lower bound on the slot index i corresponds to the case when the buffer of transmitter k^* is non-empty at instant t_0, which happens with probability $1 - p_e$. The upper bound on i is a strict inequality because it is always the case that a CRI does not terminate at a given slot if a new transmitter joins the active set during that slot. On the other hand, let $P(m, -1)$ denote the probability that a CRI of length m starts

at instant t_0, and transmitter k^* does not get involved throughout the CRI. Note that probabilities $\{P(m,i)\}_{m,i}$ and $\{P(m,-1)\}_m$ are joint unconditional probabilities. In the previous section we showed how to compute $\{P(m)\}_m$ given p_e. The computation of $\{P(m,i)\}_{m,i}$ and $\{P(m,-1)\}_m$ using $\{P(m)\}_m$ is described in Appendix A.2.

3.3.2 Number of Buffered Packets at a Transmitter

Define b_i as the number of packets that are buffered at transmitter k^* during time slot $i, 1 \leq i \leq m$ within the CRI that starts at t_0. At t_0, the number of packets in the buffer of transmitter k^* is B_0. At t_1, this number becomes B_1 given by:

$$B_1 = \begin{cases} \{b_{m,1} = B_0 + b_1 + b_2 + \cdots + b_m - 1\}_m \\ \qquad\qquad \text{w.p. } P(m,1),\ 2 \leq m \leq \tilde{K}+1 \\ \{b_{m,2} = b_1 + b_2 + \cdots + b_m - 1\}_m \\ \qquad\qquad \text{w.p. } P(m,2),\ 3 \leq m \leq \tilde{K}+1 \\ \{b_{m,3} = b_2 + b_3 + \cdots + b_m - 1\}_m \\ \qquad\qquad \text{w.p. } P(m,3),\ 4 \leq m \leq \tilde{K}+1 \\ \qquad\qquad\qquad \vdots \\ \{b_{m,\tilde{K}} = b_{m-2} + b_{m-1} + b_m - 1\}_m \\ \qquad\qquad \text{w.p. } P(m,\tilde{K}),\ m = \tilde{K}+1 \\ \{b_{m,-1} = b_m\}_m \\ \qquad\qquad \text{w.p. } P(m,-1),\ 1 \leq m \leq \tilde{K} \end{cases} \tag{3.31}$$

In (3.31), the first $\tilde{K}$ sets of expressions correspond to the case in which transmitter k^* is involved in the CRI. Note that if transmitter k^* gets involved in

the i^{th} slot of a CRI, the CRI length m is strictly greater than i. Otherwise, the CRI's length exceeds m, or transmitter k^* gets involved in a CRI of length m outside that CRI, which is a contradiction. However, for all the first $\tilde{K}$ sets in (3.31), m is at most $\tilde{K}+1$ because a maximum of $\tilde{K}$ transmitters may be active at a time. On the other hand, the last set of expressions in (3.31) corresponds to the case in which transmitter k^* is inactive. Given that, the maximum number of active transmitters is now $\tilde{K}-1$, and m is at most $\tilde{K}$ in this case.

3.3.3 Characterization of the New Packet Arrivals Per Slot

When transmitter k^* is involved, one packet in its buffer will be successfully communicated and thus may be safely removed from the buffer at the end of the CRI. This explains the deduction of one packet in all the first $\tilde{K}$ sets in (3.31). In the first set of cases, transmitter k^* gets involved in slot 1 of the CRI, so $B_0 > 0$. Variables $\{b_1, \ldots, b_m\}$ are Poisson non-negative. In the second set of cases, transmitter k^* gets involved in slot 2 of the CRI, so $B_0 = 0$. Variable b_1 is Poisson positive, while variables $\{b_2, \ldots, b_m\}$ are Poisson non-negative. In the third set of cases, transmitter k^* gets involved in slot 3 of the CRI, so $B_0 = b_1 = 0$. Variable b_2 is Poisson positive, while variables $\{b_3, \ldots, b_m\}$ are Poisson non-negative. In the $\tilde{K}^{\text{th}}$ set of cases, transmitter k^* gets involved in slot $\tilde{K}$, so $B_0 = b_1 = b_2 = \cdots = b_{\tilde{K}-2} = 0$. Variable $b_{\tilde{K}-1}$ is Poisson positive, while variables $b_{\tilde{K}}$ and $b_{\tilde{K}+1}$ are Poisson non-negative. In

the last set of cases in (3.31), transmitter k^* is not involved in the CRI, so the packets that accumulate in the buffer of transmitter k during a CRI of length m are only those b_m packets that arrive in the m^{th} slot of the CRI. Variable b_m is Poisson non-negative.

3.3.4 Probability Generating Function of the Number of Buffered Packets

By the law of total probability, the PGF of B_1 in (3.31) is given by

$$G_1(z) = \sum_{i=1}^{\tilde{K}} \sum_{m=i+1}^{\tilde{K}+1} E\left[z^{b_{m,i}}\right] P(m,i) + \sum_{m=1}^{\tilde{K}} E\left[z^{b_{m,-1}}\right] P(m,-1) \tag{3.32}$$

We now compute the individual PGFs in (3.32). Using (3.31), we have

$$E\left[z^{b_{m,1}}\right] = z^{-1} E\left[z^{B_0} | B_0 > 0\right] E\left[z^{b_1+b_2+\cdots+b_m}\right] \tag{3.33}$$

Note that

$$G_0(z) = E\left[z^{B_0}\right] = p_e \times E\left[z^0\right] + (1-p_e) \times E\left[z^{B_0} | B_0 > 0\right] \tag{3.34}$$

Moreover, $b_1 + b_2 + \cdots + b_m$ is Poisson of rate $m\lambda$, so

$$E\left[z^{b_1+b_2+\cdots+b_m}\right] = e^{-m\lambda(1-z)} \tag{3.35}$$

Substituting (3.34) and (3.35) in (3.33) we get

$$E\left[z^{b_{m,1}}\right] = z^{-1}\frac{G_0(z) - p_e}{1 - p_e}e^{-m\lambda(1-z)} \tag{3.36}$$

Similarly,

$$\begin{aligned} E\left[z^{b_{m,i}}\right] &= z^{-1}E\left[z^{b_{i-1}}|b_{i-1} > 0\right]E\left[z^{b_i + b_{i+1} + \cdots + b_m}\right] \\ &= z^{-1}\frac{E\left[z^{b_{i-1}}\right] - P(b_{i-1} = 0)}{1 - P(b_{i-1} = 0)}e^{-(m-i+1)\lambda(1-z)} \\ &= z^{-1}\frac{e^{-\lambda(1-z)} - e^{-\lambda}}{1 - e^{-\lambda}}e^{-(m-i+1)\lambda(1-z)},\ 2 \le i \le \tilde{K} \end{aligned} \tag{3.37}$$

and

$$E\left[z^{b_{m,-1}}\right] = E\left[z^{b_m}\right] = e^{-\lambda(1-z)} \tag{3.38}$$

In the steady state, $G_1(z) = G_0(z) = G(z)$. Substituting (3.36), (3.37) and (3.38) into (3.32) and equating $G_1(z)$ and $G_0(z)$ we have

$$G(z) = \frac{\begin{array}{c} z(1-p_e)\left(1-e^{-\lambda}\right)S_1(z) - \left(1-e^{-\lambda}\right)p_e S_2(z) \\ +\,(1-p_e)\left(e^{-\lambda(1-z)} - e^{-\lambda}\right)S_3(z) \end{array}}{z(1-p_e)\left(1-e^{-\lambda}\right) - \left(1-e^{-\lambda}\right)S_2(z)} \tag{3.39}$$

where

$$S_1(z) = \sum_{m=1}^{\tilde{K}} e^{-\lambda(1-z)}P(m,-1) \tag{3.40}$$

$$S_2(z) = \sum_{m=2}^{\tilde{K}+1} e^{-m\lambda(1-z)}P(m,1) \tag{3.41}$$

$$S_3(z) = \sum_{i=2}^{\tilde{K}} \sum_{m=i+1}^{\tilde{K}+1} e^{-(m-i+1)\lambda(1-z)} P(m,i) \tag{3.42}$$

3.3.5 Steady-State Probability p_e of an Empty Buffer

In (3.39) the PGF $G(z)$ of the number of packets buffered at a transmitter has unknown value p_e. This represents the probability that a transmitter buffer is empty at the start of a CRI in the network steady state. $G(z)$ becomes fully characterized by computing p_e since probabilities $\{P(m,i\}_{i,m}$ and $\{P(m,-1\}_m$ in (3.40), (3.41) and (3.42) have only one unknown parameter p_e. The dependence on p_e is described in Section 3.2 and Appendix A.2. To compute p_e we note the following. Using (3.41),

$$S_2(1) = \sum_{m=2}^{\tilde{K}+1} P(m,1) = 1 - p_e \tag{3.43}$$

This is because a transmitter gets involved in a CRI in the first time slot with probability $1 - p_e$, and such a CRI would then have length m in the range $2 \leq m \leq \tilde{K} + 1$ since at least one transmitter is active. Moreover, using (3.40), (3.41) and (3.42),

$$\begin{aligned} S_1(1) + S_3(1) &= \sum_{m=1}^{\tilde{K}} P(m,-1) + \sum_{i=2}^{\tilde{K}} \sum_{m=i+1}^{\tilde{K}+1} P(m,i) \\ &= 1 - \sum_{m=2}^{\tilde{K}+1} P(m,1) = 1 - S_2(1) = p_e \end{aligned} \tag{3.44}$$

The second equality in (3.44) follows from the fact that the probability of the set of all outcomes is unity. The third and last equalities follow from (3.43). Evaluating $G(z)$ in (3.39) at unity,

$$G(1) = 1 = \frac{(1 - p_e)\left(S_1(1) + S_3(1)\right) - p_e S_2(1)}{(1 - p_e) - S_2(1)} = \frac{0}{0} \tag{3.45}$$

Note that $G(1) = 1$ by definition of a PGF in (3.30). Form (3.45) is indeterminate, so we apply L'Hôpital's rule once to (3.39) and evaluate the expression at $z = 1$. This yields

$$[S_1'(1)] + [S_2'(1)] + \left[\frac{\lambda}{1 - e^{-\lambda}} S_3(1) + S_3'(1)\right] = 1 - S_1(1) \tag{3.46}$$

which is a polynomial equation in p_e. The derivatives in (3.46) are with respect to z. Since (3.46) may be of degree five or higher in p_e depending on the network size $\tilde{K}$, p_e admits no closed form. However, the network buffers at the transmitters converge to steady state if and only if (3.46) admits a unique solution for p_e in the range zero to unity. The condition is necessary because (3.46) is derived assuming the existence of steady-state probability p_e. The condition is sufficient because the PGF in (3.39) is unique given p_e.

3.3.6 Interpretation of the Network Convergence Condition

Per CRI, a transmitter has one of three states. In state 1, the transmitter is not involved in the CRI. In this case, new packet arrivals during the CRI

only occur during the last slot of the CRI and are Poisson of rate λ. The expected number of newly arriving packets buffered at the transmitter in state 1 during a CRI corresponds to the term in the first bracket in the LHS of (3.46).

In state 2, the transmitter is involved in the CRI starting from the first slot of the CRI. In this case, new packet arrivals during the CRI may occur throughout any of the m slots of the CRI and they follow a Poisson distribution of rate λ. The expected number of newly arriving packets buffered at the transmitter in state 2 during a CRI corresponds to the term in the second bracket in the LHS of (3.46). Note that this number only represents new packet arrivals during state 2. It does not count the old packets buffered before the start of the new CRI and because of which the transmitter gets involved at the very beginning of the new CRI.

In state 3, the transmitter is involved in the CRI starting from slot i of the CRI, $i > 1$. In this case, we distinguish between new packet arrivals within the CRI that occur during slot $i-1$, and those that occur during slots i to m. The former packet arrivals are Poisson positive as discussed in Section 3.3.3, while the latter packet arrivals are Poisson non-negative. It is easy to show that the expected value of a Poisson random variable of rate λ conditioned on being positive is given by $\lambda/(1-e^{-\lambda})$. Therefore, the expected number of newly arriving packets buffered at the transmitter in state 3 during a CRI corresponds to the two terms in the third bracket in the LHS of (3.46).

The LHS of (3.46) represents the expected number of new packet arrivals at a transmitter during a CRI over all the states of the transmitter. Using (3.40), $S_1(1)$ is the probability that a transmitter stays inactive during a CRI (state 1), so the RHS of (3.46) is the probability that a transmitter gets involved in a CRI. Now we know that a packet may be dropped from the queue of a transmitter only if the transmitter gets involved in a CRI and issues that packet (assuming successful communication). Moreover, no two distinct packets may be issued by one transmitter during a single CRI. Therefore, the RHS of (3.46) is also the expected number of packets that get transmitted during a CRI and exit the queue of the transmitter. Thus, the network convergence condition in (3.46) may unsurprisingly be interpreted as the balance point between the rate of packet arrival at a transmitter and the rate of packet departure from the transmitter.

3.3.7 Throughput Analysis

Having solved for p_e in (3.46), the probability distribution of the CRI length $\{P(m)\}_m$ derived in Section 3.2 is now fully defined. Since K distinct packets under the proposed scheme are decoded in $m = K+1$ time slots, the achieved throughput is

$$\eta(\lambda) = \sum_{k=0}^{\tilde{K}} \frac{k}{k+1} P(k+1;\lambda) \tag{3.47}$$

where probabilities $\{P(m)\}_m$ are function of data arrival rate λ. (3.47) is monotonically increasing in λ and the maximum throughput that may be achieved is

$$\eta_{\max} = \max_{\lambda^*} \ \eta(\lambda^*), \quad \lambda^* \in \{\lambda | (3.46) \text{ admits unique } p_e \in [0,1]\} \tag{3.48}$$

3.3.8 Delay Analysis

We do the same approximation as [1]. The buffer of a transmitter is modeled as M/G/1 queue with vacation. The service time denotes the waiting time m_i of a buffered packet at a transmitter while the transmitter is involved in a CRI. The vacation time denotes the waiting time m_n of a buffered packet at a transmitter while the transmitter is not involved throughout a CRI. The average delay before a buffered packet is transmitted is approximated as

$$d(\lambda) = E[m_i] + \frac{\lambda E[m_i^2]}{2(1 - \lambda E[m_i])} + \frac{E[m_n^2]}{2E[m_n]} \tag{3.49}$$

Since a transmitter in the proposed scheme may join the set of active transmitters within a CRI, the computation of the moments in (3.49) differs from [1]. While a transmitter is not involved in a CRI, a packet waits in the buffer of that transmitter for at most one slot. Therefore, $E[m_n]$ and $E[m_n^2]$ can be approximated as

$$E[m_n] = 0.5 \tag{3.50}$$

$$E[m_n^2] = 0.25 \tag{3.51}$$

On the other hand, waiting time m_i at a transmitter depends on the slot index at which the transmitter gets involved in the CRI. Having solved for p_e in (3.46), probabilities $\{P(m,i)\}_{m,i}$ may be computed as in Appendix A.2. Define the normalization factor

$$F = \sum_{i=1}^{\tilde{K}} \sum_{m=i+1}^{\tilde{K}+1} P(m,i) \tag{3.52}$$

We then have

$$E[m_i] = \frac{1}{F} \sum_{i=1}^{\tilde{K}} \sum_{m=i+1}^{\tilde{K}+1} (m-i+1) P(m,i) \tag{3.53}$$

$$E[m_i^2] = \frac{1}{F} \sum_{i=1}^{\tilde{K}} \sum_{m=i+1}^{\tilde{K}+1} (m-i+1)^2 P(m,i) \tag{3.54}$$

3.4 Results

Consider a network of $\tilde{K} = 8$ transmitters that are assigned equally spaced complex exponentials $\{r_{\tilde{k}}\}_{\tilde{k}=1}^{8}$ between 0 and π. A packet has $P = 1000$ BPSK-modulated symbols. We consider a Gaussian channel of SNR $= 10\log_{10}(1/\sigma^2)$ in the range -20 dB to 20 dB, where σ^2 is the variance of noise

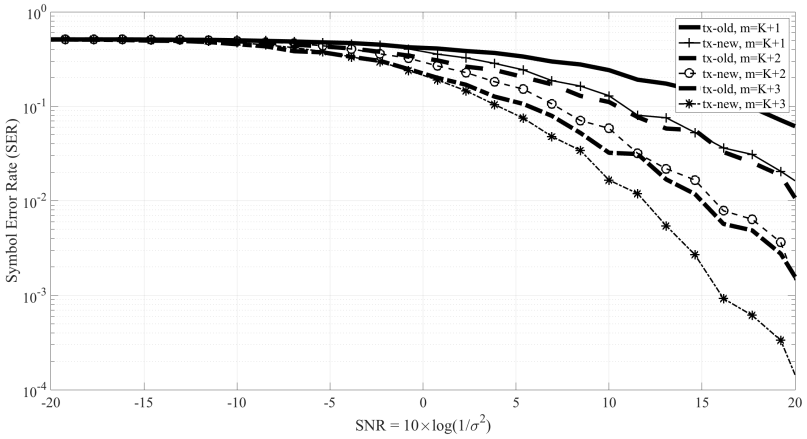

Figure 3.4: Variation of symbol error rate (SER) versus $\text{SNR} = 10\log_{10}(1/\sigma^2)$ for two transmission schemes and different number of stacked packets m. $\tilde{K} = 8$.

in (3.1). $K = 4$ transmitters are randomly selected as the active set of transmitters. We assume the receiver correctly applies the rank test of Section 3.1.2 to detect $K = 4$, so the only errors that may occur are the misidentification of the K transmitters and the decoding of the K collided packets. We consider two transmission schemes. The first scheme is that of [1], so those transmitters that are idle at the start of a CRI may not join the set of active transmitters before the CRI terminates and the packets are decoded. The second scheme is that of Section 3.1.1. We refer to the two schemes as *tx-old* and *tx-new* respectively. For the second scheme, the 14 collision patterns represented by tree $\mathcal{T}_4$ in figure 3.2 are randomly selected. We apply the root-MUSIC method of Sections 3.1.3 and 3.1.4 for the two schemes and record the symbol error rate (SER) versus the SNR. 40 points are collected on each curve and each

experiment is repeated 400 times. Figure 3.4 shows that the SER drops for higher SNR values for both *tx-old* and *tx-new*. It also drops for longer CRI lengths m: more collided mixtures $\{\overrightarrow{y}_n\}_n$ are stacked in the received matrix of packets Y_n, which expands the noise-only submatrix $U_\perp$ in (3.4) and enhances noise-averaging. It should be noted that the noise performance for *tx-new* in figure 3.4 is better compared to *tx-old* because less contention occurs on average per CRI slot for *tx-new*.

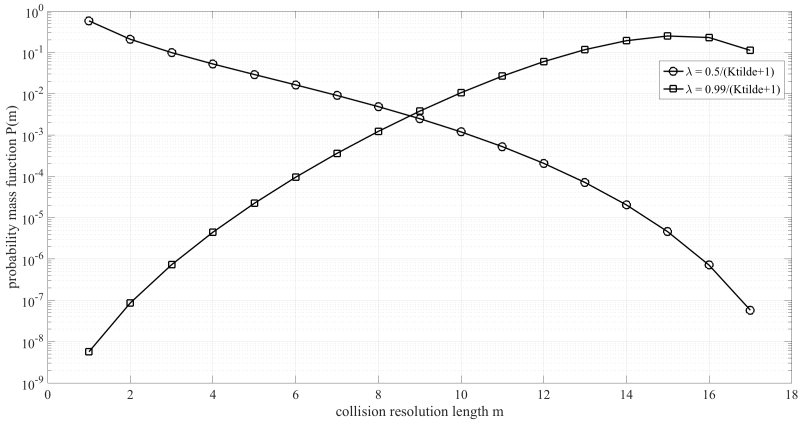

Figure 3.5: Probability mass function of the collision resolution length m for two data arrival rates λ. $\tilde{K} = 16$.

We now expand the network size to $\tilde{K} = 16$ and consider two packet arrival rates $\lambda_l = 0.5/(\tilde{K}+1)$ and $\lambda_h = 0.99/(\tilde{K}+1)$ at the transmitters. We compute the probability of an empty buffer p_e for each rate according to (3.46) and feed it into the probability mass function $P(m)$ of Section 3.2. Figure 3.5 shows $P(m)$ for the two rates. As expected, for higher λ values, longer CRI lengths

become more probable. As a sanity check, each probability mass function in figure 3.5 should add to unity.

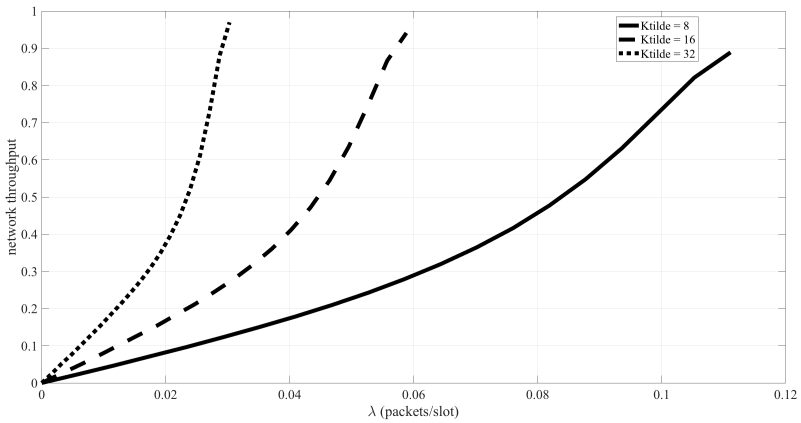

Figure 3.6: Network throughput versus data arrival rate λ for different network sizes $\tilde{K}$.

Figure 3.6 plots the network throughput $\eta(\lambda)$ in (3.47) versus λ for three network sizes $\tilde{K} = 8, 16$ and 32. As λ increases, $\eta(\lambda)$ increases because less time slots are wasted. In figure 3.6 we only show the range of λ for which (3.46) admits a solution for p_e. Note that at the same rate λ, the expected number of active transmitters in a CRI increases for larger network sizes $\tilde{K}$. This implies that the CRI length and consequently the rate of accumulation of packets at a transmitter queue tend to increase for higher $\tilde{K}$. Thus, the range of values of λ for which the network converges to steady state is reduced as the network grows in size. However, for the proposed scheme, notice that the maximum achieved throughput in figure 3.6 increases with $\tilde{K}$.

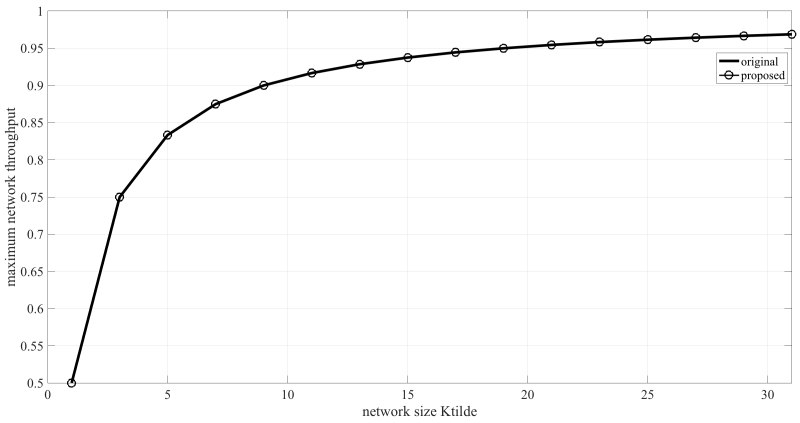

Figure 3.7: Maximum network throughput versus network size $\tilde{K}$ for the original scheme [1] and the proposed scheme.

The same observation of figure 3.6 can be made in figure 3.7 where we show the maximum throughput $\eta_{\max}$ in (3.48) versus the network size $\tilde{K}$. In addition, notice that $\eta_{\max}$ of our proposed scheme matches the maximum throughput of the collision resolution scheme of [1] for all $\tilde{K}$. Thus, $\eta_{\max}$ in (3.48) admits the same closed form expression [1]

$$\eta_{\max}(\tilde{K}) = \frac{\tilde{K}}{\tilde{K}+1} \tag{3.55}$$

From (3.55), the maximum stable value of λ for which the network reaches convergence for the proposed collision resolution algorithm is given by

$$\lambda_{\max}(\tilde{K}) = \frac{\eta_{\max}(\tilde{K})}{\tilde{K}} = \frac{1}{\tilde{K}+1} \tag{3.56}$$

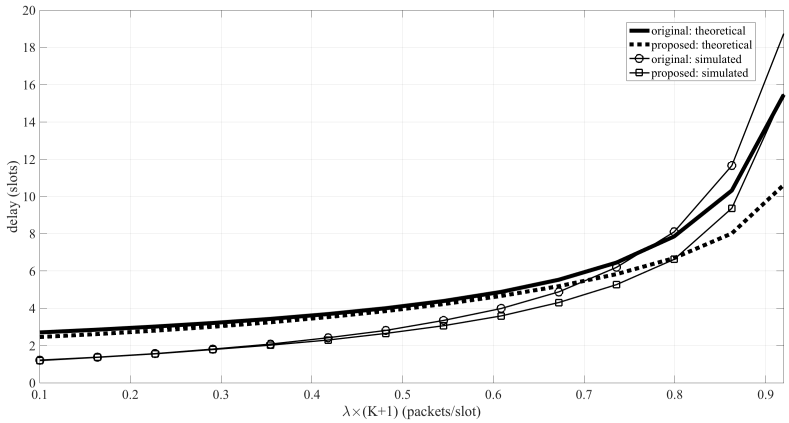

Figure 3.8: Packet queueing delay versus data arrival rate λ for the original scheme [1] and the proposed scheme. $\tilde{K} = 16$.

On the other hand, we show the derived and simulated curves for the queueing delay of the proposed algorithm and the algorithm of [1]. The simulations are run for 1e5 slots of which the queuing delay only in the second half of the simulation time is considered in order to approximate the network convergence. The experiment is repeated 20 times. The derived expression of the delay for the proposed scheme is given in (3.49). As expected, the delay increases for higher λ values. The derived approximations of the queueing delay for the two schemes tend to underestimate the simulated delay for high rates λ. However, for both the derivation and the simulation the proposed scheme reduces the queueing delay compared to [1].

3.5 Conclusion

A root-MUSIC method for blind network-assisted diversity multiple access is designed for synchronous transmissions in non-blocking mode. We carry out queueing analysis of the proposed scheme and optimize the analysis for polynomial-order complexity. Both analytical and numerical results for the network throughput and queueing delay are derived. We show that the suggested collision resolution algorithm achieves the same peak throughput as the original BNDMA scheme [1] but cuts down the queueing delay of the buffered packets at the transmitters.

Chapter 4

Asynchronous Blind Network-Assisted Diversity Multiple Access

We present a blind collision resolution algorithm in slow fading channels based on retransmission diversity. The algorithm neither assumes packet nor symbol synchronization of the different users and it does not demand estimates of the arrival times of the collided signals. The proposed scheme works independently of the relative alignment of the packets, so it can also resolve synchronous collisions. The decoding complexity does not scale with the packet size and thus does not burden the receiver. In the blocking mode, the algorithm achieves high throughputs and low queueing delay similar to synchronous network division multiple access (NDMA) protocols. In the non-blocking mode, there is longer queueing delay of the packets before transmission, but the throughput is still high due to faster accumulation of the buffered packets at the transmitters.

Section 4.1 presents the system model. In Section 4.2 we solve the collision resolution problem in the asynchronous non-blocking mode. The solution does

not apply to all collision scenarios, so a modified transmission-reception algorithm is presented in Section 4.3. Section 4.4 describes an algorithm for resolving packet collisions in the asynchronous blocking mode. In Section 4.5 we show numerical results on throughput analysis and decoding performance of the proposed algorithms. Section 4.6 concludes the chapter.

4.1 System Model

Consider a set of $\tilde{K}$ transmitters and a single receiver in a single-carrier system. A subset of K transmitters, $K \leq \tilde{K}$, may contact the receiver during the same time, on the same frequency and with no use of orthogonal codes. Moreover, all nodes have single antennas. Still, the receiver manages to listen to each of the K active transmitters by leveraging the diversity created by the transmission scheme. The receiver solves this communication problem in three stages. First, it detects the number of active transmitters K. Second, it identifies which K-subset of the $\tilde{K}$ transmitters is currently the active set of transmitters. Third, it decodes the signal of each of the K transmitters. Although the receiver has to identify the K active transmitters, we assume the receiver knows the population of $\tilde{K}$ transmitters beforehand. In particular, each transmitter $\tilde{k}$ of the $\tilde{K}$ transmitters is assigned a unique complex exponential $r_{\tilde{k}} = e^{j\angle r_{\tilde{k}}}$ lying on the unit circle, $0 \leq \angle r_{\tilde{k}} < \pi$, and the receiver is aware of this assignment.

We consider packet-switched networks. Active transmitter k wants to send packet $\overrightarrow{s}_k$ to the receiver. A packet has P symbols. A symbol may be real or complex and its duration is τ. A packet occupies one slot duration, so 1 slot $= P\tau$, and we impose $P \gg \tilde{K}$.

We assume there is a reference clock at the receiver that indicates the start of a time slot. The transmitters are not necessarily synchronized to the receiver, so packet $\overrightarrow{s}_k$ of transmitter k may not be totally received within a single time slot but might partially overlap in time with two consecutive slots. It is thus unnecessary to define slot boundaries at the receiver. We only do so for two reasons. First, we derive the collision resolution algorithm for asynchronous transmissions based on the solution for synchronous collisions, so slotted time is assumed for analytical convenience. Second, the slotted time formulation proves that the proposed algorithm in this chapter resolves the synchronous collisions as a special case. The algorithm thus also applies in a hybrid network in which only a subset of the transmitters are synchronized to the receiver such as those in its proximity.

Without loss of generality, we assume the first packet is always received at $t = 0$. The receiver identifies whether $K = 1$ by simply checking the cyclic redundancy check (CRC) bits of the collected packet. In the case $K > 1$, the receiver does not know the arrival times of the individual collided packets. In the non-blocking network operation mode, it could happen that the receiver

may not have decoded these packets yet and then another transmitter sends a packet. In this case K refers to the total number of active transmitters at the instant of successful decoding. N refers to the collision resolution interval measured in time slots. Since data availability at the transmitters is random, so are K and N. The channels between the transmitters and the receiver are slow fading with respect to N, and there is additive complex Gaussian noise $\mathcal{CN}(0, \sigma^2 I)$ of mean 0 and covariance $\sigma^2 I$ at the receiver. A collection of $p \times q$ noise samples is denoted as $\mathcal{N}_{p,q}$.

A packet is represented as a vector of symbols, were $\overrightarrow{s}_k$ is the packet to be sent by transmitter k, $1 \leq k \leq K$. During time slot n and whenever at least one transmitter is active, the receiver collects a vector of symbols

$$\overrightarrow{y}_n = \left[\overrightarrow{y}_n[1], \overrightarrow{y}_n[2], \ldots, \overrightarrow{y}_n[P]\right]^T \tag{4.1}$$

The n-time extension of the coding vector of transmitter $\tilde{k}$ is defined as

$$\overrightarrow{w}_{\tilde{k},n} = \left[r_{\tilde{k}}^0, r_{\tilde{k}}^1, \ldots, r_{\tilde{k}}^{n-1}\right]^T \tag{4.2}$$

4.2 Asynchronous Non-Blocking Mode

Transmitters that have data to send access the channel without waiting for an idle channel state. The transmitters are not necessarily synchronized

to the receiver, so in general packet $\overrightarrow{s}_k$ of transmitter k is first received at $t_k = ((n_k - 1)P + p_k)\tau$, i.e. in time slot n_k after p_k symbol durations relative to the slot start time, $1 \leq n_k \leq N$, $0 \leq p_k < P$. Shift p_k should be a decimal. We first assume $p_k \in \{0, 1, \ldots, P-1\}$ and then extend the solution to the decimal case. Resolving synchronized collisions $(n_k = 1, p_k = 0)_k$ is presented in Chapter 2. The algorithm is extended to the case of synchronized transmissions $(n_k \leq N, p_k = 0)_k$ in Chapter 3 at the cost of increased decoding complexity of the order of K. In both settings all transmitters are synchronized to the receiver. We now consider resolving collisions in the general case $(n_k \leq N, p_k < P)_k$. We emphasize that the decoding complexity does not scale with the packet size P. Otherwise it becomes prohibitive since P could be orders of magnitude larger than the number of collided packets K or decoding time N.

4.2.1 Transmission Scheme

All transmitters follow the same transmission scheme as in Chapters 2 and 3. This is important so that a decoding scheme that blindly resolves asynchronous collisions perfectly applies to synchronous collisions as a special case. Therefore, an active transmitter k sends packet $\overrightarrow{s_k}$ of length P. In case of a collision, transmitter k sends $r_k \times \overrightarrow{s_k}$, then $r_k^2 \times \overrightarrow{s_k}$ and so on. This persists until the receiver manages to decode the collided packets.

Figure 4.1 illustrates an example scenario of $K = 3$ collided signals which we

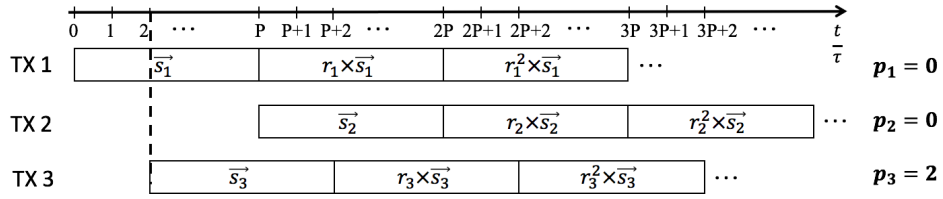

(a) Active set of transmitters — TX1 and TX2: aligned, TX3: misaligned

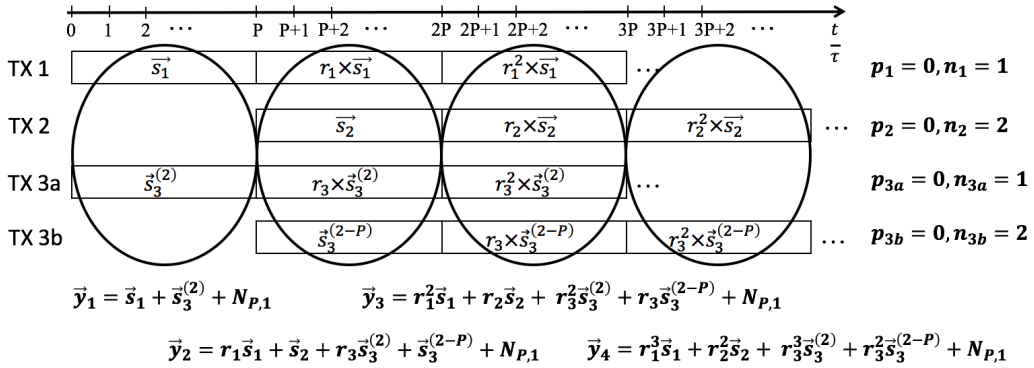

(b) Equivalent active set — all TXs aligned

Figure 4.1: Transmission scheme of $K = 3$ packets aligned with the start of a symbol duration

will use to build a decoding algorithm for a general collision setting. Assume for now there is no fading. In Figure 4.1a, packet $\overrightarrow{s}_1$ arrives at the receiver at $t = 0$, which is the start of the first time slot. Unfortunately, packet $\overrightarrow{s}_3$ arrives within the first slot at $t = 2\tau$ and collides with $\overrightarrow{s}_1$. The CRC of the collected packet is corrupted and the receiver awaits new packet arrivals. At $t = P\tau$ the second packet $r_1\overrightarrow{s}_1$ of transmitter 1 and the first packet $\overrightarrow{s}_2$ of transmitter 2 are received. Upon its second transmission, packet $r_3\overrightarrow{s}_3$ of transmitter 3 is received at $t = (P + 2)\tau$. At $t = 2P\tau$, packets $r_1^2\overrightarrow{s}_1$ and $r_2\overrightarrow{s}_2$ are received, and so on. Thus, all three transmitters follow the same transmission scheme.

4.2.2 Expressions of Collected Packets

Denote by $\overrightarrow{y}_n$ the overall received packet within time slot n. In the example of Figure 4.1a, whole packet $\overrightarrow{s}_1$ and the first $P-2$ symbols of packet $\overrightarrow{s}_3$ contribute to $\overrightarrow{y}_1$. Four signal components (beyond noise) contribute to $\overrightarrow{y}_2$: whole packets $r_1\overrightarrow{s}_1$ and $\overrightarrow{s}_2$, the last two symbols of packet $\overrightarrow{s}_3$ and the first $P-2$ symbols of packet $r_3\overrightarrow{s}_3$. In a similar manner, four signal components contribute to $\overrightarrow{y}_3$: $r_1^2\overrightarrow{s}_1$, $r_2\overrightarrow{s}_2$, last two symbols of $r_3\overrightarrow{s}_3$ and first $P-2$ symbols of $r_3^2\overrightarrow{s}_3$. This continues to be true for all received packets $\overrightarrow{y}_n$, $n>1$. For convenience, we introduce a new piece of notation. For an arbitrary vector $\overrightarrow{v}$ of length L, define

$$\overrightarrow{v}^{(d)} = \begin{cases} \big[\overbrace{0,\ldots,0}^{d \text{ zeros}}, \overrightarrow{v}[1],\ldots,\overrightarrow{v}[L-d]\big]^T, & 1 \le d \le L-1 \\ \overrightarrow{v}, & d=0 \\ \big[\overrightarrow{v}[1-d],\ldots,\overrightarrow{v}[L],\underbrace{0,\ldots,0}_{-d \text{ zeros}}\big]^T, & 1-L \le d \le -1 \\ \emptyset, & |d| > L-1 \end{cases} \tag{4.3}$$

This is easily illustrated via an example. For instance, if $\overrightarrow{v}=(a,b,c,d,e)^T$ then $\overrightarrow{v}^{(2)}=(0,0,a,b,c)^T$, $\overrightarrow{v}^{(-3)}=(d,e,0,0,0)^T$, $\overrightarrow{v}^{(0)}=\overrightarrow{v}$ and $\overrightarrow{v}^{(6)}$ is an empty vector of dimension zero.

Following the discussion above on the signal contribution to collected packets $\{\overrightarrow{y}_n\}_n$ and using the notation in (4.3) we have

- $\overrightarrow{y}_1 = \overrightarrow{s}_1^{(0)} + \overrightarrow{s}_3^{(2)} + \mathcal{N}_{P,1}$

- $\overrightarrow{y}_2 = r_1 \overrightarrow{s}_1^{(0)} + \overrightarrow{s}_2^{(0)} + \overrightarrow{s}_3^{(2-P)} + r_3 \overrightarrow{s}_3^{(2)} + \mathcal{N}_{P,1}$
- $\overrightarrow{y}_3 = r_1^2 \overrightarrow{s}_1^{(0)} + r_2 \overrightarrow{s}_2^{(0)} + r_3 \overrightarrow{s}_3^{(2-P)} + r_3^2 \overrightarrow{s}_3^{(2)} + \mathcal{N}_{P,1}$

and so on. Suppose the receiver collects $N = 5$ packets $\{\overrightarrow{y}_n\}_{n=1}^5$ and stacks them in a matrix Y_5. Thus,

$$\begin{pmatrix} \overrightarrow{y}_1^T \\ \overrightarrow{y}_2^T \\ \vdots \\ \overrightarrow{y}_5^T \end{pmatrix} = \begin{pmatrix} 1 & 0 & 1 & 0 \\ r_1 & 1 & r_3 & 1 \\ r_1^2 & r_2 & r_3^2 & r_3 \\ r_1^3 & r_2^2 & r_3^3 & r_3^2 \\ r_1^4 & r_2^3 & r_3^4 & r_3^3 \end{pmatrix} \times \begin{pmatrix} \overrightarrow{s}_1^{(0)T} \\ \overrightarrow{s}_2^{(0)T} \\ \overrightarrow{s}_3^{(2)T} \\ \overrightarrow{s}_3^{(2-P)T} \end{pmatrix} + \mathcal{N}_{5,P} \tag{4.4}$$

$$Y_5 = W_5 \times S + \mathcal{N}_{5,P}$$

4.2.3 General Expression of Received Matrix of Packets Y_n

Recall that packet $\overrightarrow{s}_k$ of active transmitter k arrives at the receiver at $t_k = ((n_k - 1)P + p_k)\tau$. In the example of Figure 4.1a, transmitters 1, 2 and 3 form the set of active transmitters, where $p_1 = p_2 = 0$ and $p_3 = 2$. The expression of the received matrix of packets in (4.4) suggests an equivalent collision scenario illustrated in Figure 4.1b. Transmitters 1, 2, 3a and 3b send packets $\overrightarrow{s}_1^{(0)}$, $\overrightarrow{s}_2^{(0)}$, $\overrightarrow{s}_3^{(2)}$ and $\overrightarrow{s}_3^{(2-P)}$ respectively to the receiver. All four packets are synchronized to the start of a time slot: $p_1 = p_2 = p_{3a} = p_{4a} = 0$.

We point out the following pattern. Transmitters 1 and 2 in Figure 4.1a have synchronized transmissions: $p_1 = p_2 = 0$. In the equivalent scenario of Figure 4.1b, each occupies one column of matrix W_5 and one row of matrix S

in (4.4). On the other hand, $p_3 \neq 0$. Transmitter 3 in Figure 4.1a is replaced by two transmitters in Figure 4.1b. It occupies two columns of W_5 and two rows of S in (4.4). Given this observation, we derive a general expression for the received matrix of packets Y_n. Using (4.2) and the notation in (4.3), transmitter k's contribution to the coding matrix W_n in the expression of Y_n is given by

$$\overrightarrow{w}_{k,n,t_k} = \begin{cases} \overrightarrow{w}_{k,n}^{(n_k-1)}, & p_k = 0 \\ \left[\overrightarrow{w}_{k,n}^{(n_k-1)}, \overrightarrow{w}_{k,n}^{(n_k)}\right], & p_k \in \{1, \ldots, P-1\} \end{cases} \tag{4.5}$$

where $[\cdot, \cdot]$ denotes horizontal stacking. Similarly, transmitter k's contribution to the matrix of packets S in the expression of Y_n is

$$\overrightarrow{s}_{k,t_k} = \begin{cases} \overrightarrow{s}_{k}^{(p_k)}, & p_k = 0 \\ \left[\overrightarrow{s}_{k}^{(p_k)}, \overrightarrow{s}_{k}^{(p_k-P)}\right], & p_k \in \{1, \ldots, P-1\} \end{cases} \tag{4.6}$$

Y_n becomes

$$\begin{aligned} Y_n &= \begin{pmatrix} \overrightarrow{w}_{1,n,t_1} & \ldots & \overrightarrow{w}_{K,n,t_K} \end{pmatrix} \times \begin{pmatrix} \overrightarrow{s}_{1,t_1}^{T} \\ \vdots \\ \overrightarrow{s}_{K,t_K}^{T} \end{pmatrix} + \mathcal{N}_{n,P} \\ &= W_n \times S + \mathcal{N}_{n,P}, \qquad 1 \leq n \leq N \end{aligned} \tag{4.7}$$

Notice that (4.4) is an instance of (4.7) for the case $K = 3$ and $n = N = 5$. So far we have assumed no fading. Along the lines of [1], slow fading relative to the collision resolution time N leads to the scaling and coloring of packets $\{\overrightarrow{s}_k\}_k$. These can be removed by equalizing packets $\{\overrightarrow{s}_k\}_k$ individually after S in (4.7) is decoded.

4.2.4 Decoding of S

Equation (4.7) shows that the received matrix of packets Y_n can be expressed as a coefficient matrix W_n times a matrix of packets S plus a noise matrix, where the columns of W_n are shifted versions of the coding vectors $\{\overrightarrow{w}_{k,n}\}_k$ in (4.2). This is the same format as the expression of Y_n in (3.1) for the case of synchronized transmissions $(n_k \leq N, p_k = 0)_k$. The receiver thus applies the same decoding algorithm as in Chapter 3 to resolve asynchronous collisions. Two main differences arise:

- In Chapter 3, the receiver identifies the set of active transmitters by solving a system of $N-1$ independent equations for characteristic roots $\{r_k\}_k$. In the case of asynchronous collisions, each transmitter k with $p_k \neq 0$ occupies two columns of W_n as in (4.5). The corresponding root r_k will be duplicate.

- In Chapter 3, the receiver decodes S which holds as its rows packets $\{\overrightarrow{s}_k\}_k$. In the case of asynchronous collisions, each transmitter k with $p_k \neq 0$ occupies two rows of S holding $\overrightarrow{s}_k^{(p_k)}$ and $\overrightarrow{s}_k^{(p_k-P)}$. The receiver reconstructs packet $\overrightarrow{s}_k$ by dropping the leading and trailing zeros of $\overrightarrow{s}_k^{(p_k)}$ and $\overrightarrow{s}_k^{(p_k-P)}$ respectively and then concatenating the resultant segments.

4.2.5 Pitfalls of Decoding Algorithm

The above decoding algorithm does not work in all collision scenarios. Successful decoding of S in (4.7) depends on the correct construction of coefficient matrix W_n by the receiver. For the latter task, roots $\{r_k\}_k$ and their multiplicities should be correctly detected. We highlight two pitfall scenarios in which the receiver cannot identify all characteristic roots $\{r_k\}_k$ and consequently fails to decode the collided packets.

4.2.5.1 Pitfall Scenario I

The receiver acquires a non-trivial left null space $U_\perp$ of Y_N in (4.7). This is always possible when $N > K$ and at high signal-to-noise ratio (SNR). Let $\overrightarrow{u}_\perp$ be an arbitrary column of the computed basis $U_\perp$. By definition, $\overrightarrow{u}_\perp^H Y_N = \mathbf{0}_{1,P}$, where $\mathbf{0}_{n,p}$ is a collection of $n \times p$ zeros. At high SNR, we also have $\overrightarrow{u}_\perp^H W_N \approx \mathbf{0}_{1,P}$ Using (4.5), this implies

$$\overrightarrow{u}_\perp^H \overrightarrow{w}_{k,N,t_k} \approx \mathbf{0}_{1,2}, \quad p_k > 0 \tag{4.8}$$

for an arbitrary transmitter k with $p_k > 0$. (4.8) is equivalent to

$$[\overrightarrow{u}_\perp^H \overrightarrow{w}_{k,N}^{(n_k-1)}, \overrightarrow{u}_\perp^H \overrightarrow{w}_{k,N}^{(n_k)}] \approx \mathbf{0}_{1,2} \tag{4.9}$$

Thus,

$$[\overrightarrow{u}_{\perp}^{H}\overrightarrow{w}_{k,N}^{(n_k-1)},\ \overrightarrow{u}_{\perp}^{H}(r_k\overrightarrow{w}_{k,N}^{(n_k)})] \approx \mathbf{0}_{1,2} \tag{4.10}$$

which implies

$$\overrightarrow{u}_{\perp}^{H}(\overrightarrow{w}_{k,N}^{(n_k-1)} - r_k\overrightarrow{w}_{k,N}^{(n_k)}) \approx 0 \tag{4.11}$$

Using (4.2) and (4.3), $(\overrightarrow{w}_{k,N}^{(n_k-1)} - r_k\overrightarrow{w}_{k,N}^{(n_k)})$ is an $N \times 1$ vector of all zeros except for unity at position n_k. (4.11) becomes

$$\overrightarrow{u}_{\perp}[n_k] \approx 0 \tag{4.12}$$

Since $\overrightarrow{u}_{\perp}$ is an arbitrary column of $U_{\perp}$, (4.12) implies that every element in row n_k of $U_{\perp}$ is almost zero. Let $\overrightarrow{w}'_N(z) = [1, z, z^2, \ldots, z^{N-1}]^T$ be a test vector in z, where z is a complex variable. Then, the $(n_k - 1)^{\text{th}}$ and n_k^{th} equations within the set of equations

$$\overrightarrow{w}_N'^{(n)H} U_{\perp} U_{\perp}^{H} \overrightarrow{w}_N'^{(n)} = 0, \quad 0 \leq n \leq N-2 \tag{4.13}$$

are equivalent. Thus, every solution of any of the two equations is also a solution of the other. This is true for root $z = r_k$, and this is also true for every root $z = r_{k'}$ such that $n_{k'} = n_k - 1$ or $n_{k'} = n_k$. Since the set of equations (4.13) are solved for characteristic complex exponentials $\{r_k\}_k$ in the decoding algorithm, a problem only arises if $p_{k'} = 0$. In the latter case, transmitter k' occupies a single column of W_n whereas root $r_{k'}$ is detected as

a duplicate solution. Thus the receiver fails to construct W_n correctly and the decoding of S fails.

4.2.5.2 Pitfall Scenario II

Consider an example collision scenario in which the receiver collects matrix Y_5 given by:

$$\begin{aligned} Y_5 &= \begin{pmatrix} \overrightarrow{w}_{1,5,t_1} & \overrightarrow{w}_{2,5,t_2} & \overrightarrow{w}_{3,5,t_3} \end{pmatrix} \times \begin{pmatrix} \overrightarrow{s}_{1,t_1}^T \\ \overrightarrow{s}_{2,t_2}^T \\ \overrightarrow{s}_{3,t_3}^T \end{pmatrix} + \mathcal{N}_{5,P} \\ &= \begin{pmatrix} 1 & 1 & 0 & 1 & 0 \\ r_1 & r_2 & 1 & r_3 & 1 \\ r_1^2 & r_2^2 & r_2 & r_3^2 & r_3 \\ r_1^3 & r_2^3 & r_2^2 & r_3^3 & r_3^2 \\ r_1^4 & r_2^4 & r_2^3 & r_3^4 & r_3^4 \end{pmatrix} \times \begin{pmatrix} \overrightarrow{s}_1^T \\ \overrightarrow{s}_2^{(P-1)^T} \\ \overrightarrow{s}_2^{(-1)^T} \\ \overrightarrow{s}_3^{(P-1)^T} \\ \overrightarrow{s}_3^{(-1)^T} \end{pmatrix} + \mathcal{N}_{5,P} \end{aligned} \tag{4.14}$$

In this example, transmitters 1, 2 and 3 form the active set. Packet $\overrightarrow{s}_1$ arrives at the receiver at $t_1 = 0$, while packets $\overrightarrow{s}_2$ and $\overrightarrow{s}_3$ arrive at $t_2 = t_3 = (P-1)\tau$. Thus, $p_1 = 0$ and $p_2 = p_3 = P-1$. From (4.3) and (4.6), rows 2 and 4 of S are linearly dependent. A sample basis of the row space of S holds four vectors $\overrightarrow{s}_1^T$, $\overrightarrow{s}_2^{(P-1)^T}$, $\overrightarrow{s}_2^{(-1)^T}$ and $\overrightarrow{s}_3^{(-1)^T}$. Y_5 in (4.14) can be expressed as

$$Y_5 = \begin{pmatrix} 1 & 1+\alpha\cdot 1 & 0 & 0 \\ r_1 & r_2+\alpha\cdot r_3 & 1 & 1 \\ r_1^2 & r_2^2+\alpha\cdot r_3^2 & r_2 & r_3 \\ r_1^3 & r_2^3+\alpha\cdot r_3^3 & r_2^2 & r_3^2 \\ r_1^4 & r_2^4+\alpha\cdot r_3^4 & r_2^3 & r_3^3 \end{pmatrix} \times \begin{pmatrix} \overrightarrow{s}_1^T \\ \overrightarrow{s}_2^{(P-1)^T} \\ \overrightarrow{s}_2^{(-1)^T} \\ \overrightarrow{s}_3^{(-1)^T} \end{pmatrix} + \mathcal{N}_{5,P} \tag{4.15}$$

where $\alpha = \overrightarrow{s}_3[1]/\overrightarrow{s}_2[1]$. The second column of the coefficient matrix in (4.15) is no longer a geometric progression. The receiver acquires a non-trivial left null space $U_\perp$ of Y_5, solves (4.13) and finds single roots r_1, r_2 and r_3. For a successful decoding of S in (4.14), the receiver should find single root r_1 and duplicate roots r_2 and r_3. This discrepancy occurs and the above decoding algorithm fails whenever S is not full rank.

We now make a general statement of pitfall scenario II. Denote by K_h the number of rows of S:

$$\begin{aligned} K_h &= \sum_{k=1}^{K} [1 \times \mathbf{1}\{p_k = 0\} + 2 \times \mathbf{1}\{p_k > 0\}] \\ &= K + \sum_{k=1}^{K} \mathbf{1}\{p_k > 0\} = K + K_a \end{aligned} \tag{4.16}$$

$\mathbf{1}\{\cdot\}$ is the indicator function. Let $\breve{S}$ be a $\breve{K}_h \times P$-matrix that holds the minimum selection of the rows of S that span its row space. Thus,

$$\exists! \overrightarrow{c}_i^T \in \mathcal{C}^{\breve{K}_h} \quad \Big| \quad S[i,:] = \overrightarrow{c}_i^T \breve{S}, \quad 1 \leq i \leq K_h \tag{4.17}$$

We stack $\{\overrightarrow{c}_i^T\}_i$ in matrix $C \in \mathcal{C}^{K_h \times \breve{K}_h}$. (4.7) becomes

$$\begin{aligned} Y_n &= W_n \times C \times \breve{S} + \mathcal{N}_{n,P} \\ &= \begin{pmatrix} W_n \times C[:,1] & \dots & W_n \times C[:,\breve{K}_h] \end{pmatrix} \times \breve{S} + \mathcal{N}_{n,P} \\ &= \breve{W}_n \times \breve{S} + \mathcal{N}_{n,P} \end{aligned} \tag{4.18}$$

If S is full rank, C is the identity matrix. Each column k of C has support $||C[:,k]||_0 = 1$. Thus, each column vector $W_n \times C[:,k]$ in (4.18) is a geometric progression. Therefore, all K_h roots $\{r_k\}_k$ ($K - K_a$ single roots and K_a duplicate roots) are detected upon solving (4.13). On the other hand, if S is not full rank, $K_h > \breve{K}_h$, so $\exists k' \quad | \quad ||C[:,k']||_0 > 1$. In this case $W_n \times C[:,k']$ is a linear combination of two or more columns of W_n and thus does not have a geometric progression format. Define

$$\mathcal{I} = \{i \quad | \quad C[i,k] \neq 0 \quad \wedge \quad ||C[:,k]||_0 > 1, \ 1 \leq i \leq K_h, 1 \leq k \leq \breve{K}_h\} \quad (4.19)$$

$\mathcal{I}$ holds the indices of the columns of W_n corresponding to roots $\{r_k\}_k$ that cannot be generated by (4.13). In the example of (4.14), $\mathcal{I} = \{2,4\}$, so the second and fourth roots in the solution list $[r_1, r_2, r_2, r_3, r_3]$ are masked.

4.3 Modified Transmission-Reception Algorithm

The algorithm of the previous section fails to resolve packet collisions in all collision scenarios. In this section we modify the transmission algorithm to eliminate pitfall scenario I. Then the reception algorithm is extended to successfully decode packets in pitfall scenario II.

4.3.1 Transmission Scheme

To break down the equivalence of an equation pair in set (4.13), $U_\perp$ should admit no rows of zeros. Therefore, the logical statement "(4.11) $\Longrightarrow$ (4.12)" should be negated. This is achieved by modifying coding vector $\overrightarrow{w}_{\tilde{k},n}$ in (4.2) or equivalently modifying the transmission scheme. In particular, each active transmitter k follows the same transmission scheme as before except for an additional scaling factor β every other transmission. Initially, transmitter k sends packet $\overrightarrow{s}_k$. If retransmissions are necessary, transmitter k sends $\beta r_k \overrightarrow{s}_k$, then $r_k^2 \overrightarrow{s}_k$, and so on. Figure 4.2a illustrates the same collision scenario as figure 4.1a for the new transmission scheme. The equivalent collision scenario with synchronized transmissions is shown in figure 4.2b. The n-time extension of the new coding vector of transmitter $\tilde{k}$ is given by

$$\overrightarrow{w}_{\tilde{k},n,\beta}[n] = \begin{cases} \overrightarrow{w}_{\tilde{k},n}[n], & n \text{ odd} \\ \beta \times \overrightarrow{w}_{\tilde{k},n}[n], & n \text{ even} \end{cases} \tag{4.20}$$

As opposed to (4.11), we choose $\beta^2 \neq 1$ so that $\overrightarrow{w}_{k,N,\beta}^{(n_k-1)}[(n_k+1):N]$ is not a scaled version of $\overrightarrow{w}_{k,N,\beta}^{(n_k)}[(n_k+1):N]$. In addition, $|\beta| = 1$ so that the average transmit power per time slot is constant. Therefore, $\beta = e^{j\theta}, \theta \neq l\pi, l \in \mathcal{Z}$.

4.3.2 Expression of Y_n

As in (4.5), define transmitter k's contribution to the coding matrix $W_{n,\beta}$ in the expression of Y_n as

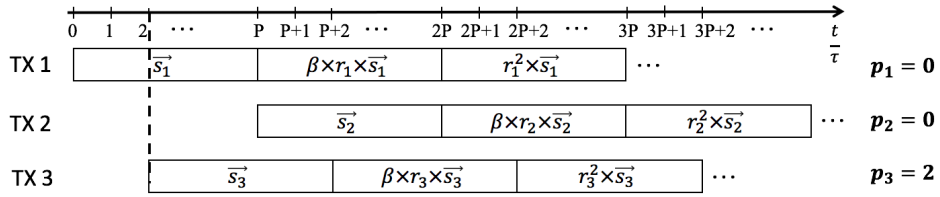

(a) Active set of transmitters — TX1 and TX2: aligned, TX3: misaligned

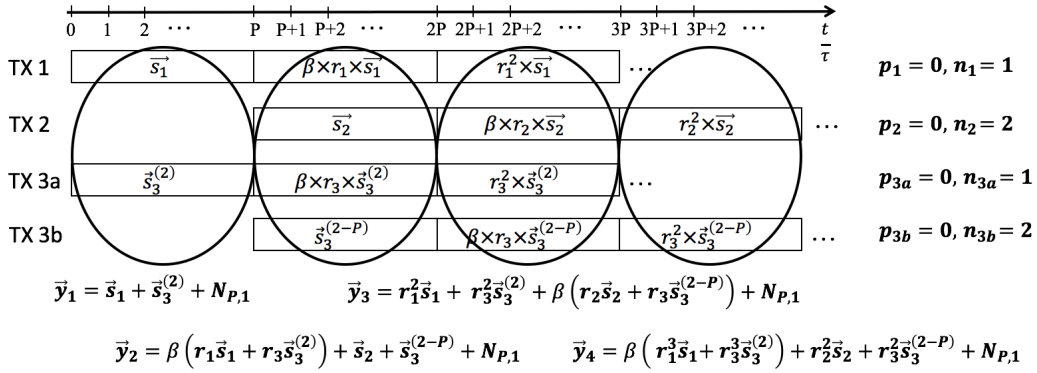

(b) Equivalent active set — all TXs aligned

Figure 4.2: Modified transmission scheme of $K = 3$ packets aligned with the start of a symbol duration

$$\overrightarrow{w}_{k,n,t_k,\beta} = \begin{cases} \overrightarrow{w}_{k,n,\beta}^{(n_k-1)}, & p_k = 0 \\ \left[\overrightarrow{w}_{k,n,\beta}^{(n_k-1)}, \overrightarrow{w}_{k,n,\beta}^{(n_k)} \right], & p_k \in \{1, \ldots, P-1\} \end{cases} \tag{4.21}$$

Y_n becomes

$$\begin{aligned} Y_n &= \left(\overrightarrow{w}_{1,n,t_1,\beta} \quad \ldots \quad \overrightarrow{w}_{K,n,t_K,\beta} \right) \times S + \mathcal{N}_{n,P} \\ &= W_{n,\beta} \times S + \mathcal{N}_{n,P} = W_{n,\beta} \times C \times \breve{S} + \mathcal{N}_{n,P} \\ &= \breve{W}_{n,\beta} \times \breve{S} + \mathcal{N}_{n,P} \end{aligned} \tag{4.22}$$

where S, C and $\breve{S}$ are defined in the previous section.

4.3.3 Detection of Pitfall Scenario II

We show how the receiver detects linear dependencies among the rows of S before S is decoded. Referring to Appendix B.1, the rank of $W_{n,\beta}$ strictly increases as more transmitters become active almost surely. Thus, as the receiver sequentially stacks more packets into matrix Y_n over time index n, the rank of Y_n in (4.22) increases from 1 to $\breve{K}_h$ and saturates at $\breve{K}_h$ at high SNR. Therefore, the receiver detects rank $\breve{K}_h$ of $\breve{S}$ in $N = \breve{K}_h + 1$ slots. The receiver computes left null space $U_\perp$ of Y_N and solves the set of equations

$$\overrightarrow{w}'^{(n)}_{N,\beta}{}^H U_\perp U_\perp^H \overrightarrow{w}'^{(n)}_{N,\beta} = 0, \quad 0 \leq n \leq N-2 \tag{4.23}$$

where $\overrightarrow{w}'_{N,\beta}(z) = [1, \beta z, z^2, \ldots, \beta^{(N-1)\%2} z^{N-1}]^T$. Compared to (4.13), test vector $\overrightarrow{w}'_{N,\beta}$ in (4.23) accounts for the extra β-factor in the modified transmission scheme.

Denote by $\hat{K}_h$ the number of correctly detected roots $\{r_k\}_k$ upon solving (4.23). If S is full rank, all the columns of $\breve{W}_{n,\beta}$ in (4.22) have the same format as $\overrightarrow{w}'_{N,\beta}$, so $\hat{K}_h = \breve{K}_h$ $(= K_h)$. On the other hand, if S is not full rank, at least one column of $\breve{W}_{N,\beta}$ is a linear combination of two or more columns of $W_{N,\beta}$. Such a column does not have the same format as $\overrightarrow{w}'_{N,\beta}$, so $\hat{K}_h < \breve{K}_h$ $(< K_h)$. Therefore, the receiver detects pitfall scenario II by comparing the number $\hat{K}_h$ of found solutions $\{r_k\}_k$ to the saturated rank value $\breve{K}_h$ of Y_N. In the example of (4.15), $\hat{K}_h = 3 < \breve{K}_h = 4$ $(< K_h = 5)$.

4.3.4 Identifiability of the K Active Transmitters

We show that the receiver successfully identifies the K active transmitters at high SNR even when S is not full rank. We first prove the following theorem.

Theorem: A row of S that holds at least $P/2$ packet symbols cannot be spanned by the other rows of S and forms a row of $\breve{S}$.

Proof: Without loss of generality, suppose the first $P/2$ entries of row 1 of S are packet symbols (instead of zeros). For notational convenience, P is assumed even. We prove that row 1 of S cannot be expressed as a linear combination of the other rows of S almost surely:

$$
\begin{aligned}
& P\left(\exists \overrightarrow{v} \middle| \overrightarrow{v}^T S[2:K_h,:] = S[1,:]\right) \quad \ldots \text{ L1} \\
& = P\left(\exists \overrightarrow{v} \middle| \overrightarrow{v}^T S[2:K_h,1:(K_h-1)] = S[1,1:(K_h-1)]\right) \\
& \qquad \times P\left(\overrightarrow{v}^T S[2:K_h,K_h:P] = S[1,K_h:P] \middle| \overrightarrow{v}\right) \quad \ldots \text{ L2} \\
& \leq P\left(\overrightarrow{v}^T S[2:K_h,K_h:P] = S[1,K_h:P] \middle| \overrightarrow{v}\right) \quad \ldots \text{ L3} \\
& \leq P\left(\overrightarrow{v}^T S[2:K_h,K_h:P/2] = S[1,K_h:P/2] \middle| \overrightarrow{v}\right) \quad \ldots \text{ L4} \\
& = \prod_{p=K_h}^{P/2} P\left(\overrightarrow{v}^T S[2:K_h,p] = S[1,p] \middle| \overrightarrow{v}\right) \quad \ldots \text{ L5} \\
& \leq \prod_{p=K_h}^{P/2} \frac{1}{2^B} = \left(\frac{1}{2}\right)^{B(P/2-K_h+1)} \quad \ldots \text{ L6} \\
& \approx 0 \quad \ldots \text{ L7}
\end{aligned}
\tag{4.24}
$$

Line 1 of (4.24) denotes the probability that row 1 of S falls in the span of rows 2 to K_h of S. Using Bayes' rule in line 2, this is the probability that the partitions of row 1 of S fall in the span of the corresponding partitions of rows 2 to K_h of S. In particular, row 1 is partitioned into two groups: entries 1 to $K_h - 1$, and entries K_h to P. The inequality in line 3 follows from the fact that a probability is at most unity. The event in line 4 is implied by the event in line 3, so it is at least as probable. The equality in line 5 follows from the independence of the random packet symbols. $\overrightarrow{v}$ is determined by a system of linear equations defined in line 2, so $\overrightarrow{v}^T S[2 : K_h, p]$ in line 5 is not necessarily a valid symbol. Moreover, symbol $S[1, p]$ is random. It attains one of 2^B values for a modulation scheme of B bits per symbol, $B \geq 1$. This sets the upper probability bound in line 6. Typically, $K_h \leq 2\tilde{K} \ll P/2$, so this bound is approximately zero. Therefore, row 1 of S is not spanned by the other rows of S. It is thus a basis vector in matrix $\breve{S}$. This is true for all rows of S that hold at least $P/2$ packet symbols.

Assume row $S[i, :]$ holds at least $P/2$ packet symbols. By the above theorem, $S[i, :]$ is also row i' of $\breve{S}$. Consider row $S[j, :]$ for some $j \neq i$. By (4.17),

$$S[j, :] = \overrightarrow{c}_j[i']\breve{S}[i', :] + \sum_{k=1, k\neq i'}^{\breve{K}_h} \overrightarrow{c}_j[k]\breve{S}[k, :] \tag{4.25}$$

S and $\breve{S}$ have the same row span. Since row i of S is row i' of $\breve{S}$, then the row span of S excluding its i^{th} row is the same as that of $\breve{S}$ excluding its i'^{th} row.

Therefore, $\exists \overrightarrow{c'}_j$ such that (4.25) can be expressed as

$$S[j,:] = \overrightarrow{c}_j[i']S[i,:] + \sum_{k=1,k\neq i}^{K_h} \overrightarrow{c'}_j[k]S[k,:] \tag{4.26}$$

(4.26) implies $\overrightarrow{c}_j[i'] = 0$ or row i of S can be expressed as a linear combination of the other rows of S. Using the above theorem, the latter result is false almost surely, so $\overrightarrow{c}_j[i'] = 0 \ \forall j \neq i$. Thus, $||C[:,i']||_0 = 1$. Consequently, column $W_{n,\beta} \times C[:,i']$ of $\breve{W}_{n,\beta}$ admits the same format as $\overrightarrow{w}'^{(n)}_{N,\beta}$ in (4.23), so root r_k corresponding to row i of S is successfully detected by (4.23) at high SNR. This is true for every row of S with $P/2$ or more packet symbols. From (4.6), each active transmitter k contributes to S at least one such row. Thus, for each active transmitter k there is at least one column of $\breve{W}_{n,\beta}$ of the same format as $\overrightarrow{w}'^{(n)}_{N,\beta}$. The receiver thus detects all roots $\{r_k\}_{k=1}^K$ at least once, so all K active transmitters are identifiable even when pitfall scenario II occurs.

4.3.5 Decoding of S

We show that the receiver is able to decode S at high SNR even when S is not full rank. The receiver detects single roots $\{r_{i_1}, \ldots, r_{i_A}\}$ and duplicate roots $\{r_{j_1}, \ldots, r_{j_B}\}$ where $[i_1, \ldots, i_A, j_1, \ldots, j_B]$ is a permutation of index vector $[1, \ldots, K]$. Equivalently, the receiver detects columns $\{\overrightarrow{w}^{(n'_{i_1})}_{i_1,n,\beta}, \ldots, \overrightarrow{w}^{(n'_{i_A})}_{i_A,n,\beta}\} \cup \{\overrightarrow{w}^{(n_{j_1}-1)}_{j_1,n,\beta}, \ldots, \overrightarrow{w}^{(n_{j_B}-1)}_{j_B,n,\beta}\} \cup \{\overrightarrow{w}^{(n_{j_1})}_{j_1,n,\beta}, \ldots, \overrightarrow{w}^{(n_{j_B})}_{j_B,n,\beta}\}$ of $W_{n,\beta}$ upon collecting $n \geq$

$\breve{K}+1$ packets and solving (4.23).

$\hat{K}_h = A + 2B$. If $\hat{K}_h = \breve{K}$, $n'_{i_a} = n_{i_a} - 1,\ 1 \leq a \leq A$ as in (4.21). The receiver fully identifies $W_{n,\beta}$. No additional packets are collected into Y_n, so $N \geq \breve{K}+1$. S may be decoded as

$$\hat{S} = (W_{N,\beta}^H W_{N,\beta})^{-1}(W_{N,\beta})^H Y_N \tag{4.27}$$

On the other hand, if $\hat{K}_h < \breve{K}$, pitfall scenario II occurred. Since a transmitter occupies at most two columns of $W_{n,\beta}$ there is no ambiguity about column pair $[\overrightarrow{w}_{j_b,n,\beta}^{(n_{j_b}-1)}, \overrightarrow{w}_{j_b,n,\beta}^{(n_{j_b})}],\ 1 \leq b \leq B$. However, by (4.21), for each column $\overrightarrow{w}_{i_a,n,\beta}^{(n'_{i_a})}, 1 \leq a \leq A$ there are three possibilities:

- $n'_{i_a} = n_{i_a}$ and column $\overrightarrow{w}_{i_a,n,\beta}^{(n'_{i_a}-1)}$ of $W_{n,\beta}$ is masked.
- $n'_{i_a} = n_{i_a} - 1$ and column $\overrightarrow{w}_{i_a,n,\beta}^{(n'_{i_a}+1)}$ of $W_{n,\beta}$ is masked.
- $n'_{i_a} = n_{i_a} - 1$ and no pair column for $\overrightarrow{w}_{i_a,n,\beta}^{(n'_{i_a})}$ of $W_{n,\beta}$ is masked.

A naive approach to decode S is then to test all possible constructions of $W_{n,\beta}$, decode S according to (4.27) and check the CRCs of the recovered packets. The correct solution will be detected in $\mathcal{O}(3^A)$ order of complexity.

Instead, the receiver distinguishes between three types of rows of S in (4.6): full (holds only symbols), right-aligned (holds zeros followed by symbols) and

left-aligned (holds symbols followed by zeros). Denote by $\mathcal{F}$, $\mathcal{R}$ and $\mathcal{L}$ the set of indices of the three categories respectively. Then (4.22) can be expressed as a sum of rank-1 matrices plus a noise matrix as follows:

$$Y_n = \sum_{k_f \in \mathcal{F}} W_{n,\beta}[:, k_f] S[k_f, :] + \sum_{k_r \in \mathcal{R}} W_{n,\beta}[:, k_r] S[k_r, :] + \sum_{k_l \in \mathcal{L}} W_{n,\beta}[:, k_l] S[k_l, :] + \mathcal{N}_{n,P} \quad (4.28)$$

Upon the detection of pitfall scenario II, the receiver collects a total of $n \geq 2K$ packets into Y_n and computes the length-n version of each column within set $\{\overrightarrow{w}^{(n'_{i_1})}_{i_1,n,\beta}, \ldots, \overrightarrow{w}^{(n'_{i_A})}_{i_A,n,\beta}\} \cup \{\overrightarrow{w}^{(n_{j_1}-1)}_{j_1,n,\beta}, \ldots, \overrightarrow{w}^{(n_{j_B}-1)}_{j_B,n,\beta}\} \cup \{\overrightarrow{w}^{(n_{j_1})}_{j_1,n,\beta}, \ldots, \overrightarrow{w}^{(n_{j_B})}_{j_B,n,\beta}\}$ for the new value of n. Since $n \geq 2K$, there exists $\overrightarrow{v}_{n,a^*,R}$ and $\overrightarrow{v}_{n,a^*,L}$ in $\mathcal{C}^n$ such that

$$\overrightarrow{v}_{n,a^*,R} \perp \{\overrightarrow{w}^{(n'_{i_a})}_{i_a,n,\beta}\}_{a=1}^{A} \cup \{\overrightarrow{w}^{(n'_{i_a}-1)}_{i_a,n,\beta}\}_{a=1,a\neq a^*}^{A} \cup \{\overrightarrow{w}^{(n_{j_b}-1)}_{j_b,n,\beta}\}_{b=1}^{B} \cup \{\overrightarrow{w}^{(n_{j_b}-1)}_{j_b,n,\beta}\}_{b=1}^{B} \quad (4.29)$$

$$\overrightarrow{v}_{n,a^*,L} \perp \{\overrightarrow{w}^{(n'_{i_a})}_{i_a,n,\beta}\}_{a=1}^{A} \cup \{\overrightarrow{w}^{(n'_{i_a}+1)}_{i_a,n,\beta}\}_{a=1,a\neq a^*}^{A} \cup \{\overrightarrow{w}^{(n_{j_b}-1)}_{j_b,n,\beta}\}_{b=1}^{B} \cup \{\overrightarrow{w}^{(n_{j_b}-1)}_{j_b,n,\beta}\}_{b=1}^{B} \quad (4.30)$$

for each index $a^* \in \{1, \ldots, A\}$. The receiver finds sample vectors $\overrightarrow{v}_{n,a^*,R}$ and $\overrightarrow{v}_{n,a^*,L}$ and computes

$$\overrightarrow{v}^{H}_{n,a^*,R} Y_n = \begin{cases} \overrightarrow{0}_{1\times P} & \text{if } \overrightarrow{w}^{(n'_{i_{a^*}}-1)}_{i_{a^*},n,\beta} \notin \{W_{n,\beta}[:,k_r]\}_{k_r\in\mathcal{R}} \\ (\overrightarrow{v}^{H}_{n,a^*,R} \overrightarrow{w}^{(n'_{i_{a^*}}-1)}_{i_{a^*},n,\beta}) S[i_{a^*},:] & \text{o.w.} \end{cases} \tag{4.31}$$

$$\overrightarrow{v}^{H}_{n,a^*,L} Y_n = \begin{cases} \overrightarrow{0}_{1\times P} & \text{if } \overrightarrow{w}^{(n'_{i_{a^*}}+1)}_{i_{a^*},n,\beta} \notin \{W_{n,\beta}[:,k_l]\}_{k_l\in\mathcal{L}} \\ (\overrightarrow{v}^{H}_{n,a^*,L} \overrightarrow{w}^{(n'_{i_{a^*}}+1)}_{i_{a^*},n,\beta}) S[i_{a^*},:] & \text{o.w.} \end{cases} \tag{4.32}$$

(4.31) and (4.32) follow the expression of Y_n in (4.28) and the orthogonality in (4.29) and (4.30). Therefore, for each column $\overrightarrow{w}^{(n'_{i_{a^*}})}_{i_{a^*},n,\beta}, 1 \le a^* \le A$:

- If $\overrightarrow{v}^{H}_{n,a^*,R} Y_n$ is a right-aligned row vector, column $\overrightarrow{w}^{(n'_{i_{a^*}}-1)}_{i_{a^*},n,\beta}$ of $W_{n,\beta}$ is masked.
- Else if $\overrightarrow{v}^{H}_{n,a^*,L} Y_n$ is a left-aligned row vector, column $\overrightarrow{w}^{(n'_{i_{a^*}}+1)}_{i_{a^*},n,\beta}$ of $W_{n,\beta}$ is masked.
- Else, no pair column for $\overrightarrow{w}^{(n'_{i_{a^*}})}_{i_{a^*},n,\beta}$ of $W_{n,\beta}$ is masked.

Thus, the receiver resolves the ambiguity about roots $\{r_{i_1}, \ldots, r_{i_A}\}$ and fully identifies $W_{n,\beta}$ in $\mathcal{O}(A)$ order of complexity. The receiver decodes S by (4.27) for $N \ge 2K$. In general, this is larger than the number of packets collected when S is full rank. However, in the simulations we show that pitfall scenario II occurs only with low probability.

4.3.6 Symbol Asynchronization

So far p_k is assumed an integer. We now forgo symbol synchronization and let $0 \leq p_k < P$. Consider the two transmission schemes described in the previous sections. Transmissions of weighted versions of the same packet are assumed to be contiguous. In practice, transmitter k waits for a guard interval after each transmission of weighted packet $\overrightarrow{s}_k$ and watches for an acknowledgement from the receiver. New packets may be sent once the acknowledgement is received. Therefore, we may abstract the packet as having $P = P' + G$ entries of which P' values are actual symbols and G values are zeros. The information signal extends over $P'\tau$, and $G\tau$ is the length of the guard interval. The total slot time is $P\tau$.

Packet $\overrightarrow{s}_k$ of transmitter k fits within the slot boundaries if $p_k < G$. Therefore, each transmitter k with $p_k < G$ occupies one column of $W_{n,\beta}$ and one row of S in (4.22). On the other hand, if $G \leq p_k < P$, transmitter k occupies two columns of $W_{n,\beta}$ and two rows of S. Therefore, the receiver may apply the same decoding algorithm as above. Since p_k is no longer an integer, the information in packet $\overrightarrow{s}_k$ of duration $P\tau$ does not necessarily align to a symbol boundary. Therefore, $P' + 1$ entries of S extending over one or two rows depict the content of packet $\overrightarrow{s}_k$. The receiver recovers the actual P' symbols of packet $\overrightarrow{s}_k$ by compensating for the fractional symbol delay as in single channel communication.

4.4 Asynchronous Blocking Mode

Packet $\overrightarrow{s}_k$ of transmitter k is first collected by the receiver at $t_k = ((n_k - 1)P + p_k)\tau$. In the blocking mode, $n_k = 1$ for $1 \leq k \leq K$. If a transmitter has no data to send within the first time slot of a collision resolution interval, this transmitter may not send a packet to the receiver until the currently collided packets get decoded. The transmitters follow the transmission scheme of Section 4.2. For ease of notation, p_k is assumed an integer and the transmissions are contiguous. Define

$$\overrightarrow{\xi}_k = \begin{cases} r_k \overrightarrow{s}_k & \text{if} \quad p_k = 0 \\ \left[\overrightarrow{s}_k[P - p_k + 1 : P]; r_k \overrightarrow{s}_k[1 : P - p_k]\right] & \text{o.w.} \end{cases} \tag{4.33}$$

where $[\cdot;\cdot]$ is vertical stacking. Suppose the receiver drops packet $\overrightarrow{y}_1$ from Y_n. We have

$$\begin{pmatrix} \overrightarrow{y}_2^T \\ \vdots \\ \overrightarrow{y}_n^T \end{pmatrix} = \left(\overrightarrow{w}_{1,n-1} \ldots \overrightarrow{w}_{K,n-1}\right) \times \begin{pmatrix} \overrightarrow{\xi}_1^T \\ \vdots \\ \overrightarrow{\xi}_K^T \end{pmatrix} + \mathcal{N}_{n-1,P}, n \geq 2 \tag{4.34}$$

This has the same form as synchronous collisions in the blocking mode. Thus, the receiver applies the decoding scheme of Chapter 2 onto $Y_n[2 : n, :]$ in (4.34) to decode packets $\{\overrightarrow{\xi}_k\}_k$. Packet $\overrightarrow{s}_k$ is recovered by detecting its start in $\overrightarrow{\xi}_k$ using the marking symbol(s) appended to $\overrightarrow{s}_k$ before transmission. Therefore,

K packets in the asynchronous blocking mode are decoded in $K+2$ slots at high SNR. Compared to synchronous collisions in Chapter 2, only one additional slot is wasted because $\overrightarrow{y}_1$ is discarded. This is still more efficient compared to the non-blocking mode of the previous section in which two extra time slots are needed per transmitter k whenever $p_k \in \{1, \ldots, P-1\}$.

4.5 Results

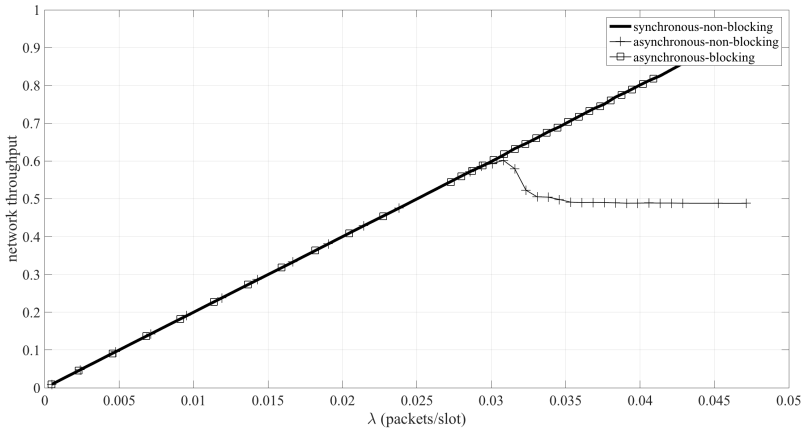

Figure 4.3: Network throughput versus mean data arrival rate λ for three network operation modes, $\tilde{K} = 20$.

Consider a network of $\tilde{K} = 20$ transmitters and one receiver. Packet arrivals at each transmitter are modeled by a Poisson distribution of mean λ. The network is operated in three modes: synchronous non-blocking (SN) mode of Chapter 3, asynchronous non-blocking (AN) mode of Section 4.3 and

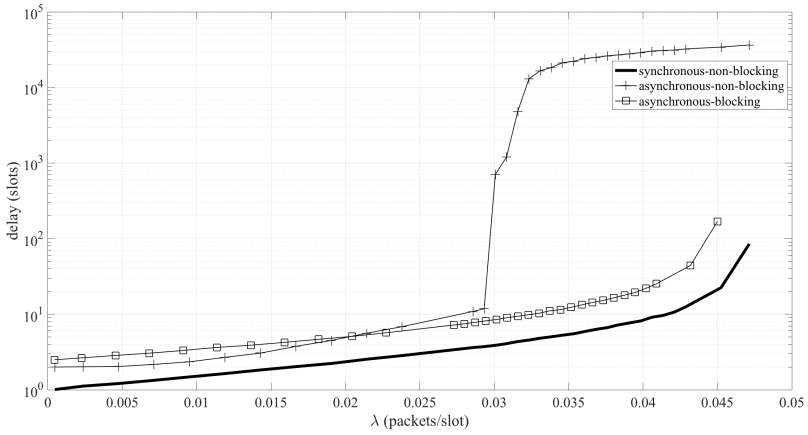

Figure 4.4: Packet queueing delay versus data arrival rate λ for three network operation modes, $\tilde{K} = 20$.

asynchronous blocking (AB) mode of Section 4.4. Define the network throughput as the average number of packets successfully decoded by the receiver over time. Figure 4.3 shows the network throughput versus λ for the three operation modes. Figure 4.4 shows the average queueing delay experienced by a packet at a transmitter. The SNR is assumed infinite, so the mean time to decode a set of collided packets only depends on the multiplicity of the collision. A transmitter buffer is infinitely long, so no packets are dropped. Only one packet per transmitter is decoded in a single collision resolution interval (CRI). Initially, the buffers of all transmitters are empty. The network is run for 5e4 slots before throughput and queueing delay are recorded.

As expected, both throughput and queueing delay are monotonically increas-

ing in λ. For K collided packets, the CRI length is $K+1$ slots for the SN mode and $K+2$ slots for the AB mode. The network throughput for the SN and AB modes is similar for the whole range of λ in figure 4.3. However, the queueing delay in the AB mode is slightly higher in figure 4.4 due to the extra slot per CRI. In a symmetric network of size $\tilde{K}$, the maximum stable value of λ is $1/(\tilde{K}+1)$ in the SN mode and $1/(\tilde{K}+2)$ in the AB mode. Beyond this value, the queueing delay at a transmitter grows arbitrarily large and the network throughput no more increases.

On the other hand, a longer CRI length is obtained in the AN mode. For low λ, the network throughput is similar to the SN and AB modes. This is because the packets exit the buffer of a transmitter in the AN mode at a lower rate, so the accumulation of the buffered packets is faster. Consequently, the expected number $E[K]$ of active transmitters or equivalently decoded packets per CRI is higher in the AN mode, which compensates for the longer CRI length. However, the maximum stable value of λ is reduced in the AN mode compared to the SN and AB modes. The network throughput saturates early for high λ and the queueing delay increases unboundedly.

Figure 4.5 shows the maximum network throughput in the AB mode of Section 4.4 versus the network size $\tilde{K}$. This is obtained by increasing mean data arrival rate λ to its maximum stable value. The maximum throughput in the simulated network is plotted along with function $\tilde{K}/(\tilde{K}+2)$. The two curves

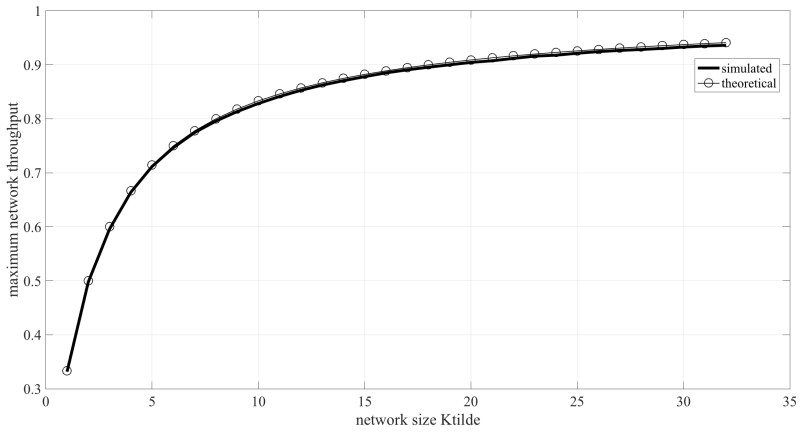

Figure 4.5: Maximum network throughput $\eta_{\max}$ versus network size $\tilde{K}$ for the asynchronous blocking mode: $\eta_{\max} = \tilde{K}/(\tilde{K}+2)$.

are matching. This result can be derived similarly to the throughput analysis of the synchronous blocking (SB) mode in [1]. This also shows that the decoding algorithm in the AB mode is asymptotically optimal: $\tilde{K}/(\tilde{K}+2) \xrightarrow{\tilde{K}\to\infty} 1$.

In Section 4.3.5 we show that a larger number of packets is required to decode S in the AN mode when S is not full rank. Figure 4.6 shows the mean absolute difference between the rank of S and that of a full rank matrix of the same dimensions. $P = 1000$, and S is randomly generated 5000 times. This is repeated for different collision multiplicities in the range $0 \leq K \leq 100$. Clearly the mean rank difference increases with K. However, the difference is less than 0.1 even for 100 collided packets. This shows that the probability of pitfall scenario II is low.

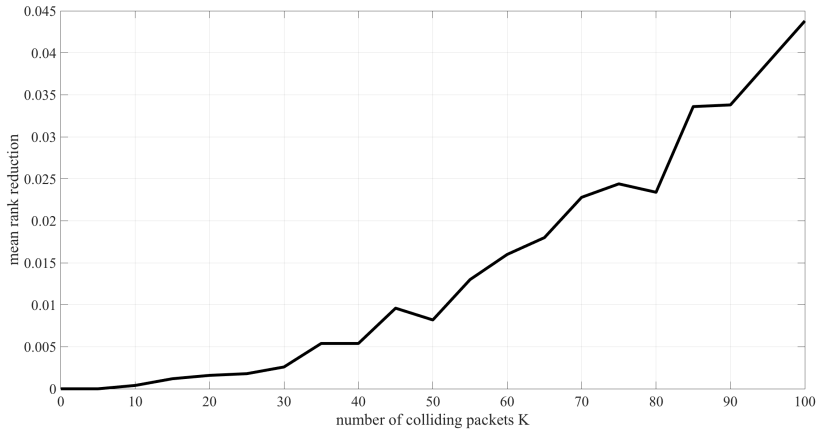

Figure 4.6: Absolute difference between rank of packets S and that of a full rank matrix of same dimensions as S versus the number of collided packets K.

Figure 4.7 plots the symbol error rate (SER) versus the SNR upon decoding a mixture of $K = 3$ packets for two modes: the SB mode of Chapter 2 and the AN mode. The K active transmitters are randomly selected from a network of $\tilde{K} = 8$ transmitters. The characteristic complex exponentials $\{r_{\tilde{k}}\}_{\tilde{k}=1}^{\tilde{K}}$ are equally spaced on the upper half of the unit circle. Each packet has $P = 1000$ BPSK modulated symbols. As expected, the SER drops for higher SNR values in the two modes. Lower SER is obtained in the AN mode because not all K transmitters are necessarily active within every slot of the CRI in the non-blocking mode, thus being less contended. In addition, the SER drops as more packets are stacked into Y_n for the same value of K in the SB and AN modes. This is due to noise-averaging that results from expanding the noise-

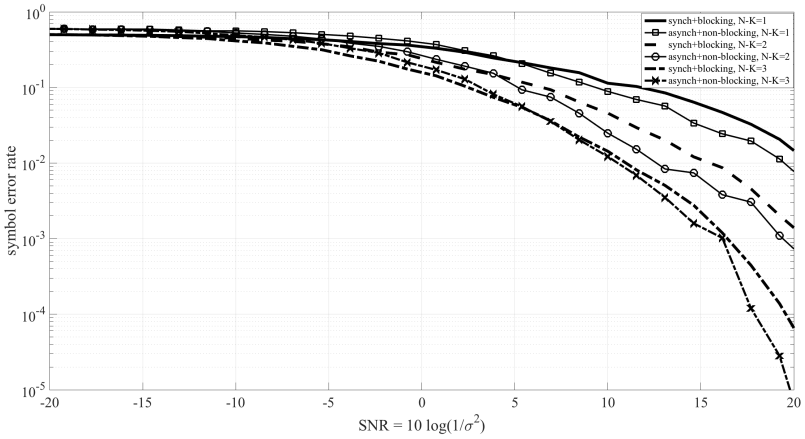

Figure 4.7: Symbol error rate versus $SNR = 10\log_{10}(1/\sigma^2)$ for $K = 3$ collided packets and N collected mixtures of packets in fully synchronous and fully asynchronous network operation modes, $\tilde{K} = 8$.

only subspace $U_\perp$ of Y_n.

4.6 Conclusion

We presented a blind collision resolution algorithm based on temporal diversity for slow fading channels. The method supports immediate transmissions in blocking and non-blocking modes. It also perfectly applies to synchronous networks similar to slot-synchronized NDMA protocols. The decoding complexity solely depends on the number of collided packets. Simulation results show high throughputs at a minimal increase of the queueing delay in the blocking mode. The stable range of the data arrival rate at a transmitter is reduced in the non-blocking mode.

Chapter 5

Conclusion

5.1 Summary

We presented a set of blind network-assisted diversity multiple access schemes using root-MUSIC-like algorithms. We first considered the collision resolution problem in the synchronous blocking mode and presented an analysis of the noise performance of the decoding algorithm. Then we extended the solution to the non-blocking mode in which the active set of transmitters may expand within the collision resolution interval. A corresponding throughput and delay analysis was presented. Finally we dismissed slot and symbol synchronization and tackled the collision resolution problem again in the blocking and non-blocking modes.

5.2 Future Research Directions

In this work we assumed a slow fading channel with additive white Gaussian noise. On each path from an involved transmitter to the receiver, fading does not change for the length of the collision resolution interval. One research direction is to extend the presented algorithms to fast fading channels, i.e. the channel may vary over consecutive time slots or within one slot. This

complicates the signal processing techniques used for signal separation. This also poses a network challenge to estimate the channels within the collision resolution interval. On a related note, in this work we assumed the involved transmitters are static. We may have to address channel estimation in a mobile scenario.

Another research direction is to exploit frequency and space diversity along with temporal diversity. Temporal diversity has the advantage that the number of retransmissions per collision resolution interval is dynamically adapted to the number of involved transmitters. However, transmissions on multi-frequency and space dimensions may yield diversity gains and enhance the robustness of the proposed algorithms.

Appendices

Appendix A

Appendix to Chapter 3

A.1 Rank(W_n)

Denote by θ_k the angle of complex exponential r_k. Let

$$\theta_k = \frac{k\pi}{\tilde{K}+1} + \phi_k, \quad 1 \leq k \leq \tilde{K} \tag{A.1}$$

where ϕ_k is a random variable that is uniformly distributed over $[-\frac{\pi}{2(\tilde{K}+1)}, \frac{\pi}{2(\tilde{K}+1)}]$, and $\{\phi_k\}_{k=1}^{\tilde{K}}$ are independent. Transmitter k joins the set of active transmitters at $t_k = (n_k - 1)P\tau$. Without loss of generality, assume $1 = n_1 \leq n_2 \leq \cdots \leq n_K$. The columns of W_n are arranged from left to right in non-decreasing order of $\{n_k\}_k$.

We prove by mathematical induction that

$$\text{rank}\left(W_{T_k}[:, 1:k]\right) = k, \tag{A.2}$$

where $T_k = \max(k, n_k)$. The proof goes as follows:

Base case: At $n = n_1 = 1$, the top left 1×1 submatrix of W_1 is a non-zero scalar, so $\text{rank}(W_1[:, 1:1]) = 1$.

Inductive step: Assume $\text{rank}(W_{T_{k-1}}[:, 1:(k-1)]) = k-1$.

For $T_{k-1} \leq n < T_k$, the top T_{k-1} rows of W_n are matrix $W_{T_{k-1}}$, so $\text{rank}(W_n[:, 1:(k-1)]) = k-1$ by the inductive step.

Let M hold the first $k-1$ columns of W_{T_k-1}. M has rank $k-1$. At $n = T_k$, we partition $W_{T_k}[:, 1:k]$ as follows:

$$W_{T_k}[:, 1:k] = \left(\begin{array}{c|c} M & \overrightarrow{w}_{k,T_k}^{(n_k-1)}[1:(T_k-1)] \\ \hline \overrightarrow{C}^T & \overrightarrow{w}_{k,T_k}^{(n_k-1)}[T_k] \end{array} \right) \tag{A.3}$$

where row vector $\overrightarrow{C}^T$ holds the T_k^{th} element of the shifted coding vectors of the first $k-1$ active transmitters: $\overrightarrow{C}^T = [\overrightarrow{w}_{1,T_k}^{(n_1-1)}[T_k], \ldots, \overrightarrow{w}_{k-1,T_k}^{(n_{k-1}-1)}[T_k]]$. Column $W_{T_k}[:, k]$ is simply the shifted coding vector of transmitter k, partitioned into its first $T_k - 1$ elements and the last element. The notation in (A.3) follows (3.2).

Since M in (A.3) is full rank almost surely, $W_{T_k}[:, 1:k]$ will be rank deficient only if its last column is in the span of the first $k-1$ columns, i.e.

$$\begin{aligned}\overrightarrow{w}_{k,T_k}^{(n_k-1)}[T_k] &= \left(\overrightarrow{C}^T \times M^\dagger\right) \times \overrightarrow{w}_{k,T_k}^{(n_k-1)}[1:(T_k-1)] \\ &= \overrightarrow{x}^T \times \overrightarrow{w}_{k,T_k}^{(n_k-1)}[1:(T_k-1)]\end{aligned} \tag{A.4}$$

where $M^\dagger = (M^H M)^{-1} M^H$ is the left inverse of M (it exists almost surely since M is full rank almost surely), and x^T is a row vector of length $T_k - 1$. We distinguish between two cases: if $n_k = T_k$, then $\overrightarrow{w}_{k,T_k}^{(n_k-1)}[T_k] = 1$ and $\overrightarrow{w}_{k,T_k}^{(n_k-1)}[1:(T_k-1)]$ is all zeros. In this case (A.4) is always false and $\text{rank}\,(W_{T_k}[:, 1:k]) = k$. On the other hand, if $n_k < T_k$, by rearranging (A.4) we get

$$[\overrightarrow{x}^T, -1] \times \begin{bmatrix} \overrightarrow{w}_{k,T_k}^{(n_k-1)}[1:(T_k-1)] \\ \overrightarrow{w}_{k,T_k}^{(n_k-1)}[T_k] \end{bmatrix} = [\overrightarrow{x}^T, -1] \times \overrightarrow{w}_{k,T_k}^{(n_k-1)} = 0 \tag{A.5}$$

$[\overrightarrow{x}^T, -1]$ is the horizontal concatenation of $\overrightarrow{x}^T$ and -1 while $\overrightarrow{w}_{k,T_k}^{(n_k-1)}$ is the vertical concatenation of $\overrightarrow{w}_{k,T_k}^{(n_k-1)}[1:(T_k-1)]$ and $\overrightarrow{w}_{k,T_k}^{(n_k-1)}[T_k]$. From (3.2), $\overrightarrow{w}_{k,T_k}^{(n_k-1)}$ is function of r_k. Suppose there are $T_k - n_k + 1$ values $\{r_{k,j}\}_{j=1}^{T_k-n_k+1}$ of r_k that satisfy (A.5). The corresponding vectors are denoted as $\{\overrightarrow{w}_{k,T_k}^{(n_k-1),j}\}_{j=1}^{T_k-n_k+1}$. In this case and using (A.5) we have

$$[\overrightarrow{x}^T, -1] \times \left(\overrightarrow{w}_{k,T_k}^{(n_k-1),1} \quad \dots \quad \overrightarrow{w}_{k,T_k}^{(n_k-1),T_k-n_k+1}\right) = \overrightarrow{0}^T \tag{A.6}$$

From (3.2), the top $n_k - 1$ rows of W^*, the matrix of vectors $\{\overrightarrow{w}_{k,T_k}^{(n_k-1),j}\}_{j=1}^{T_k-n_k+1}$ in (A.6), are all zeros. Therefore, the last $T_k - n_k + 1$ elements of vector $[\overrightarrow{x}^T, -1]$ in (A.6) form a left null vector of the bottom $T_k - n_k + 1$ rows of

W^*. However, from (3.2), these $T_k - n_k + 1$ rows are themselves a full rank Vandermonde matrix of rank $T_k - n_k + 1$. Therefore, the last $T_k - n_k + 1$ elements of row vector $[\overrightarrow{x}^T, -1]$ should be zero. However, the last element of $[\overrightarrow{x}^T, -1]$ is $-1 \neq 0$. This is a contradiction. Therefore, it is impossible to find $T_k - n_k + 1$ values $\{r_{k,j}\}_{j=1}^{T_k - n_k + 1}$ of r_k that satisfy (A.5). Thus, the number of valid roots r_k that satisfy (A.5) is at most $T_k - n_k$ which is finite. Since $\theta_k = \angle r_k$ in (A.1) is randomly selected from a continuous range, (A.5) is not satisfied almost surely. Thus, $\text{rank}\,(W_{T_k}[:, 1:k]) = \text{rank}(M) + 1 = k$ almost surely. This completes the proof by induction.

A.2 Computation of $P(m, i)$

$P(m, -1)$ denotes the probability that a CRI of length m starts at instant t_0, and some particular transmitter k^* does not get involved throughout the CRI. The latter event happens with probability $p_e e^{-\lambda(m-1)}$. The probability of the former event is that of a CRI of length m assuming the network size is $\tilde{K} - 1$. Therefore,

$$P(m, -1|\tilde{K}) = \begin{cases} p_e e^{-\lambda(m-1)} \times P(m|\tilde{K} - 1), & 1 \leq m \leq \tilde{K} \\ 0, & m = \tilde{K} + 1 \end{cases} \tag{A.7}$$

The dependence on the network size is stated explicitly in (A.7) for clarity. The computation of $P(m|\tilde{K} - 1)$ is described in Section 3.2.

$P(m,i)$ denotes the probability that a CRI of length m starts at instant t_0, and transmitter k^* gets involved in that CRI in the i^{th} slot, where $1 \leq i < m$. The event that a CRI of length m occurs may be partitioned into three cases:

1. A CRI of length m occurs and transmitter k^* gets involved in slot i. This happens with probability $P(m,i)$.

2. A CRI of length m occurs and transmitter k^* gets involved in some slot other than slot i. This happens with probability $\text{pb}_{m,i}$.

3. A CRI of length m occurs and transmitter k^* is not involved at all. This happens with probability $P(m,-1)$.

Therefore, $P(m,i)$ is given by

$$P(m,i) = \begin{cases} P(m) - P(m,-1) - \text{pb}_{m,i}, & m > 1, \quad i < m \\ 0, & \text{o.w.} \end{cases} \tag{A.8}$$

$P(m)$ may be computed as in Section 3.2, and $P(m,-1)$ may be computed as in (A.7). A polynomial-time algorithm to compute $\text{pb}_{m,i}$ is presented in the code below. The derivation of the algorithm is tedious and thus is skipped for brevity.

```
function pb_m_i = P_m_involved_not_at_i(m,i,Ktilde,
    lambda,pi_vec, pe)
```

```
%pb_m_i: probability that a CRI has length m and that a
   transmitter gets
%involved in the CRI but not at slot i
%i:index of slot at which desired transmitter involved
%m: length of CRI
%lambda: rate of packets per slot
%Ktilde: size of network
%pi_vec: vector holding probabilities of equation 6
%pe: probability that the buffer of a transmitter is
   empty before the start
%of a CRI

assert(i<m); %Otherwise, need not call this function
   since it is
              %definitely the case that for a CRI of
                 length m a tx cannot
              %get involved at i>=m

K = m-1;    %nb of active txs

%first row of treeStructure corresponds to last level of
    T_K
%next two rows of treeStructure correspond to
   penultimate level of T_K
%...
%last K rows of treeStructure correspond to first level
   of T_k(the root)
%below memory requirement not necessary but only assumed
    for simplicity
treeStructure = -1*ones(K*(1+K)/2,K);

treeStructure(1,:) = pi_vec;
%scaling below to account for the fact that one of the K
    transmitters
%cannot be assigned to slot i, which reduces the number
   of orderings of
%the K transmitters
```

```
treeStructure(1,i) = treeStructure(1,i) *(K-1)/ K;

cnt = 1;
for e = 1:(K-1) %moving up tree T_K
    temp = sum(treeStructure(cnt:-1:(cnt-e+1),1:(size(
       treeStructure,2)-(e-1))),1);
    temp = cumsum(temp(end:-1:2));
    temp = temp(end:-1:1);
    cnt = cnt+1;
    treeStructure(cnt,1:length(temp)) = temp.*pi_vec
       (1,1:length(temp));
    cnt2 = cnt;
    for e2 = 1:e
        cnt = cnt+1;
        treeStructure(cnt,1:length(temp)) = 1/(e2+1)*
           treeStructure(cnt2-e+e2-1,1:length(temp)).*
           pi_vec(1,1:length(temp));
    end
    if i <= (K-e)
        a = 1;
        for e3 = (cnt-e):cnt
            %scaling below to account for the fact that
               one of the K transmitters
            %cannot be assigned to slot i, which reduces
                the number of orderings of
            %the K transmitters
            treeStructure(e3,i) = treeStructure(e3,i) *
               (K - a) / (K-(a-1));
            a = a+1;
        end
    end
end

pb_normalized = sum(treeStructure((end-K+1):end,1));
pb_m_i = pb_normalized * nchoosek(Ktilde-1,K-1) *
   factorial(K) * pe^(Ktilde-K) * exp(-(Ktilde-K)*(m-1)*
   lambda);
```

```
return;
```

Appendix B

Appendix to Chapter 4

B.1 Rank(W_n)

Denote by θ_k the angle of complex exponential r_k. Let

$$\theta_k = \frac{k\pi}{\tilde{K}+1} + \phi_k, \quad 1 \le k \le \tilde{K} \tag{B.1}$$

where ϕ_k is a random variable that is uniformly distributed over $[-\frac{\pi}{2(\tilde{K}+1)}, \frac{\pi}{2(\tilde{K}+1)}]$, and $\{\phi_k\}_{k=1}^{\tilde{K}}$ are independent. Transmitter k joins the set of active transmitters at $t_k = ((n_k-1)P + p_k)\tau$. Without loss of generality, assume $1 = n_1 \le n_2 \le \cdots \le n_K$. Column blocks $\{\overrightarrow{w}_{k,n,t_k,\beta}\}_k$ of $W_{n,\beta}$ are arranged in $W_{n,\beta}$ from left to right in non-decreasing order of $\{n_k\}_k$. Moreover, $p_1 = 0$ and $p_k = (t_k - t_1)\%(P\tau)$. We prove by mathematical induction that

$$\begin{aligned} &\text{rank}\left(W_{T_k,\beta}[:, 1:h_k]\right) = h_k \\ &\text{rank}\left(W_{T_k+\mathbf{1}\{p_k>0\},\beta}[:, 1:(h_k+\mathbf{1}\{p_k>0\})]\right) = h_k + \mathbf{1}\{p_k>0\} \end{aligned} \tag{B.2}$$

where

$$h_k = k + \sum_{k'=1}^{k-1} \mathbf{1}\{p_{k'} > 0\} = h_{k-1} + \mathbf{1}\{p_{k-1} > 0\} + 1 \tag{B.3}$$

$\mathbf{1}\{\cdot\}$ is the indicator function. T_k is defined by the following recurrence relation

$$\begin{aligned} T_1 &= 1 \\ T_k &= \max\left(T_{k-1} + \mathbf{1}\{p_{k-1} > 0\} + 1, n_k\right) \end{aligned} \tag{B.4}$$

The proof goes as follows:

Base case: At $n = n_1 = 1$, the top left 1×1 submatrix of $W_{1,\beta}$ is a non-zero scalar, so $\text{rank}(W_{1,\beta}[:, 1:1]) = 1$.

Inductive step: Assume $\text{rank}(W_{T_{k-1},\beta}[:, 1 : h_{k-1}]) = h_{k-1}$. Moreover, if $p_{k-1} > 0$, assume $\text{rank}(W_{T_{k-1}+1,\beta}[:, 1 : (h_{k-1} + 1)]) = h_{k-1} + 1$.

For $(T_{k-1} + \mathbf{1}\{p_{k-1} > 0\}) \leq n < T_k$, the top $T_{k-1} + \mathbf{1}\{p_{k-1} > 0\}$ rows of $W_{n,\beta}$ are matrix $W_{T_{k-1}+\mathbf{1}\{p_{k-1}>0\},\beta}$, so $\text{rank}(W_{n,\beta}[:, 1 : h_{k-1} + \mathbf{1}\{p_{k-1} > 0\}]) = h_{k-1} + \mathbf{1}\{p_{k-1} > 0\}$ by the inductive step.

Consider $W_{n,\beta}$ for $n = T_k$. Let M hold the first $h_{k-1} + \mathbf{1}\{p_{k-1} > 0\}$ columns of $W_{T_k-1,\beta}$. M has rank $h_{k-1} + \mathbf{1}\{p_{k-1} > 0\} = h_k - 1$. We partition $W_{T_k,\beta}[:, 1 : h_k]$ as follows:

$$W_{T_k,\beta}[:, 1:h_k] = \left(\begin{array}{c|c} M & \overrightarrow{w}_{k,T_k,\beta}^{(n_k-1)}[1:(T_k-1)] \\ \hline C_1^T & \overrightarrow{w}_{k,T_k,\beta}^{(n_k-1)}[T_k] \end{array} \right) \tag{B.5}$$

where $C_1^T = [\overrightarrow{w}_{1,T_k,t_1,\beta}[T_k,:], \ldots, \overrightarrow{w}_{k-1,T_k,t_{k-1},\beta}[T_k,:]]$. Using (4.21), note that row vector C_1^T has $h_{k-1} + \mathbf{1}\{p_{k-1} > 0\}$ elements.

Column $W_{T_k,\beta}[:, h_k]$ is spanned by columns $W_{T_k,\beta}[:, 1:h_k-1]$ for at most $T_k - n_k$ values of r_k. The proof is analogous to the synchronous case in Appendix A.1 where we show that column $W_{T_k}[:, k]$ is spanned by columns $W_{T_k}[:, 1:k-1]$ for only a finite number of values of r_k. Since $\theta_k = \angle r_k$ in (B.1) is randomly selected from a continuous range, then $W_{T_k,\beta}[:, h_k]$ is not spanned by $W_{T_k,\beta}[:, 1:h_k-1]$ almost surely. Moreover, $\text{rank}(W_{T_k,\beta}[:, 1:h_k-1]) = \text{rank}(M) = h_k - 1$. Thus, $\text{rank}(W_{T_k,\beta}[:, 1:h_k]) = h_k$. This proves the first equality in (B.2).

In the case where $p_k > 0$, let $\Omega = W_{T_k+1,\beta}[:, 1:(h_k+1)]$ and $\overrightarrow{\omega}_k = \overrightarrow{w}_{k,T_k+1,\beta}$. Ω can be partitioned as

$$\Omega = \left(\begin{array}{c|c|c} M & \overrightarrow{\omega}_k^{(n_k-1)}[1:(T_k-1)] & \overrightarrow{\omega}_k^{(n_k)}[1:(T_k-1)] \\ \hline C_1^T & \overrightarrow{\omega}_k^{(n_k-1)}[T_k] & \overrightarrow{\omega}_k^{(n_k)}[T_k] \\ \hline C_2^T & \overrightarrow{\omega}_k^{(n_k-1)}[T_k+1] & \overrightarrow{\omega}_k^{(n_k)}[T_k+1] \end{array} \right) \tag{B.6}$$

where $C_2^T = [\overrightarrow{w}_{1,T_k+1,t_1,\beta}[T_k+1,:], \ldots, \overrightarrow{w}_{k-1,T_k+1,t_{k-1},\beta}[T_k+1,:]]$. Ω has dimensions $(T_k+1) \times (h_k+1)$. Note that $W_{T_k,\beta}[:, 1:h_k]$ in (B.5) is the 2×2 top left subblocks of Ω in (B.6).

Let D be the 2×2 bottom right submatrix of Ω. Let $C_{1,2}^T$ be the vertical concatenation of C_1^T and C_2^T in (B.6), so $C_{1,2}^T$ has dimensions $2 \times (h_k - 1)$. On the other hand, M is a $(T_k - 1) \times (h_k - 1)$ matrix that has rank $h_k - 1$ almost surely. Let $M_{\mathcal{S}}$ be the selection of $h_k - 1$ rows of M that are full rank, so $M_{\mathcal{S}}$ is a square matrix. Denote by $\overrightarrow{\omega}_a$ and $\overrightarrow{\omega}_b$ the corresponding selections of the elements of column vectors $\overrightarrow{\omega}_k^{(n_k-1)}[1 : (T_k - 1)]$ and $\overrightarrow{\omega}_k^{(n_k)}[1 : (T_k - 1)]$ respectively. Let $\overrightarrow{\omega}_{a,b}$ be the horizontal concatenation of $\overrightarrow{\omega}_a$ and $\overrightarrow{\omega}_b$, so $\overrightarrow{\omega}_{a,b}$ is $(h_k - 1) \times 2$. Form the matrix

$$\Omega_{\mathcal{S}} = \left(\begin{array}{c|c} M_{\mathcal{S}} & \overrightarrow{\omega}_{a,b} \\ \hline C_{1,2}^T & D \end{array} \right) \tag{B.7}$$

$\Omega_{\mathcal{S}}$ is thus a selection of $h_k + 1$ rows of Ω and is a square matrix. Since $M_{\mathcal{S}}$ is a square matrix that is invertible almost surely, we can factorize $\Omega_{\mathcal{S}}$ using the Schur complement:

$$\Omega_{\mathcal{S}} = \begin{pmatrix} I & 0 \\ C_{1,2}^T M_{\mathcal{S}}^{-1} & I \end{pmatrix} \times \begin{pmatrix} M_{\mathcal{S}} & 0 \\ 0 & \Omega_{\mathcal{S}}/M_{\mathcal{S}} \end{pmatrix} \times \begin{pmatrix} I & M_{\mathcal{S}}^{-1} \overrightarrow{\omega}_{a,b} \\ 0 & I \end{pmatrix} \tag{B.8}$$

where

$$\Omega_{\mathcal{S}}/M_{\mathcal{S}} = D - C_{1,2}^T M_{\mathcal{S}}^{-1} \overrightarrow{\omega}_{a,b} \tag{B.9}$$

Apply the determinant to both sides of (B.8). We obtain

$$|\Omega_{\mathcal{S}}| = |M_{\mathcal{S}}| \times |\Omega_{\mathcal{S}}/M_{\mathcal{S}}| \tag{B.10}$$

Determinant $|M_{\mathbb{S}}|$ is non-zero almost surely. Therefore, $\Omega_{\mathbb{S}}$ is full rank almost surely if the 2×2 matrix $\Omega_{\mathbb{S}}/M_{\mathbb{S}}$ is full rank almost surely. Expanding (B.9), we have

$$\Omega_{\mathbb{S}}/M_{\mathbb{S}} = \begin{pmatrix} D[1,1] - C_1^T M_{\mathbb{S}}^{-1} \overrightarrow{\omega}_a & D[1,2] - C_1^T M_{\mathbb{S}}^{-1} \overrightarrow{\omega}_b \\ D[2,1] - C_2^T M_{\mathbb{S}}^{-1} \overrightarrow{\omega}_a & D[2,2] - C_2^T M_{\mathbb{S}}^{-1} \overrightarrow{\omega}_b \end{pmatrix} \tag{B.11}$$

The elements of D, $\overrightarrow{\omega}_a$ and $\overrightarrow{\omega}_b$ hold exponents of r_k. However, from (B.6), $D[1,1]$ and $D[2,1]$ hold higher-order exponents of r_k compared to $\overrightarrow{\omega}_a$. Similarly, $D[1,2]$ and $D[2,2]$ hold higher-order exponents of r_k compared to $\overrightarrow{\omega}_b$. Thus, determinant $|\Omega_{\mathbb{S}}/M_{\mathbb{S}}|$ can be expressed as

$$|\Omega_{\mathbb{S}}/M_{\mathbb{S}}| = |D| + \text{lower-order exponents of } r_k \tag{B.12}$$

Expanding $|D|$ we get

$$|D| = \overrightarrow{\omega}_k^{(n_k-1)}[T_k] \times \overrightarrow{\omega}_k^{(n_k)}[T_k+1] - \overrightarrow{\omega}_k^{(n_k-1)}[T_k+1] \times \overrightarrow{\omega}_k^{(n_k)}[T_k] \tag{B.13}$$

From (B.4), $T_k \geq n_k$. Thus

$$|D| = \begin{cases} r_k^{2(T_k-n_k)} = 1 & \text{if } T_k = n_k \\ (\beta^2 - 1)\, r_k^{2(T_k-n_k)} & \text{if } T_k > n_k, (T_k - n_k)\%2 = 1 \\ (1-\beta^2)\, r_k^{2(T_k-n_k)} & \text{if } T_k > n_k, (T_k - n_k)\%2 = 0 \end{cases} \tag{B.14}$$

Since $\beta^2 \neq 1$, (B.12) and (B.14) imply that $|\Omega_{\mathbb{S}}/M_{\mathbb{S}}|$ is a non-trivial polynomial in r_k of degree $2(T_k - n_k)$. Thus, $|\Omega_{\mathbb{S}}/M_{\mathbb{S}}| = 0$ admits at most $2(T_k - n_k)$ unit

circle roots r_k, which is a finite number of solutions. Since $\theta_k = \angle r_k$ in (B.1) is randomly selected from a continuous range,

$$|\Omega_{\mathcal{S}}/M_{\mathcal{S}}| \neq 0 \tag{B.15}$$

almost surely. (B.10) and (B.15) imply

$$|\Omega_{\mathcal{S}}| \neq 0 \tag{B.16}$$

Thus, $\text{rank}(\Omega) = \text{rank}(\Omega_{\mathcal{S}}) = \text{rank}(M_{\mathcal{S}}) + 2 = h_k + 1$. This proves the second equality in (B.2) and completes the proof by induction.

Bibliography

[1] R. Zhang, N. D. Sidiropoulos, and M. K. Tsatsanis, "Collision resolution in packet radio networks using rotational invariance techniques," *IEEE Transactions on Communications*, vol. 50, pp. 146–155, Jan 2002.

[2] R. G. Dimitri Bertsekas, *Data Networks*. Prentice Hall, Inc, 1992.

[3] W. Z. Jon W. Mark, *Wireless Communications and Networking*. Pearson Education, Inc., 2003.

[4] S. Gollakota, S. D. Perli, and D. Katabi, "Interference alignment and cancellation," *SIGCOMM Comput. Commun. Rev.*, vol. 39, pp. 159–170, Aug. 2009.

[5] O. E. Ayach, S. W. Peters, and R. W. Heath, "The practical challenges of interference alignment," *IEEE Wireless Communications*, vol. 20, pp. 35–42, February 2013.

[6] G. Dimic, N. D. Sidiropoulos, and R. Zhang, "Medium access control - physical cross-layer design," *IEEE Signal Processing Magazine*, vol. 21, pp. 40–50, Sept 2004.

[7] H. Jin, S. W. Jeon, and B. C. Jung, "Opportunistic interference alignment for random access networks," *IEEE Transactions on Vehicular Technology*, vol. 64, pp. 5947–5954, Dec 2015.

[8] Y. Liang, X. Li, J. Zhang, and Y. Liu, "A novel random access scheme based on successive interference cancellation for 5g networks," in *2017 IEEE Wireless Communications and Networking Conference (WCNC)*, pp. 1–6, March 2017.

[9] M. Kontik and S. C. Ergen, "Distributed medium access control protocol for successive interference cancellation-based wireless ad hoc networks," *IEEE Communications Letters*, vol. 21, pp. 354–357, Feb 2017.

[10] M. K. Tsatsanis, R. Zhang, and S. Banerjee, "Network-assisted diversity for random access wireless networks," *IEEE Transactions on Signal Processing*, vol. 48, pp. 702–711, Mar 2000.

[11] R. Zhang and M. K. Tsatsanis, "Network-assisted diversity multiple access in dispersive channels," *IEEE Transactions on Communications*, vol. 50, pp. 623–632, Apr 2002.

[12] R. Lin and A. P. Petropulu, "A new wireless network medium access protocol based on cooperation," *IEEE Transactions on Signal Processing*, vol. 53, pp. 4675–4684, Dec 2005.

[13] H. Yang, A. P. Petropulu, X. Yang, and T. Camp, "A novel location relay selection scheme for alliances," *IEEE Transactions on Vehicular Technology*, vol. 57, pp. 1272–1284, March 2008.

[14] L. Dong and A. P. Petropulu, "Multichannel alliances: A cooperative cross-layer scheme for wireless networks," *IEEE Transactions on Signal*

Processing, vol. 56, pp. 771–784, Feb 2008.

[15] R. Zhang, M. K. Tsatsanis, and N. D. Sidiropoulos, "Performance analysis of a random access packet radio system with joint network-spatial diversity," in *2000 IEEE International Conference on Acoustics, Speech, and Signal Processing. Proceedings (Cat. No.00CH37100)*, vol. 5, pp. 2593–2596 vol.5, 2000.

[16] Y. Yu and G. B. Giannakis, "High-throughput random access using successive interference cancellation in a tree algorithm," *IEEE Transactions on Information Theory*, vol. 53, pp. 4628–4639, Dec 2007.

[17] R. Samano-Robles, M. Ghogho, and D. C. McLernon, "A contention binary tree algorithm assisted by source separation," in *2007 IEEE 8th Workshop on Signal Processing Advances in Wireless Communications*, pp. 1–5, June 2007.

[18] R. Samano-Robles, M. Ghogho, and D. C. McLernon, "A multiaccess protocol assisted by retransmission diversity and multipacket reception," in *2008 IEEE International Conference on Acoustics, Speech and Signal Processing*, pp. 3005–3008, March 2008.

[19] R. Samano-Robles, M. Ghogho, and D. C. McLernon, "An infinite user model for random access protocols assisted by multipacket reception and retransmission diversity," in *2008 IEEE 9th Workshop on Signal Processing Advances in Wireless Communications*, pp. 111–115, July 2008.

[20] Y. H. Nam, P. K. Gopala, and H. El-Gamal, "Resolving collisions via incremental redundancy: Arq diversity," in *IEEE INFOCOM 2007 - 26th IEEE International Conference on Computer Communications*, pp. 285–293, May 2007.

[21] R. Dinis, P. Montezuma, L. Bernardo, R. Oliveira, M. Pereira, and P. Pinto, "Frequency-domain multipacket detection: a high throughput technique for sc-fde systems," *IEEE Transactions on Wireless Communications*, vol. 8, pp. 3798–3807, July 2009.

[22] A. P. Liavas and P. A. Regalia, "On the behavior of information theoretic criteria for model order selection," *IEEE Transactions on Signal Processing*, vol. 49, pp. 1689–1695, Aug 2001.

[23] M. Wax and T. Kailath, "Detection of signals by information theoretic criteria," *IEEE Transactions on Acoustics, Speech, and Signal Processing*, vol. 33, pp. 387–392, Apr 1985.

[24] Q. T. Zhang, K. M. Wong, P. C. Yip, and J. P. Reilly, "Statistical analysis of the performance of information theoretic criteria in the detection of the number of signals in array processing," *IEEE Transactions on Acoustics, Speech, and Signal Processing*, vol. 37, pp. 1557–1567, Oct 1989.

[25] B.Escrig, "Random matrix theory applied to the estimation of collision multiplicities," 01 2012.

[26] B. Ozgul and H. Delic, "Blind collision multiplicity detection for wireless access with retransmission diversity," in *IEEE 60th Vehicular Technology Conference, 2004. VTC2004-Fall. 2004*, vol. 2, pp. 1078–1082 Vol. 2, Sept 2004.

[27] R. Ahlswede, N. Cai, S. Y. R. Li, and R. W. Yeung, "Network information flow," *IEEE Transactions on Information Theory*, vol. 46, pp. 1204–1216, Jul 2000.

[28] S. Y. R. Li, R. W. Yeung, and N. Cai, "Linear network coding," *IEEE Transactions on Information Theory*, vol. 49, pp. 371–381, Feb 2003.

[29] R. Koetter and M. Medard, "An algebraic approach to network coding," *IEEE/ACM Transactions on Networking*, vol. 11, pp. 782–795, Oct 2003.

[30] T. Ho, M. Medard, J. Shi, M. Effros, and D. R. Karger, "On randomized network coding," in *In Proceedings of 41st Annual Allerton Conference on Communication, Control, and Computing*, 2003.

[31] P. Ostovari, J. Wu, and A. Khreishah, *Network Coding Techniques for Wireless and Sensor Networks*, pp. 129–162. Berlin, Heidelberg: Springer Berlin Heidelberg, 2014.

[32] S. Katti, S. Gollakota, and D. Katabi, "Embracing wireless interference: Analog network coding," *SIGCOMM Comput. Commun. Rev.*, vol. 37, pp. 397–408, Aug. 2007.

[33] S. Katti, H. Rahul, W. Hu, D. Katabi, M. Medard, and J. Crowcroft, "Xors in the air: Practical wireless network coding," *IEEE/ACM Transactions on Networking*, vol. 16, pp. 497–510, June 2008.

[34] J. s. Park, M. Gerla, D. S. Lun, Y. Yi, and M. Medard, "Codecast: a network-coding-based ad hoc multicast protocol," *IEEE Wireless Communications*, vol. 13, pp. 76–81, October 2006.

[35] S. Zhang, S. C. Liew, and P. P. Lam, "Physical layer network coding," *CoRR*, vol. abs/0704.2475, 2007.

[36] S. Chachulski, M. Jennings, S. Katti, and D. Katabi, "Trading structure for randomness in wireless opportunistic routing," *SIGCOMM Comput. Commun. Rev.*, vol. 37, pp. 169–180, Aug. 2007.

[37] A. Vahid, M. A. Maddah-Ali, and A. S. Avestimehr, "Communication through collisions: Opportunistic utilization of past receptions," *CoRR*, vol. abs/1312.0116, 2013.

[38] J. Goseling, M. Gastpar, and J. H. Weber, "Random access with physical-layer network coding," *IEEE Transactions on Information Theory*, vol. 61, pp. 3670–3681, July 2015.

[39] G. Cocco, C. Ibars, D. Gunduz, and O. del Rio Herrero, "Collision resolution in slotted aloha with multi-user physical-layer network coding," in *2011 IEEE 73rd Vehicular Technology Conference (VTC Spring)*, pp. 1–4, May 2011.

[40] H. C. Bui, J. Lacan, and M. Boucheret, "NCSA: A new protocol for random multiple access based on physical layer network coding," *CoRR*, vol. abs/1009.4773, 2010.

[41] E. Casini, R. D. Gaudenzi, and O. D. R. Herrero, "Contention resolution diversity slotted aloha (crdsa): An enhanced random access schemefor satellite access packet networks," *IEEE Transactions on Wireless Communications*, vol. 6, pp. 1408–1419, April 2007.

[42] E. Paolini, G. Liva, and M. Chiani, "High throughput random access via codes on graphs: Coded slotted aloha," in *2011 IEEE International Conference on Communications (ICC)*, pp. 1–6, June 2011.

[43] G. Liva, "Graph-based analysis and optimization of contention resolution diversity slotted aloha," *IEEE Transactions on Communications*, vol. 59, pp. 477–487, February 2011.

[44] D. Halperin, T. Anderson, and D. Wetherall, "Taking the sting out of carrier sense: Interference cancellation for wireless lans," in *Proceedings of the 14th ACM International Conference on Mobile Computing and Networking*, MobiCom '08, (New York, NY, USA), pp. 339–350, ACM, 2008.

[45] Y. Yu and G. B. Giannakis, "Sicta: a 0.693 contention tree algorithm using successive interference cancellation," in *Proceedings IEEE 24th Annual Joint Conference of the IEEE Computer and Communications Societies.*, vol. 3, pp. 1908–1916 vol. 3, March 2005.

[46] C. Ware, J. Chicharo, and T. Wysocki, "Modelling capture behaviour in ieee 802.11 radio modems," 01 2001.

[47] J. Lee, W. Kim, S.-J. Lee, D. Jo, J. Ryu, T. Kwon, and Y. Choi, "An experimental study on the capture effect in 802.11a networks," in *Proceedings of the Second ACM International Workshop on Wireless Network Testbeds, Experimental Evaluation and Characterization*, WinTECH '07, (New York, NY, USA), pp. 19–26, ACM, 2007.

[48] X. Li and Q.-A. Zeng, "Performance analysis of the ieee 802.11 mac protocol over a wlan with capture effect," *Information and Media Technologies*, vol. 1, no. 1, pp. 679–685, 2006.

[49] M. G. Jibukumar, S. Shajahan, P. Preetha, and G. Sethulekshmi, "Impact of capture effect on receiver initiated collision detection with sequential resolution in wlan," in *2015 International Computer Science and Engineering Conference (ICSEC)*, pp. 1–6, Nov 2015.

[50] S. Gollakota and D. Katabi, "Zigzag decoding: Combating hidden terminals in wireless networks," *SIGCOMM Comput. Commun. Rev.*, vol. 38, pp. 159–170, Aug. 2008.

[51] M. S. Rahman, Y. Li, and B. Vucetic, "An iterative zigzag decoding for combating collisions in wireless networks," *IEEE Communications Letters*, vol. 14, pp. 242–244, March 2010.

[52] L. Zheng and L. Cai, "Afda: Asynchronous flipped diversity aloha for emerging wireless networks with long and heterogeneous delay," *IEEE Transactions on Emerging Topics in Computing*, vol. 3, pp. 64–73, March 2015.

[53] D. Ismail, M. Rahman, A. Saifullah, and S. Madria, "Rnr: Reverse replace decoding for collision recovery in wireless sensor networks," in *2017 14th Annual IEEE International Conference on Sensing, Communication, and Networking (SECON)*, pp. 1–9, June 2017.

[54] X. Zhang and K. G. Shin, "Cooperation without synchronization: Practical cooperative relaying for wireless networks," *IEEE Transactions on Mobile Computing*, vol. 14, pp. 937–950, May 2015.

[55] L. Kong and X. Liu, "mzig: Enabling multi-packet reception in zigbee," in *Proceedings of the 21st Annual International Conference on Mobile Computing and Networking*, MobiCom '15, (New York, NY, USA), pp. 552–565, ACM, 2015.

[56] `http://www.zigbee.org`.

[57] L. Lu, S. C. Liew, and S. Zhang, "Collision resolution by exploiting symbol misalignment," *CoRR*, vol. abs/0810.0326, 2008.

[58] S. Verdu, "Minimum probability of error for asynchronous gaussian multiple-access channels," *IEEE Transactions on Information Theory*, vol. 32, pp. 85–96, January 1986.

[59] L. Lu, S. C. Liew, and S. Zhang, "Channel-coded collision resolution by exploiting symbol misalignment," in *2010 IEEE International Conference on Communications*, pp. 1–6, May 2010.

[60] D. D. Lin and T. J. Lim, "Subspace-based active user identification for a collision-free slotted ad hoc network," *IEEE Transactions on Communications*, vol. 52, pp. 612–621, April 2004.

[61] X. Wang and H. V. Poor, "Blind multiuser detection: a subspace approach," *IEEE Transactions on Information Theory*, vol. 44, pp. 677–690, Mar 1998.

[62] X. Wang and A. Host-Madsen, "Group-blind multiuser detection for uplink cdma," *IEEE Journal on Selected Areas in Communications*, vol. 17, pp. 1971–1984, Nov 1999.

[63] S. Verdu, *Multiuser Detection*. New York, NY, USA: Cambridge University Press, 1st ed., 1998.

[64] B. Ozgul and H. Delic, "Wireless access with blind collision-multiplicity detection and retransmission diversity for quasi-static channels," *IEEE Transactions on Communications*, vol. 54, pp. 858–867, May 2006.

[65] J. Yao, X. Yang, J. Li, Z. Li, and Y. Zhang, "Blind collision resolution using cooperative transmission," in *2010 IEEE 71st Vehicular Technology Conference*, pp. 1–5, May 2010.

[66] J. Yao, X. Yang, and J. Li, "A blind collision resolution protocol based on cooperative transmission," *Wireless Personal Communications*, vol. 64, pp. 273–286, May 2012.

[67] S. Talwar, M. Viberg, and A. Paulraj, "Blind separation of synchronous co-channel digital signals using an antenna array. i. algorithms," *IEEE Transactions on Signal Processing*, vol. 44, pp. 1184–1197, May 1996.

[68] T. Li and N. D. Sidiropoulos, "Blind digital signal separation using successive interference cancellation iterative least squares," *IEEE Transactions on Signal Processing*, vol. 48, pp. 3146–3152, Nov 2000.

[69] S. Feng, M. Wang, J. Yan, Y. Zhu, and Z. Li, "Independent component analysis based tag anti-collision algorithm in multi-antenna radio frequency identification," in *2015 5th International Conference on Information Science and Technology (ICIST)*, pp. 519–524, April 2015.

[70] X. Liu, A. P. Petropulu, H. V. Poor, and V. Koivunen, "Blind separation of two users based on user delays and optimal pulse-shape design," *EURASIP Journal on Wireless Communications and Networking*, vol. 2010, p. 939340, Jun 2010.

[71] A. P. Petropulu, M. Olivieri, Y. Yu, L. Dong, and A. Lackpour, "Pulse-shaping for blind multi-user separation in distributed miso configurations," in *2008 IEEE International Conference on Acoustics, Speech and Signal Processing*, pp. 2741–2744, March 2008.

[72] X. Liu, S. Oymak, A. P. Petropulu, and K. R. Dandekar, "Collision resolution based on pulse shape diversity," in *2009 IEEE 10th Workshop on Signal Processing Advances in Wireless Communications*, pp. 409–413, June 2009.

[73] X. Liu, J. Kountouriotis, A. P. Petropulu, and K. R. Dandekar, "Aloha with collision resolution: Physical layer description and software defined radio implementation," in *2010 IEEE International Conference on Acoustics, Speech and Signal Processing*, pp. 3330–3333, March 2010.

[74] C. Zhang, Y. Wang, and F. Jing, "Underdetermined blind source separation of synchronous orthogonal frequency hopping signals based on single source points detection," *Sensors*, vol. 17, no. 9, 2017.

[75] Q. Zhao and L. Tong, "Semi-blind collision resolution in random access wireless ad hoc networks," *IEEE Transactions on Signal Processing*, vol. 48, pp. 2910–2920, Oct 2000.

[76] R. Djapic, A. J. van der Veen, and L. Tong, "Synchronization and packet separation in wireless ad hoc networks by known modulus algorithms," *IEEE Journal on Selected Areas in Communications*, vol. 23, pp. 51–64, Jan 2005.

[77] A. G. Orozco-Lugo, M. M. Lara, D. C. McLernon, and H. J. Muro-Lemus, "Multiple packet reception in wireless ad hoc networks using polynomial phase-modulating sequences," *IEEE Transactions on Signal Processing*, vol. 51, pp. 2093–2110, Aug 2003.

[78] S. Jochen, *Mobile Communications*. Boston, MA, USA: Addison-Wesley Longman Publishing Co., Inc., 2 ed., 2003.

[79] S. Khurana, A. Kahol, and A. P. Jayasumana, "Effect of hidden terminals on the performance of ieee 802.11 mac protocol," in *Local Computer Networks, 1998. LCN '98. Proceedings., 23rd Annual Conference on*, pp. 12–20, Oct 1998.

[80] A. Baiocchi and A. Todini, "Collision recovery in ieee 802.11 wlans,"

[81] H. Hwang, A. Zekeriya, G. Marshall, and A. Yakovlev, "Direction of arrival estimation using a root-music algorithm," *Lecture Notes in Engineering and Computer Science*, vol. 2169, 03 2008.

[82] J. Liu, X. Liu, and X. Ma, "First-order perturbation analysis of singular vectors in singular value decomposition," in *2007 IEEE/SP 14th Workshop on Statistical Signal Processing*, pp. 532–536, Aug 2007.

[83] R. J. Vaccaro, "A second-order perturbation expansion for the svd," *SIAM J. Matrix Anal. Appl.*, vol. 15, pp. 661–671, Apr. 1994.

[84] Z. Xu, "Perturbation analysis for subspace decomposition with applications in subspace-based algorithms," *IEEE Transactions on Signal Processing*, vol. 50, pp. 2820–2830, Nov 2002.

[85] F. Li, H. Liu, and R. J. Vaccaro, "Performance analysis for doa estimation algorithms: unification, simplification, and observations," *IEEE Transac-*

tions on Aerospace and Electronic Systems, vol. 29, pp. 1170–1184, Oct 1993.

[86] N. P. Waweru, D. B. O. Konditi, and P. K. Langat, "Performance Analysis of MUSIC, Root-MUSIC and ESPRIT DOA Estimation Algorithm," Mar. 2014.

[87] T. B. Lavate, V. K. Kokate, and A. M. Sapkal, "Performance analysis of music and esprit doa estimation algorithms for adaptive array smart antenna in mobile communication," in *2010 Second International Conference on Computer and Network Technology*, pp. 308–311, April 2010.

[88] A. Samadhiya, "Performance analysis of music and mvdr doa estimation algorithm," 2014.

[89] H. Krim, P. Forster, and J. G. Proakis, "Operator approach to performance analysis of root-music and root-min-norm," *IEEE Transactions on Signal Processing*, vol. 40, pp. 1687–1696, Jul 1992.

[90] B. D. Rao and K. V. S. Hari, "Performance analysis of root-music," *IEEE Transactions on Acoustics, Speech, and Signal Processing*, vol. 37, pp. 1939–1949, Dec 1989.

[91] A. L. Swindlehurst and T. Kailath, "A performance analysis of subspace-based methods in the presence of model errors. i. the music algorithm," *IEEE Transactions on Signal Processing*, vol. 40, pp. 1758–1774, Jul 1992.

[92] P. Forster and E. Villier, "Simplified formulas for performance analysis of music and min norm," in *OCEANS '98 Conference Proceedings*, vol. 3, pp. 1486–1490 vol.3, Sep 1998.

[93] K. R. Srinivas and V. U. Reddy, "Finite data performance of music and minimum norm methods," *IEEE Transactions on Aerospace and Electronic Systems*, vol. 30, pp. 161–174, Jan 1994.

[94] G. Dimic, N. D. Sidiropoulos, and L. Tassiulas, "Wireless networks with retransmission diversity access mechanisms: stable throughput and delay properties," *IEEE Transactions on Signal Processing*, vol. 51, pp. 2019–2030, Aug 2003.

[95] R. Samano-Robles, M. Ghogho, and D. C. McLernon, "Wireless networks with retransmission diversity and carrier-sense multiple access," *IEEE Transactions on Signal Processing*, vol. 57, pp. 3722–3726, Sept 2009.

[96] G. Z. Dimic and N. D. Sidiropoulos, "Stability analysis of collision resolution protocols with retransmission diversity," in *2002 IEEE International Conference on Acoustics, Speech, and Signal Processing*, vol. 3, pp. III–2133–III–2136, May 2002.

[97] R. Samano-Robles, M. Ghogho, and D. C. McLernon, "Adaptive detection for wireless network diversity multiple access protocols," in *2007 9th International Symposium on Signal Processing and Its Applications*, pp. 1–4, Feb 2007.